KJPS
AL-Kitab Journal For Pure Sciences

AL-Kitab Journal For Pure Sciences

Volume : 6 (2022)

Issue: 1

ISSN: 2617-1260 (print)

ISSN: 2617-8141 (online)

DOI: http://10.32441/kjps

Deposit Number of Iraqi National Library of Books and Documents 2271 in 2017

Al-Kitab Journal for Pure Science

KJPS

ISSN: 2617-1260 (print), 2617-8141(online)
DOI: http://10.32441/kjps
www.kjps.isnra.org

An Academic Semi-Annual Journal

Volume: 6 Issue: 1 June 2022

University Website: www.uoalkitab.edu.iq
Journal Website: www.kjps.isnra.org
E-mail: kjps@uoalkitab.edu.iq

Editors

Authors Guidelines

Rules and Instructions for Publication in Al-Kitab Journal for Pure Sciences

First: General requirements

1. The paper is submitted to the Editorial Secretariat directly in four copies with CD-ROM or E-mail of the magazine in MS Word and PDF files.
2. Research before being sent to scientific evaluators is subject to the quotation Turnitin program.
3. Research shall be accepted for publication after being judged by scientific evaluators and according to the rules.
4. The publication fee is (50$) for researchers from Iraqi Universities and (free of charge) for foreign researchers.

Second: To prepare research for publication, authors must follow the following procedures.

1. **The article:**

   The article needs to be typed on one side of A4 paper (Right margin =2.5 cm, left margin =2.5 cm, and 2cm for the top and bottom) with 1.5 space, and the pages must be numbered.

2. **The content organization:**

   MS Word is to be used as follows: "Simplified Arabic" font for the Arabic articles, and "Times New Roman" for the English articles. The Size of the title is 18 bold. The name of the authors will be typed in 11 bold in Arabic and 11 bold in English. Abbreviations, keywords, the main headings, the reference, and the acknowledgment will be typed in 14. Subheadings will be in 12 bold. The abstract will be size 12. The body of the article/paper is in size 12. The order of the content of the paper will be as follows: The article heading, the names of authors and their addresses, and the abstract (Both in Arabic and English).

3. **Research paper title:**

   The title must be as short as possible and indicates the contents of the subject together with the name (names) of the authors. The names of the authors to whom correspondence is to be made should be indicated with (*) and show his / her email.

4. **The size:**

The paper should contain no more than 15 pages of journal pages including charts and diagrams. Extra pages will be charged at (3$) each.

5. **Abstract:**

The abstract should include the purpose and the means of the founding results and the conclusions. It should also contain the knowledge values of the subject of research. It is meant to be no more than 250 words. It should also emphasize the content of the subject and includes the keywords used throughout the paper.

6. **Diagrams:**

Figures and diagrams must be given following the explanation referring to the diagram. Each diagram must contain its title below the diagram at the first size of 12. The diagram should be editable in terms of enlargement or reduction within the margins of the paper size. The parts of each diagram must be grouped into drawing parts.

7. **Tables:**

The tables should follow the parts of the main body and should be located below the indicated part of the text. Tables must have titles with a text size of 12. The text used inside the tables should be of size 12 and kept within the cells of the table.

8. **References:**

The references used in the paper must be given in order and their numbers given inside the square bracket [ ]. The following instructions are to be followed:

If the reference is a book, the First name of the reference must be given first followed by the other names. Then the title (bold and Italic) of the book, edition, year of publication, the publisher, and place of publication (year of publication).

Example: [1] P. Ring and P. Schuck, "**The Nuclear Many-Body Problem**", First Edition, Springer-Varlag, New York (1980).

(b) If the reference is a research paper or an article in a journal: The name of the author must be given first, the title of the article, the name of the journal, the volume (issue), page (Year). **Example:** [1] Ali H. Taqi, R. A. Radhi, and Adil M. Hussein, **"Electroexcitation of Low-lying Particle-Hole RPA States of ^{16}O with WBP Interaction"**, Communication

Theoretical Physics, 62(6), 839 (2014).

c) If the reference is an M.Sc. or Ph.D. thesis, the name of the anther must be written with the first name first followed by the surname, title of the thesis, the name of the university, and Country (Year).

Example: [1] R. A. Radhi, **"Calculations of Elastic and Inelastic Electron Scattering in Light Nuclei with Shell-Model Wave Functions"**, Ph.D. Thesis, Michigan State University, USA (1983).

(d) If the reference is from the conference. Authors Name, "**Paper Title**", Conference, Country, Publisher, volume, page (Year).

Example: [1] Ali H. Taqi and Sarah S. Darwesh, **"Charge-Changing Particle-Hole Excitation of ^{16}N and ^{16}F Nuclei"**, 3rdInternational Advances in Applied Physics and Materials Science Congress, Turkey, AIP Conf. Proc., 1569, 27 (2013)

Third: Privacy Statement

1. The names and e-mail addresses entered into the journal's website will be used exclusively for the purposes stated in this journal and will not be provided for any other purpose or to any other party.
2. The editor of the journal has the right to change any statement or phrase of the research content he may find necessary in order of expressing the work suitable to the general style of the journal.
3. After publishing the paper and its presentation on the journal page, the editors' team will destroy all the scrap papers. The author has no right to ask for them in any case.

Fourth: Modernity of sources:

The percentage of modern references used in the research should not be less than 50% of the total references used in the research. Modernity is measured within the last ten years of the year of submission of the research. For example, when submitting the research in 2018, the references should be from 2008 upwards and not less than 50%. The journal prefers to have at least one of the reference types of research published in the previous journal issues.

Note: For more information, visit:

Al-Kitab University Website: www.uoalkitab.edu.iq

Or Journal Website: www.kjps.isnra.org

The Journal can also be e-mailed to kjps@uoalkitab.edu.iq

Table of Contents

Volume: 6 Issue: 1 June 2022

https://doi.org/10.32441/kjps.06.01.p1

Al-Kitab Journal for Pure Sciences
ISSN: 2617-1260 (print), 2617-8141(online)
www.kjps.isnra.org

Performance Improvements Using Deep Learning Based Object-Identification

Shouket Abdulrahman Ahmed[*1], **Hazry Desa**[1], **Abadal-Salam T. Hussain**[12]

[1] Centre of Excellence for Unmanned Aerial Systems (COEUAS), Universiti Malaysia Perlis, Malaysia.
[2] Department of Medical Instrumentation Engineering Techniques, Al-Kitab University, Iraq.

[*]Corresponding Author: shouketunimap@gmail.com

Citation: Ahmed S., Desa H., Hussain A. Performance Improvements Using Deep Learning Based Object-Identification. Al-Kitab Journal for Pure Sciences (2021); 6(1): 1-13. DOI: https://doi.org/10.32441/kjps.06.01.p1

Keyword
Deep Learning, Artificial Neural Networks, Object-Identification.

Article History

Received	15 Jan.	2022
Accepted	12 Feb.	2022
Available online	10 April	2022

Abstract:

Deep Learning incorporates numerous hidden layers and more rooted combinations that average Artificial Neural Networks (ANN), to produce more refined and better performing autonomy in learning algorithms. An incredible volume of literature details and improves upon Deep Learning related methods and their improvement through the years as well as their suitability in uses. Nevertheless, the primary focus of the literature review is not the enlistment of these techniques hence a concise overview will be provided over the mechanisms before delving into the intended applications.

Keywords: Deep Learning, Artificial Neural Networks, Object-Identification.

تحسينات الأداء باستخدام التعرف على المكونات القائمة على التعلم العميق

شوكت عبد الرحمن احمد[1*]، حزري ديسي[1]، عبد السلام طه حسين[12]

المركز الاستشاري للطائرات المسيرة، جامعة بيرليس الماليزية، بيرليس، ماليزيا [1]

قسم هندسة تقنيات الأجهزة الطبية، الكلية التقنية الهندسية، جامعة الكتاب، كركوك، العراق[2]

[*]shouketunimap@gmail.com

الخلاصة:

يشتمل التعلم العميق على العديد من الطبقات المخفية ومجموعات أكثر تجذرًا من الشبكات العصبية الاصطناعية لإنتاج استقلالية أكثر دقة وأفضل أداءً في خوارزميات التعلم. حجم لا يصدق من التوصيلات والتفاصيل وتحسن أساليب التعلم العميق ذات الصلة وتحسينها خلال عملية التعلم وكذلك مدى ملاءمتها في الاستخدامات المختلفة. ومع ذلك، فإن التركيز الأساسي لمراجعة التوصيلات ليس هو تجنيد هذه التقنيات ومن ثم سيتم تقديم نظرة عامة موجزة على الآليات قبل الخوض في التطبيقات المقصودة.

الكلمات المفتاحية: التعلم العميق، الشبكات العصبية الاصطناعية، التعرف على الأشياء.

1. INTRODUCTION:

The performance of DNNs (Deep Neural Networks) in operations concerning the processing of images improved considerably in the past decade because of the abundance of samples (labeled examples) and increased computer functionality. Deep Neural Networks have shown promising results when utilized for information handling operations, but there is yet much unexplored regarding the capabilities and constraints that this approach may have. For this reason, many studies were devised to more accurately detail the perspective contributions that deep learning may provide in the field of image segmentation.

2. Deep Neural Networks Overview:

Deep Neural Networks (DNNs) is a concept of neural-networks that are made up of “neurons”, referred to as units, and contain a specific incitation (or activation) and specifications (or parameters) functioning as processes that convert input data such as UAV-imagery to the desired output, which in this case is scenario-based maps, simultaneously gaining a greater level of knowledge **[1, 2]**. This dynamic knowledge enhancement is carried in layers called the “hidden layers” that lie between the input layer and output layer **[3]**. Deep

Neural Networks exist as the most simplified Deep Learning approach, as such containing at the very least two hidden layers. They were introduced in the mid-20th century and the ideology of this concept was derived from AI (Artificial Intelligence) produced under the natural neural networks present in human biology. Deep Neural Networks have resurfaced in many important domains of science only after the improvements in computation technology and the rising abundancy of sample image datasets. Due to the benefits gained in performance with the implementation of Deep Learning networks in image-processing operations, it has caught the of many researchers and scientists in the image segmentation field in the previous decade **[4, 5]**.

The operation of a Deep Neural Network is identical to that of an Artificial Neural Network such that it can be instructed to evaluate specific input characteristics that are examined through various layers, and the required data is provided by a final output layer. However, there are many differences between the more conventional Artificial Neural Networks and Deep Neural Networks that need to be examined. One of the most prevalent pieces of literature in the scope of Deep Learning, details Deep Neural Networks as "Representation-Learning" algorithms with several bands of representation. The concept of Representation Learning is a prominent subject in Deep Learning as it provides the capability for the model to autonomously generate the required representations from raw data, commonly in text, image, and video formats.

Usually, Deep Neural Networks consist of activation instructions that are applied to the dense layers in the network as illustrated in **Figure 1** below. The purpose of these activation instructions is to evaluate the importance score of the input data and provided biases and accordingly activate (or not activate) a unit **[6]**. These instructions contain decision-making parameters that assist in studying inherent patterns **[7]** hence, this process is essential in allowing different units to interact and gain knowledge. Some Activation algorithms that are broadly implemented are Rectified Linear Unit (ReLu) and others based on its structure e.g., Leaky ReLu, Parametric Rectified Linear unit (PReLU), Exponential Linear Unit (ELU), max-out, linear, tahn, and sigmoid **[8]**. Out of these ReLu, a piecewise linearly structured algorithm is the most prevalent of the modern Deep Neural Network algorithms. Its popularity can be attributed to its lower processing-power requirements than other functions, effectively handles the vanishing-gradient issue, allows broader representation of information, and provides the capability to alter data structure. On the other hand, a novel approach for implementing activation algorithms has been introduced as Mish, an autonomously organized and multi-

parametric activation algorithm, which is providing encouraging results, as further studies are being implemented.

Besides the Activation instructions, other constituent operations of a layer present in a Deep Neural Networks model can be batch normalization, convolution and deconvolution, max pooling, dropout, encoding and decoding, and memory holding units among many others. Out of these, dropout and batch normalization will be discussed currently while others will be detailed in further sections of this literature. Due to the nature of Deep Learning models to inconsistently discard neurons and connections using a configured probability, dropout layers are introduced to provide normalization in this process. They assist the network in reducing overfitting through the removal of connections showing correlation, along with enhancing rationalization allowing for more refined and quicker learning processes **[9, 10]**. Similarly, batch normalization also assists in enhancing rationalization by operating as a catalyst and stabilizing the path of loss-gradient. It is often implemented on problems pertaining to covariance shift in land use maps **[11]**. The systemization of these various types of layers and their construction is a defining feature of this network.

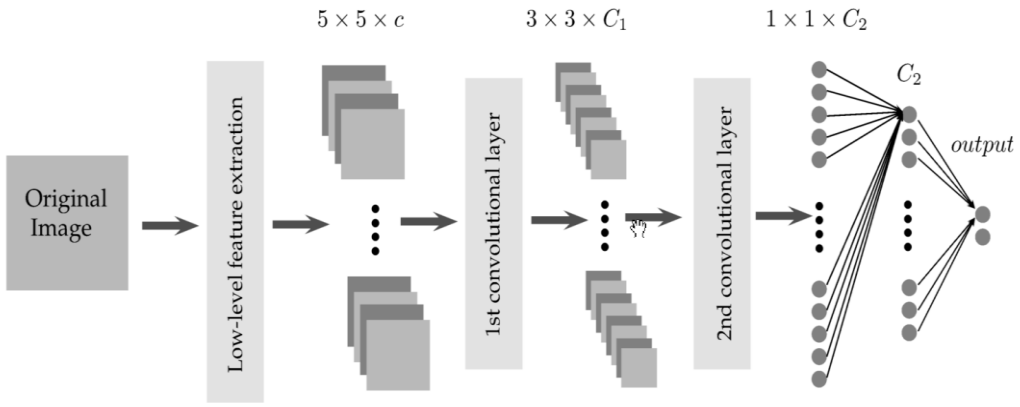

Figure 1: Deep learning model architecture

When assembling a network, its configuration requires some elementary pieces of information. The “optimizer” is one such piece that is applied to evaluate the rate of learning. A few reliable optimizer algorithms that are commonly used are momentum algorithm, Adam, Root Mean Squared Propagation (RMSprop), and Stohastic Gradient Descent (SGD). Choosing the most suitable optimizer for every application or architecture can assist greatly in refining the precision. The simplest of the above algorithms is SGD, in which the units are combined

and processed with the optimum-cost operation at a rate of a single sample-per-step. Another method, the Momentum algorithm aims to overcome the limitation caused by being bound to the local bottleneck by employing a transitory model. On the basis of gradient-based refinement strategies, RMSprop incorporates the momentum and AdaGrad (Adaptive Gradient) algorithms to apply an increasingly diminishing mean value of the gradients. The most prominent optimizer model, Adam, provides the capability to conjoin the adaptive-learning flow with the momentum algorithm, further examination of which can be found in **[12]**. These functions are essential in Deep Learning models as when used with a suitable loss algorithm, they can greatly enhance the precision of the network.

In the scope of optimization, the algorithm responsible for examining the network is the cost function, also commonly referred to as an objective function or loss function. The purpose of the loss function is to evaluate the capability of a network to provide a single-scalar score from the test information. Due to this often the focus of enhancing the learning ability of a network is directed towards varying the networks specifications to reduce the cost function. This assists in novel approaches to be scored and then benchmarked against different unit operations **[13]**. Cost functions utilize numerical statistics to perform their computation. This representation is analogous to the context of the issue, for instance, if a model is responsible for performing object classification or regression-based operations. In the case of object classification, the statistical loss can be evaluated using various approaches such as Poisson, cross-entropy, KL divergence (Kullback- Leibler), etc. In the case of regression-based operations, approaches such as Mean Squared Logarithmic Error (MSLE), Mean Absolute Error (MAE), Mean-Squared Error (MSE), Mean Absolute Percentage Error (MAPE), etc., are often applied. A more thorough approach to objective functions can be found in the literature by **[4]**.

To assess the capabilities of a Deep Neural Network several criteria have been applied **[5]**, as scientists often consult these evaluations. In the context of object classification, the general parameter used is accuracy, or by extension sensitivity or recall, other metrics such as F-Score, an area under the ROC curve path, precision, Intersection over Union can also be utilized to evaluate the efficiency of a model. An additional parameter is the “Kappa Co-efficient” which has been discredited as an accurate metric in the publication by **[6]**. Furthermore, in the context of regression-based operations, the preferred parameters are MAE, MSE, Mean Relative Error (MRE), Correlation Co-efficient (r), Root-Mean-Squared (RMS) Error, and others. Evaluation of such qualities is necessary to benchmark the performance of sample and acquired data and compare novel models with existing ones **[7]**. Despite regression-based evaluation not being as

prevalently applied in the examination of image-processing, it is still essential as UAV-related operations are often dependent on both processes.

Various variants of network models have been introduced in the past decade to advance and refine Deep Neural Networks by applying numerous types of layers, activation and optimizer algorithms, cost functions, level of depth, etc. Albeit the rise in Deep Neural Network's prevalence in the computer vision community can most accurately be attributed to the abundance of openly accessible data available to train these models. The prominent criterion among data-scientists suggested that at the very least 5000 samples should be available for every data class **[8]**. However, the direction taken by modern research in Deep Neural Networks focuses on achieving similar levels of feature detection using fewer samples than those suggested. Due to fewer expenditures and manpower needed to acquire samples, many applications with special requirements can profit from this. As such, despite efforts being made at this front, modern research in the computer-vision field is also advancing towards accommodating approaches for data augmentation, self-sufficiency, and unsupervised data-learning techniques, and many others. More details on these approaches are provided at the end of this literature, as such the study by **[9]** can also be consulted.

3. Image Segmentation Algorithms

Unsupervised image segmentation algorithms have progressed to the stage they can produce segmentations that match human intuition to a great extent. It is about time for segmentations to be implemented in the recognition of objects. Unsupervised segmentation can clearly be used to aid in the cueing and refinement of many recognition algorithms; however, a major stumbling block is the fact that it is not yet clear how efficiently these segmentation schemes can perform objectively. Most segmentation algorithms include cursory evaluations that only show visual clues of the segmentation process and rely on the instincts of the reader for decisions. Considering the persistent absence of numerical findings, it is tedious to determine the best segmentation scheme that will produce beneficial performances and in what scenarios. While appealing to human intuition is convenient, objective findings on huge datasets are necessary if the method is to be employed in an automated system.

4. Convolutional and Recurrent Neural Networks

Deep Neural Networks can be constructed using various models, where the sophistication of the architecture can be dependent on the number and constitution of layers in the networks and

the mathematical processing that is applied. The various types of Deep Learning models that are used commonly are Recurrent Neural Networks (RNN) as show in **Figure 2**, Convolutional Neural Networks (CNN), Deep Belief Networks (DBN) **[9]**, and Generative Adversarial Networks, that has been newly introduced. These Convolutional Neural Networks and Recurrent Neural Networks have been the most prominently used in the context of supervised networks **[1]**.

Modern research in the context of image-processing and object-identification operations is primarily implemented with Convolutional Neural Network models. They are prominently recognized in the field of computer vision despite having recently come into the spotlight. Despite having been predicted to provide great enhancements in image-classification operations, its promise only became recognized in 2012, when **[2]** developed an approach incorporating CNN that severely outperformed all others in an image-classification contest. This model is referred to as AlexNet consisting of 8 total layers. The starting 5 were entirely convolutional based, of which a few were accompanied with max-pooling layers, and the final 3 were fully connected layers, all of which used the ReLu activation algorithm **[5]**. This architecture is currently thought of as a basic Deep Learning model and its efficiency is attributed to the comprehensiveness of its layers.

Convolutional Neural Networks (comprehensively illustrated in **Figure 2**) primarily consists of three discrete systemized webs of layers, i.e., convolutional, fully connected, and pooling layers **[2]**, and have several assigned metrics such as biases, weights, the number of units and layers, stride, activation instructions, learning-rate, size of filters, etc. **[11]**. As the data passes through every layer several filters and incorporated biases are applied to allow the network to develop a land-use map **[13]**. Convolution processes utilize the size of filters to explore the correlation between pixels from the input data **[11]**. Due to the regular arrangement of pixels in multi-band image segmentation image-data Convolutional Neural Networks, that were initially introduced to compute data in the format of multiple arrays. As such this model has garnered a reputation as one of the most prevalent Deep Neural Network architectures currently **[1]** and has contributed greatly to the enhancement of numerous UAV-related image-processing operations.

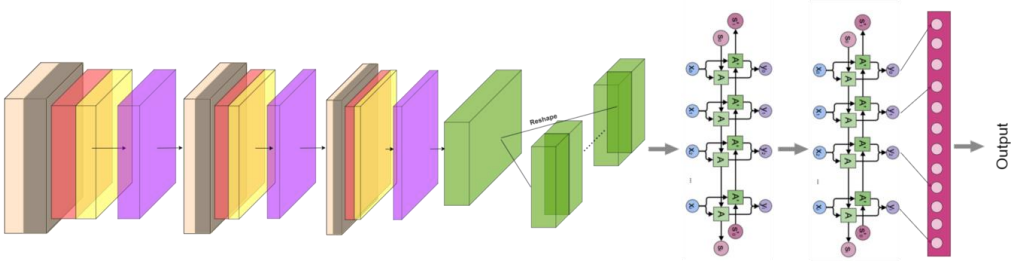

Figure 2: Convolutional Recurrent Neural Networks

Another architecture built upon the concept of Deep Learning is Recurrent Neural Networks, which implement a supervised-learning approach. Its advent in image segmentation applications is a recent development despite having been commonly utilized for numerous computer-vision-related operations. The Recurrent Neural Network architecture was introduced with the aim of handling discrete-sequence data examinations [1].

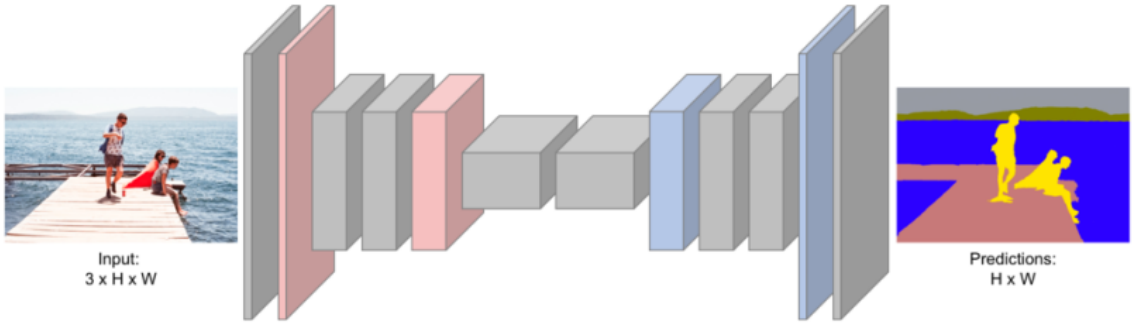

Figure 3: A Convolutional Neural Network-based model consisting of convolution layers and deconvolutional layers

The fundamental benefit received in using Recurrent Neural Networks is their ability to enhance their knowledge database through repeated examination of a specific setting or object, commonly pertaining to data of a time series-related format. A variant of Recurrent Neural Networks that is gaining importance and is being utilized with many applications is the Long Short-Term Memory model. They are useful in time-series-based operations as they overcome the diminishing gradient issue encountered with Recurrent Neural Networks. To accomplish these specific parameters and functions are included to smoothen the generated gradients [3]. Neurons found in an LSTM-based architecture consist of a cell along with an input and output gate and a forget gate. These gates exist to assist the unit in retaining and discarding information at discretely specified time-intervals.

Within the domain of image segmentation, Recurrent Neural Network architectures have been implemented in operations requiring handling and examination of time-series image-data intending to, for instance, generate land-use maps [4,5]. When working with pixel-related time-series image-data to classify categories of winter-time herbage density utilizing the SAR Sentinel-1 model, traditional Machine Learning networks paled in comparison to the performance demonstrated by the Recurrent Neural Network architecture. Furthermore, a modern model built for performing more precise herbage-density mapping been introduced, incorporated a multi-domain Convolutional Neural Network to derive spatial-characteristics from UAV-acquired RGB-based image data and then processed through an attention focused

Recurrent Neural Network to examine the flowing reliance withing multi-transient characteristics. The collective spatial temporal properties are utilized to deduce the class of vegetation. Examples such as these prove the promise of applying Recurrent Neural Networks to image segmentation information. Another promising model is the CNN-LSTM Architecture (illustrated in **Figure 4**). In this model, the convolution layers are applied to the image-data for feature-extraction which are then input into the LSTM-model. Very few implementations of this architecture can be found in literature as it caters to distinct applications such as, operations involving multi-temporal data.

Accordingly, besides Convolutional and Recurrent Neural Networks, many other models of Deep Neural Networks are being introduced for image-data processing applications. Among these Generative Adversarial Networks are considered to be the most innovatory approach in the context of un-supervised Deep Learning architectures. Generative Adversarial Networks consist of two models, namely “generative” and “discriminative”, that are designed to compete with each other. The generative model focuses on deriving the required properties from a specific data-format, for example image-data, while on the other hand the discriminative model discriminates between the reference, also known as real or ground-truth, data and the data provided by the generative network i.e., the fake data) **[6,8]**. Currently, GAN-based Deep Learning models that assist the process of image-data computation such as object-classification of image segmentation imagery and image to image transcription operations are providing promising outcomes **[9]**.

Originally, the majority of DNN-based architecture types, such as RNN, CNN, and CNN-LSTM were introduced to handle a distinct problem. These models can be conveniently categorized according to image-classification operations, for instance setting-specific classification, object sensing, semantic-segmentation, pixel-based instance-segmentation, and regression operations. These operations are followed through and detailed further in consequent sub-sections. As such the upcoming subsections will demonstrate the way in which these technologies are being used in image-processing operations and how they aid in overcoming problems encountered with previously applied models.

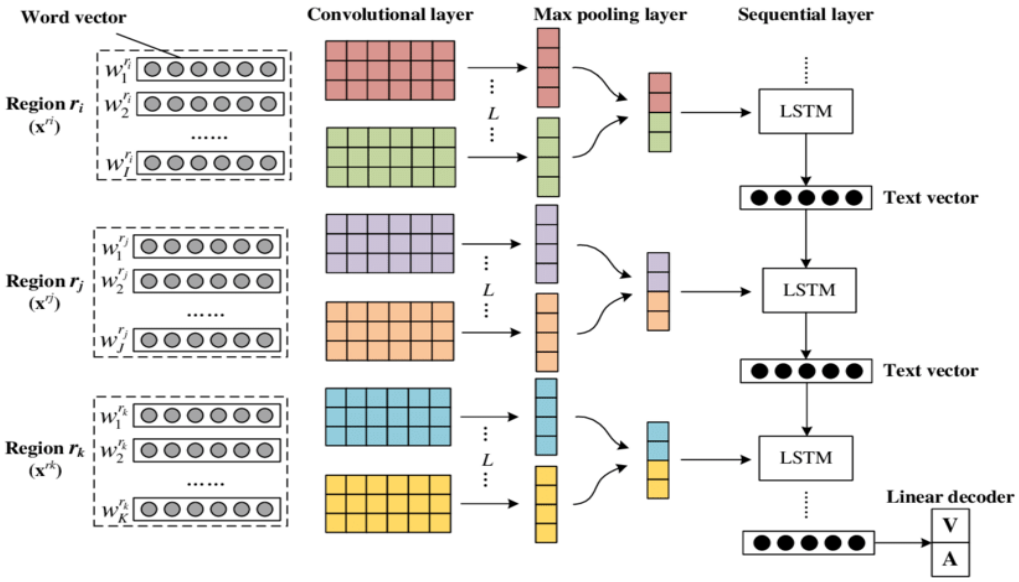

Figure 4: A sample of an architecture of type CNN-LSTM

5. Classification and Regression Approaches

In the context of implementing Deep Learning models to compute image segmentation image-data, the most common operations performed are, setting-specific classification, semantic-segmentation, instance-segmentation, and object-identification. The aim of setting-specific image-classification is to appoint a class-label to every input image, while the process of object detection is focused on building boundary-boxes that outline the detected image in an image and then assigning labels to these boundary-boxes. As such the process of identification is thought to be a more complex operation as it performs both detection and classification tasks. Additionally, identification can also be done with outlining sections or patches around an object rather than boundary-boxes, which specifies the category of an object at the pixel level. This operation is referred to as semantic segmentation. A drawback of this method is that it is unable to discriminate between objects of the same class owing to the capacity of a pixel to hold a single class-label [5]. As a means of overcoming this limitation a new approach called instance-segmentation was introduced that incorporated concepts of both semantic segmentation and object detection. It allows to perform identification of different objects in pixel level clouds, and these clouds are then labelled with corresponding class-labels [10].

To develop a regression-based model, the network requires readjustment in that its end layer i.e., the fully connected layer is modified to handle regression operations in place of the more regularly implemented image-classification tasks. Due to this modification, sequential data is evaluated with different criteria from that of classification operations. The implementation of regression-based operations utilizing Deep Learning models is not as common as that of

classification-task, albeit recent research has demonstrated the promise shown by using this combination in processing of image segmentation related data. One such research is by [9] in which an in-depth investigation of deep-regression models was carried out and was shown that commonly used refined networks such as ResNet-50 **[6]** and VGG-16 _bookmark51**[11]** showed incredibly promising outcomes. One disadvantage of these models is that they have been tailored to perform distinct functions, meaning they are not that well suited for general purpose problems. Another drawback is that deep-regression methods are not successful every time. A useful technique is to categorize the output-space and to allow the model to handle the operation as an image-classification task. In the context of UAV-based image segmentation operations, it is preferred to utilize popular models. Models other than the "ResNet-50" and VGG-16" **[11]**, include VGG-11 and AlexNet, used by **[10]**. A prospect for future research-considerations in retrospect of the required implementations is optimizer functions. Currently models that incorporate dynamic learning-rates, for instance RMSProp, AdaGrad, Adam, and AdaDelta are the most prominently recognized.

6. Scene-Wise Classification, Object Detection, and Segmentation

Setting-specific image-classification or scene-recognition are operations that assign a theme or label for an image, also referred to as a patch, according to other sample-images, for instance in agricultural, beach, and urban settings, among others **[2,4]**. Simple Deep Neural Network models were introduced for these operations of which there are many that are broadly used for conventional image-classification tasks. In the scope of image segmentation implementations, it is not common to employ a scene wise classification approach. Rather, applications in this field would find it more advantageous to adopt object-identification and instance-segmentation methods. In terms of scene wise categorization, the approach requires only a labeling of the class-label present in the image, whereas for object-identification every object present in the image is required to be outlined by a boundary-box, hence increasing the cost required to construct such sample data clusters. The abundancy reduces even further for data clusters related to instance-segmentation as a "mask" needs to be constructed around every pixel the object is present in, meaning more accuracy is required for such an operation. **Figure 5** illustrates the operation of the annotation step for both object identification and pixel-wise semantic segmentation processes.

7. Conclusions

Object-identification models can be classified in two elementary approaches: regression-based mechanisms and region-proposal based mechanisms, also referred to as one stage and

two stage detectors respectively [3-6]. Utilizing the common two stage object detector approach requires construction of probable regularly shaped boundary-boxes on the landscape map. Each object is then categorized with a class-label and the successful detections are reinforced through boundary-box regression. A broadly implemented technique utilized in many studies to compute region-proposals was through the Faster-RCNN model combined with a Region-Proposal-Network (RPN) [7]. Several other modern models are also available such as Cascade-RCNN [9-13]. Dynamic-RCNN [4], DetectoRS [6]. In the case of one stage detectors, they omit the region-proposal task and immediately outline the position of objects and label them accordingly. The omission of this task improves the speed of the identification process, but the accuracy is compromised as a result. This technique is commonly referred to as region free detection due to the nature of the model to utilize the image grid to segment the image and classify the objects with a class-label. Accordingly, there are a few detectors present that can perform both regression-based and region-proposal based approaches.

Object-identification related approaches can be thought to be built from three constituents namely:

- The backbone that is focused on deriving the inherent characteristics from the images.
- The neck, a mediatory element of the structure that lies in the middle of the head and backbone, its purpose being to refine the information generated by the backbone and lastly.
- The head, the structure responsible for constructing the boundary-boxes by performing the identification and classification operations on the image.

8. REFERENCES

[1] Adão, T., Hruška, J., Pádua, L., Bessa, J., Peres, E., Morais, R., & Sousa, J. J. ***Hyperspectral imaging: A review on UAV-based sensors, data processing and applications for agriculture and forestry. Remote Sensing***, 9(11), 1110. (2017).

[2] Adayel, R., Bazi, Y., Alhichri, H., & Alajlan, N. ***Deep open-set domain adaptation for cross-scene classification based on adversarial learning and pareto ranking. remote sensing***, 12(11), 1716. (2020).

[3] Al-Najjar, H. A., Kalantar, B., Pradhan, B., Saeidi, V., Halin, A. A., Ueda, N., & Mansor, S. ***Land cover classification from fused DSM and UAV images using convolutional neural networks. Remote Sensing***, 11(12), 1461. (2019).

[4] Ammour, N., Alhichri, H., Bazi, Y., Benjdira, B., Alajlan, N., & Zuair, M. ***Deep learning approach for car detection in UAV imagery. Remote Sensing***, 9(4), 312. (2017).

[5] Ampatzidis, Y., & Partel, V. ***UAV-based high throughput phenotyping in citrus utilizing multispectral imaging and artificial intelligence. Remote Sensing***, 11(4), 410. (2019).

[6] Apolo-Apolo, O. E., Martínez-Guanter, J., Egea, G., Raja, P., & Pérez-Ruiz, M. ***Deep learning techniques for estimation of the yield and size of citrus fruits using a UAV. European Journal of Agronomy***, 115, 126030. (2020).

[7] Audebert, N., Le Saux, B., & Lefèvre, S. ***Deep learning for classification of hyperspectral data: A comparative review***. IEEE geoscience and remote sensing magazine, 7(2), 159-173. (2019).

[8] Bachman, P., Hjelm, R. D., & Buchwalter, W. ***Learning representations by maximizing mutual information across views***. arXiv preprint arXiv:1906.00910. (2019).

[9] Badrinarayanan, V., Kendall, A., & Cipolla, R. ***Segnet: A deep convolutional encoder-decoder architecture for image segmentation***. IEEE transactions on pattern analysis and machine intelligence, 39(12), 2481-2495. (2017).

[10] Bah, M. D., Hafiane, A., & Canals, R. ***Deep learning with unsupervised data labeling for weed detection in line crops in UAV images. Remote sensing***, 10(11), 1690. (2018).

[11] Ball, J. E., Anderson, D. T., & Chan Sr, C. S. ***Comprehensive survey of deep learning in remote sensing: theories, tools, and challenges for the community***. Journal of Applied Remote Sensing, 11(4), 042609. (2017).

[12] Banerjee, K., Gupta, R. R., Vyas, K., & Mishra, B. ***Exploring Alternatives to Softmax Function***. arXiv preprint arXiv:2011.11538. (2020).

[12] Barbedo, J. G. A., Koenigkan, L. V., Santos, P. M., & Ribeiro, A. R. B. ***Counting cattle in UAV images dealing with clustered animals and animal/background contrast changes. Sensors***, 20(7), 2126. (2020).

Acknowledgment:

The authors Mr. Shouket Abdulrahman Ahmed, Prof Dr. Hazry Desa, and Ass. Prof Dr. Abadal-Salam T. Hussain of University Malaysia Perlis (Malaysia) would like to acknowledge and thanks Al-Kitab university, Kirkuk, Iraq and its scientific journal "Al-Kitab Journal for Pure Sciences" for acceptance and support our research titled "Performance Improvements Using Deep Learning Based Object-Identification".

---

https://doi.org/10.32441/kjps.06.01.p2

Al-Kitab Journal for Pure Sciences
ISSN: 2617-1260 (print), 2617-8141(online)
www.kjps.isnra.org

Bismuth oxyiodide nanocomposites supported on strontium hydroxyapatite enhance UV-Vis light-driven photocatalytic activity

*Mohammed K. Kzar, Zaki N. Kadhim, Ali H. Al-Mowali

Department of Chemistry,College of Science, University of Basrah, Basrah, Iraq

*Corresponding Author: mohammedkadhikzar@utq.edu.iq

Citation: Kzar M. K., Kadim Z. N., Al-Mowali A. H. Bismuth oxyiodide nanocomposites supported on strontium hydroxyapatite enhance UV-Vis light-driven photocatalytic activity. Al-Kitab Journal for Pure Sciences (2022); 6(1): 14-29. DOI: https://doi.org/10.32441/kjps.06.01.p2.

Keyword
Bismuth Oxyiodide (BiOl), Strontium Hydroxyapatite (SrHA), Cationic Dyes, Photocatalytic, XRD, EDX, and SEM.

Article History

Received	02 May	2022
Accepted	08 July	2022
Available online	02 August	2022

Abstract:

In this research, we discuss the removal of basic fusion (BF), and crystal violet (CV) dyes by strontium hydroxyapatite supported BiOI. In a modified hydrothermal model, one can synthesize BiOI/SrHA. BiOI/SrHA was characterized using Fourier transform-infrared spectroscopy (FTIR), UV-visible (UV-vis) analysis, X-ray diffraction (XRD), energy diffraction X-ray (EDX), and scanning electron microscopy (SEM). SEM outcome confirmed the dispersion of BiOI onto strontium hydroxyapatite. The shape of the BiOI catalytic samples overlapped with each other to form 3D hierarchical flower-like structures. The UV-visible was used as a radiation source during photocatalysis. BiOI/SrHA had an effect on malachite green dye degradation. The oxidative removal occurred through hydroxyl radical formation. UV-visible (UV-vis) BiOI/SrHA showed perfect photocatalytic property for the decay of Basic Fuchsin (BF) and Crystal Violet (CV) from an aqueous solution. According to kinetics analysis, the dye degradation rates could be in a pseudo-first-order model.

Keywords: Bismuth Oxyiodide (BiOl), Strontium Hydroxyapatite (SrHA), Cationic Dyes, Photocatalytic, XRD, EDX, SEM.

مركبات البزموت أوكسي يوديد النانوية المستندة على هيدروكسيباتيت السترونتيوم لتعزز نشاط التحفيز الضوئي بواسطة اشعة *UV-Vis*

محمد كاظم كزار*، زكى ناصر كاظم، على حسين الموالى

قسم الكيمياء، كلية العلوم، جامعة البصرة، البصرة، العراق

*mohammedkadhikzar@utq.edu.iq

Zaki.kadhim@uebasreh.edu.iq / ali-almoaali1946@yaho.com

الخلاصة:

في هذا البحث، نناقش إزالة صبغات الفوكسين الأساسي (BF) والبنفسجي البلوري (CV) بواسطة هيدروكسيباتيت السترونتيوم المستندة على BIOI. بواسطة التحلل الحراري المعدل، يمكن تحضير BIOI / SRHA. تم تشخيص BIOI / SRHA باستخدام التحليل الطيفي بالأشعة تحت الحمراء المحولة من فورييه (FTIR)، وتحليل الأشعة فوق البنفسجية المرئية (UV-VIS)، وحيود الأشعة السينية (XRD)، والأشعة السينية لحيود الطاقة (EDX)، والمجهر الإلكتروني الماسح (SEM). أكدت نتائج SEM تشتت BIOI على هيدروكسيباتيت السترونتيوم. تداخل شكل العينات الحافزة BIOI مع بعضها البعض لتشكيل هياكل D3 الهرمية الشبيهة بالزهور. تم استخدام الأشعة فوق البنفسجية المرئية كمصدر إشعاعي أثناء التحفيز الضوئي. كان ل BIOI / SRHA تأثير على تدهور صبغات الفوكسين الأساسي (BF) والبنفسجي البلوري (CV). حدثت إزالة الأكسدة من خلال تشكيل جذر الهيدروكسيل. أظهرت BIOI / SRHA المرئية للأشعة فوق البنفسجية (UV-VIS) خاصية مثالية للتحفيز الضوئي لاضمحلال الفوكسين الأساسي (BF) والبنفسجي البلوري (CV) من محلول مائي. وفقا لتحليل الحركية، معدل ازالة هذه الاصباغ يمكن تطبيق معادلة درجة الاولى الكاذبة.

الكلمات المفتاحية: أوكسي يوديد البزموت (BiOl)، هيدروكسيباتيت السترونتيوم (SrHA)، الأصباغ الكاتيونية، التحفيز الضوئي، XRD، EDX، SEM.

1. INTRODUCTION:

Pollutants can be elements, molecules, or particles with greatly benefit on living organisms and cause problems for the environment [1]. Plants and trees cannot grow in the absence of clean water. That is, there is no source of food, and this, in turn, can affect the economic conditions of humans, and here we must admit that people are the main source of environmental pollution [2]. One of the most important water pollutants are includes insecticides and herbicides, nutrition processing waste, pollutants from cattle operations, volatile organic compounds, heavy metals, chemical waste, and others [3,4]. Recently, the world has paid a lot of attention to the photocatalytic process. In this field researchers and scientists have conducted many types of experimental research. Heterogeneous photocatalysis is a promising new alternative method for the removal of organic pollutants from water. The photocatalytic mechanism is based on the advanced oxidation process (AOP), which has shown a high ability to decompose, mineralize harmful organic and inorganic compounds in the environment. One of the most important compounds that are used in the photocatalytic process is TiO_2 and ZnO, the importance of these two compounds is their non-toxicity and because of their strong

oxidizing power. The incorporation of bismuth into a given material yields an additional filled Bi 6s state, which appears to be more than O 2p. The transition to the s/d states of a transition metal from Bi 6s (or hybrid Bi 6s–O 2p states) becomes possible, which decreases the band gap. Compounds of the bismuth oxyhalide (BiOX) group exhibit some semiconducting and optical properties. In 1935, the scientist Bannister discovered the BiOX crystal structure and found that it possessed layers linked by covalent bonds of the three elements that made up [X-Bi-O-Bi- X, and X= halogens Cl, Br, I respectively] **[5,6]**. The geometric structure of BiOl/SrHA is tetragonal, so an electric field can be generated by work that activates photocatalytic thus preventing recombination between electrons and Holes formation **[7]**. Zhang et al. (2006) investigated the photocatalytic properties of bismuth oxyiodide (BiOl) as the first BiOX compound **[8]**. In recent years, there have been numerous medical, domestic, and industrial pollution problems. So as a result, efforts have been made to address this serious issue through practical research **[9]**. In this field, nanoparticles have been used extensively to reduce this dangerous phenomenon **[10]**. Many nanomaterials have been used, including bismuth oxyhalide BiOX, the unusual properties of these compounds made them distinguished in this field (passive voice and active voice). The formed Bi nanoparticles in the BiOl surface accelerate the transfer of photo-induced electrons from BiOl to Bi, and the surface oxygen vacancies in the BiOl photocatalyst result in its bandgap narrowing down to the visible light range **[11]**. Many experiments have been conducted in the process of replacing the element strontium (Sr^{+2}) to replace the element calcium (Ca^{+2}) in the compound hydroxyapatite, particularly in biological experiments, specifically in bones, where experiments have proven that the element strontium (Sr^{+2}) is non-toxic and stable when bound to hydroxyapatite **[12-16]**. BiOI displays a small bandgap (~1.7 eV) and is an active visible light photocatalyst for the photodegradation of different pollutants **[17-19]**. Li et.al offers BiOI with 3D hierarchical structures applied in the degradation of methyl orange (MO) and phenol with effective photocatalytic action **[20]**. Zan et.al elucidate that the photodegradation efficiency of cationic Rhodamine B (RhB) with BiOI was remarkably increased highly due to its distinctive structure containing single crystal nanosheets with high symmetry **[21]**. The structure of the two dyes examined is depicted in **Figure1**.

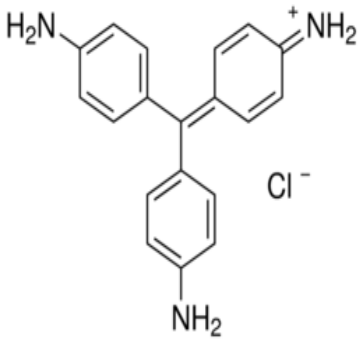

Basic Fuchsin (BF)

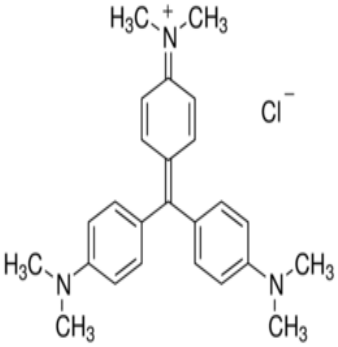

Crystal Violet (CV)

Figure 1: The chemical structure of dyes

2 .Experimental

2.1. Preparation of SrHA

A solution of H_3PO_4 0.3 mol. L-1 was vigorously mixed with a solution of Sr $(NO_3)_2$ 0.5 mol. L-1 (Merck, 99.67%) (molar ratio Sr/P =1.67. By adding NH_4OH (Merck, 30%), the pH of the solution was adjusted to 9.0. A white precipitate was formed, and the suspension was stirred for 2 h. Thereafter, the precipitate was washed with distilled water and vacuum filtered **[22,23]**. The preparation reaction occurs according to the **equation (1)**.

$$10\ Sr\ (NO_3)_{2(aq)} + 6\ H_3PO_{4(aq)} + 2\ NH_4OH_{(aq)} \rightarrow Sr_{10}(PO)_6(OH)_{2(s)} + 18\ HNO_{3(aq)} + 2NH_4NO_{3(aq)} \text{-------(1)}$$

2.2. Preparation of BiOCl/SrHA

BiOl/SrHA nanoparticles were synthesized by a modified hydrothermal method using bismuth oxide, Hl, and SrHA as precursors. The Bi_2O_3 (1.5g) was dissolved in excess concentrated hydrochloric acid (10 mol/L, 10 mL) to obtain a transparent BiO_3-Hl aqueous solution. To this solution, 1.2 g of SrHA was added with simultaneous stirring. The obtained mixture was sonicated for 15 min. The pH of the solution was adjusted between 2 and 3 using ammonia. The mixture was heated at 90 ^oC for half an hour to obtain white precipitates. The precipitates were washed several times with water and ethanol and then dried at 75 ^oC for 10 h. The acquired product is calcined in an electric furnace for 3 h at 550 ^oC. to obtain BiOl/SrHA nanoparticles

3. Photocatalytic dyes degradation and reactor

A photoreactor (as seen in **Figure 2**) experiment was carried out in a mode photoreactor. It was irradiated with UV light using (λ=254nm, 30V). The photocatalytic dye's degeneration tests

were performed by mixing different number of BiOl/SrHA nanoparticles in a photoreactor with a capacity of 1000 mL of each dye solution (15, and 20 mg/L, respectively) at 25°c. At predictable time intervals, the solution patterns were removed from the reaction medium. With the use of a UV–vis spectrophotometer (Perkin-Elmer Lambda 25), we separate BiOl/SrHA from the solution and observe the change in the catalyst adsorption process for these dyes at maximum wavelengths 545 and 591 nm for Basic Fuchsin and Crystal Violet, correspondingly. The concentration of BiOl/SrHA nanoparticles has an effect on the degeneration of photocatalytic dyes by contacting 1000 mL of dye solution (15 and 20 mg/L for Basic Fuchsin and Crystal Violet, respectively) at room temperature of 25°C for 5 h. various number of BiOl/SrHA nanoparticles were used. The initial dye concentration was calculated to see how it affects photocatalytic dye degradation. The BiOl/SrHA nanoparticles (0.05 g Basic Fuchsin, and 0.05 g for Crystal Violet) were added to 1000 mL of different dye concentrations (15, 30, 45, and 60 mg/l) of Basic Fuchsin (BF) and (20, 40, 60, and 80 mg/l) of Crystal Violet (CV).

4. Result and discussion

4.1. Characterization of specimens

Figure 3 shows the FT-IR spectra of BiOl/SrHA, the range of (3417.98 – 3346.76) cm−1 may refer to the stretching vibrations of −OH that existed in the adsorbed water molecule. As well the distinctive peaks at range (1615.41) cm-1 are referring to the O-H bending vibrations. for pure BiOl, 442.73 cm−1 corresponds to valence symmetrical (A2u-type) vibrations of the Bi-O bond, a reference that the compounds of BiOl are obtained. The broadband at 3417.98 cm-1 is refer to O–H vibration of H_2O absorbed in the specimen. 1404.71 cm-1 peak is refer to the carbon-related pollution and a small amount of $(CO3)^{2-}$ caused by the CO2 in an aqueous solution or air during the synthesis. 1615.41 cm-1 peak is refer to carbon-related pollution. The bands at 1018.19 are a marker of asymmetric stretching. The two groups of bands in the low wavenumber ranging from 605.22-510.04 cm-1 are attributed to the bending vibrations of O–P–O in (PO4)3- groups. Confirmed the formation of BiOl/SrHA. **Figure 4** note sample BiOl/SrHA overlapped with each other. The morphology of BiOl/SrHAp diagnosed by scanning electron microscopy (SEM) are fixed in SEM visual data shows a quite different morphology. notable, the surface structure of BiOl/SrHA changes to marked rise with some holes which look like bunches of grapes that were not present before being installed when modified, this explains the presence of a large surface area, which increased the adsorption process of the dyes Basic Fuchsin, and Crystal Violet, widely used dyes, were chosen as the

test pollutant to evaluate the photocatalytic activity of synthesized BiOl/SrHA. The phase structures of the as-synthesis BiOl/SrHA specimens were examined by XRD. As displayed in **Figure 5** peaks from BiOI/SrHA sample appear at 13.1, 23, 27.3, 31.7, 32.8, 35.25, 39.95, 40.95, 42.95, 46.25, 49.55, and 58.53, 2θ values with corresponding hkl values as 002, 012, 110, 013, 004, 020, 005, 114, 122, 016, 025, and 017, respectively, as per JCPDS card No. 73-2062.**[20]**. describe the EDX pattern of BiOl and BiOl/SrHA. in **Figure 6**, The presence of the components O, P, I, Sr, and Bi in BiOl/SrHA verified its formation.

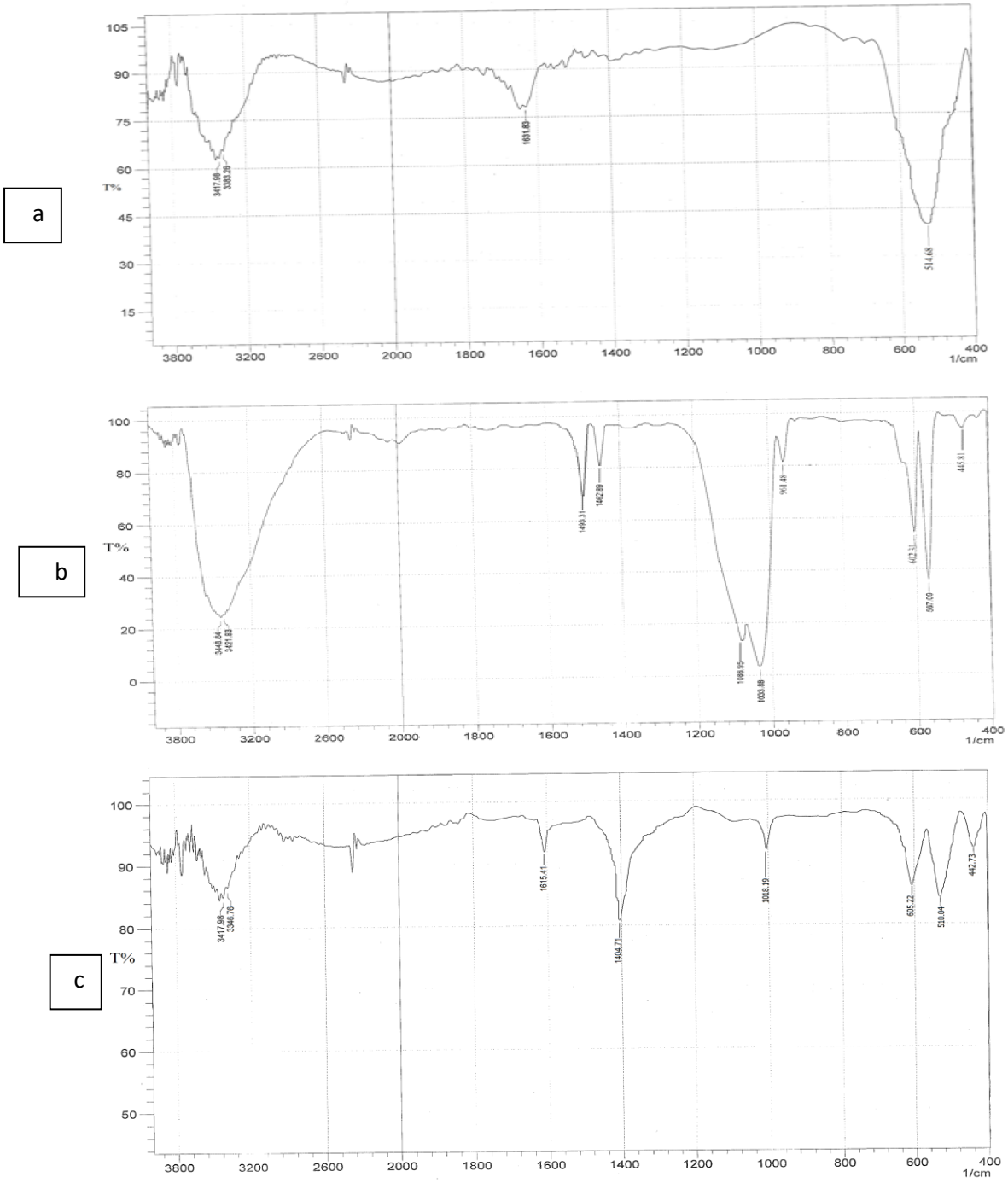

Figure 2: FTIR patterns of (a) BiOl, (b) SrHA, and (c) BiOl/SrHA

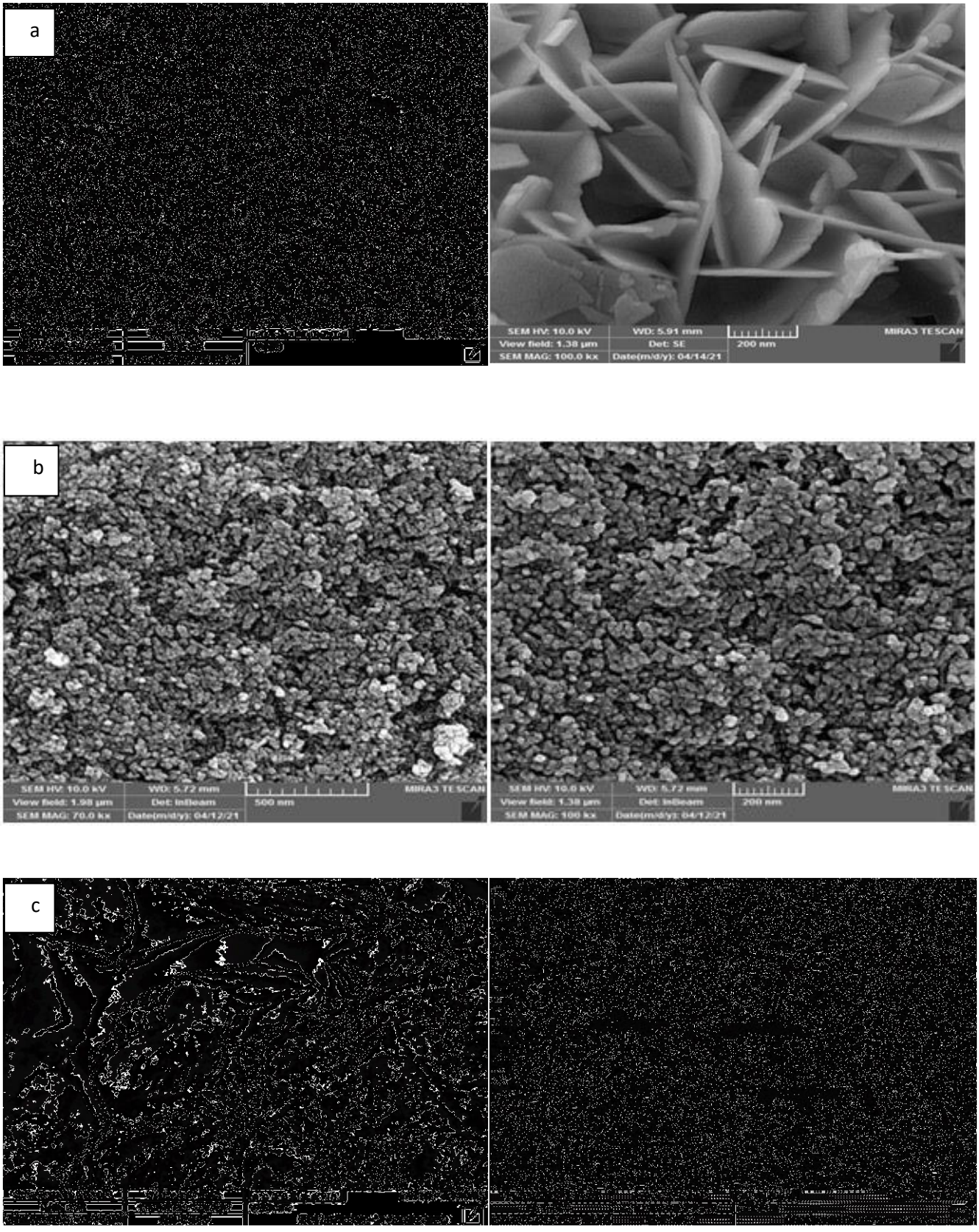

Figure 3: SEM of BiOl (a), SrHA (b) and BiOl/SrHA (c)

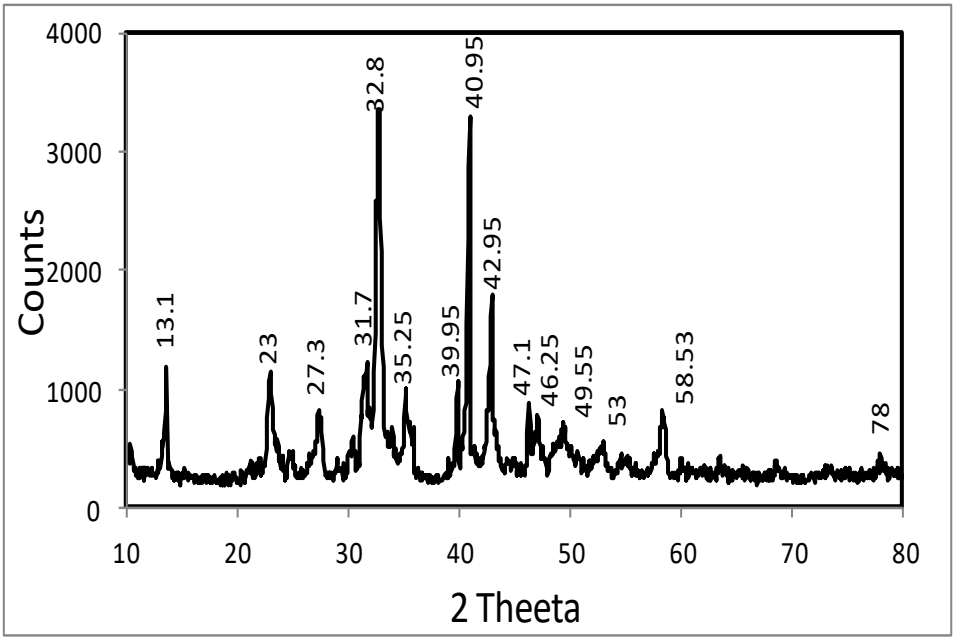

Figure 4: XRD patterns of BiOl/SrHA

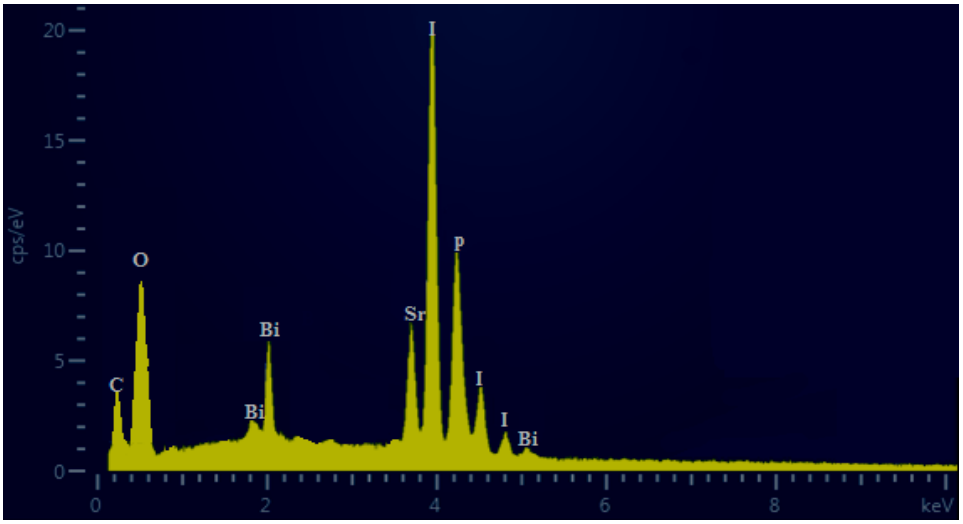

Figure 5: EDX pattern of BiOI/SrHA

5. Impact of some parameters on dyes degradation

5.1. Effect of BiOl/SrHA concentration

Figure 7 shows the effect of BiOl/SrHA concentration on photocatalytic dyes decomposition. In the absence of BiOl/SrHA, photodegradation for BF and CV is (5 and 3.5) %, correspondingly. Believing ultraviolet light alone was insufficient to oxidize dyes included in colourful wastewater samples; photocatalysts must be used to activate the UV. It is when the

use of BiOl/SrHA is as a photocatalyst with UV produces a significant improvement of dyes decay on the reverse when using UV alone to decomposition dyes [24]. The nanoparticles BiOl on SrHA as support are an experimentally efficient photocatalyst that uses light energy to form the e-/h+ pair on its surface. Where this pair e^-/h^+ leads to on decomposing the dyes through the formation of active oxygen superoxide radical anions ($O2^{\bullet-}$) and hydroxyl radicals ($HO^{\bullet}$) Which is the main sources in the pollutant decay. The kinetics of photocatalytic dye degradation by the photocatalyst BiOI/ SrHA were investigated at zero-order (eq. 2), first order (eq. 3), and second order (eq. 4).

$$Co - Ct = kot \quad \text{----------(2)}$$

Where Co and Ct are the initial and equilibrium concentration at any time dye concentration (mg/l), KO is the rate constant of pseudo-first order kinetic equation. The value of ko was determined from the slope of the linear plots of Co-Ct vs t.

$$\frac{dq}{dt} = k1(q_e - q_t) \quad \text{----------(3)}$$

The integrated form of the above expression is (4):

$$Ln(q_e-q_t) = lnq_e - k_1t \quad \text{----------(4)}$$

Where k_1 (min^{-1}) is the rate constant of pseudo-first order kinetic equation, qe and qt, respectively are the amounts of adsorbate adsorbed at equilibrium and at any time (mg /g). The value of k_1 was determined from the slope of the linear plots of ln ($q_e - q_t$) vs t.

$$\frac{t}{qt} = 1/k_2q_e + t/q_e \quad \text{----------(5)}$$

Where k_2 (g mg^{-1} min^{-1}) is the rate constant of pseudo-second order kinetic equation. The value of qe and k_2 can be determined by the slopes and intercepts of the straight line of the plots (t/q_t vs t).

The insertion of the applicability of pseudo zero, first, and second-order kinetics models for photocatalytic dye degradation by the nanoparticles of BiOX (X= Cl, Br, or I)/SrHA at different catalyst dosages, ko, k1, and k2 and R2 (correlation coefficient values) are shown in Table 1 respectively. The results shown in that the kinetics of photo catalytic dye degeneration via BiOX (X= Cl, Br, or I)/SrHA at various catalyst dosages followed the first-order kinetics.

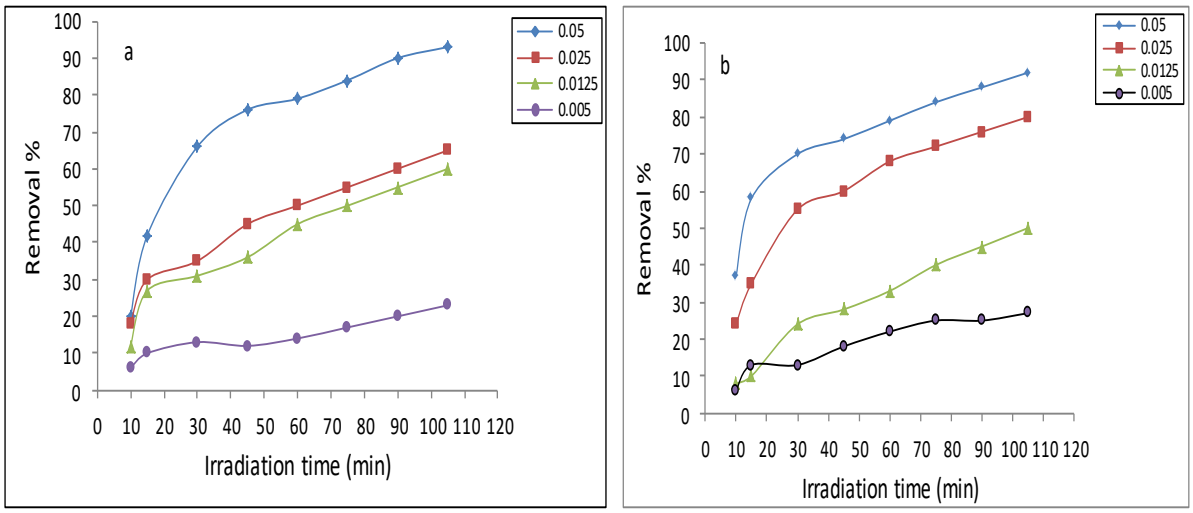

Figure 6: The effect of BiOl/SrHA concentration on the degradation of dyes in the presence of UV/BiOl/SrHA BF(a) and CV(b)

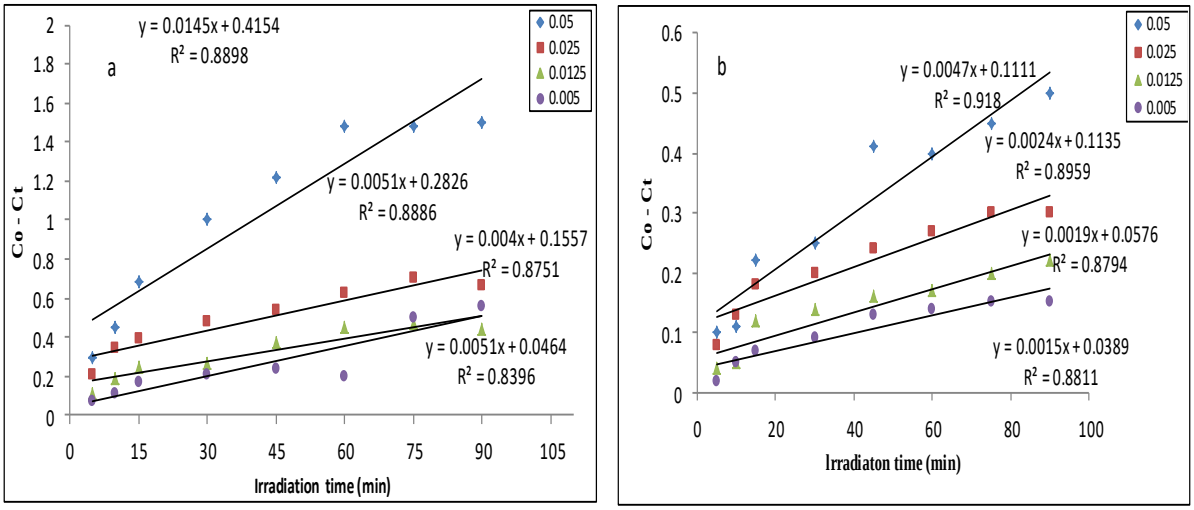

Figure 7: Shows the zero-order kinetics of photocatalytic dye degradation using BiOl/SrHA at varied catalyst concentrations BF(a) and CV (b)

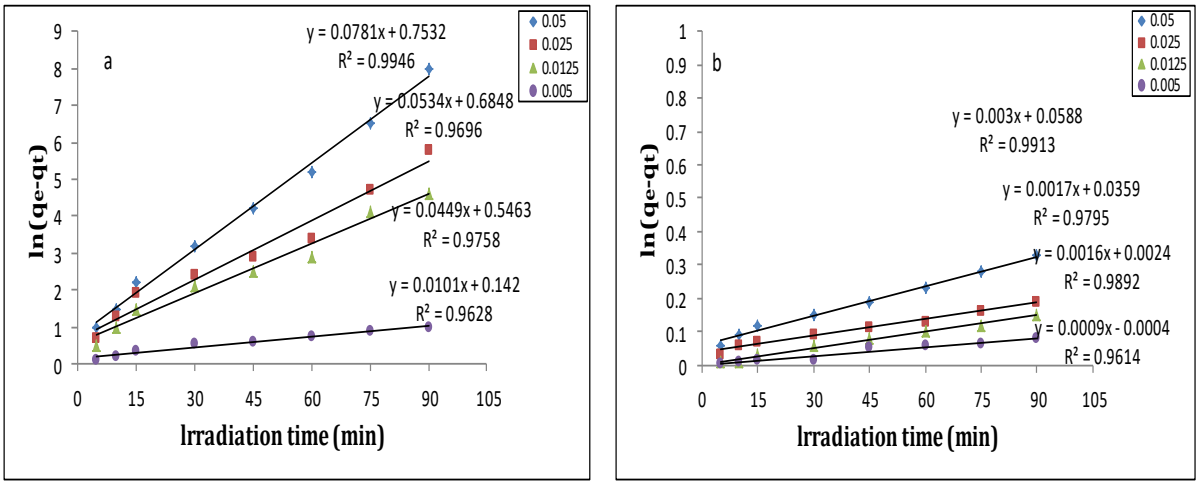

Figure 8: Shows the first-order kinetics of photocatalytic dye degradation using BiOl/SrHA at varied catalyst concentrations BF(a) and CV (b)

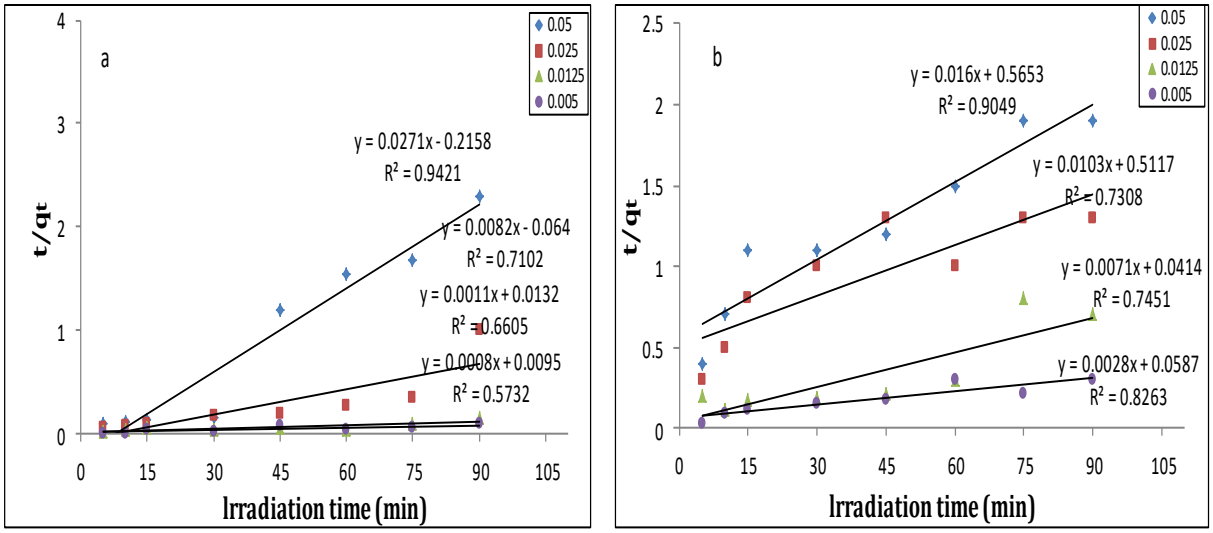

Figure 9: Shows the second-order kinetics of photocatalytic dye degradation using BiOl/SrHA at varied catalyst concentrations BF(a) and CV (b)

Table 1: The kinetics constants of photocatalytic Basic Fuchsin dye degradation by BiOl/SrHA at various catalyst dosages

BiOI/SrHA(g)	Pseudo-zero order		Pseudo-first order		Pseudo-second order	
BF	K_0	R^2	K_1	R^2	K_2	R^2
0.05	0.0145	0.8898	0.0781	0.9946	0.0034	0.9421
0.025	0.0051	0.8886	0.0543	0.9696	0.0010	0.7102
0.0125	0.004	0.8751	0.0449	0.9758	9.1E-05	0.6605
0.005	0.0051	0.8396	0.0101	0.9628	6.7E-05	0.5732
VC						
0.05	0.0047	0.918	0.003	0.9913	0.0004	0.9094
0.025	0.0024	0.8959	0.0017	0.9795	0.0002	0.7308
0.0125	0.0019	0.8794	0.0016	0.9892	0.0012	0.7451
0.005	0.0015	0.8811	0.0009	0.9614	0.0001	0.8263

5.2. Initial dye concentration

Figure 11 shows the effect of initial dye concentration on the photocatalytic dye decomposition at various time intervals. The results show that dye degradation decreases through initial dye concentration increasing. With the increase in the dye concentration, the potential reason is the intervention from intermediates composed upon the decay of the parental dye molecules. The degradation inhibition repression would be more obvious in the presence of a high level of degradation intermediates composed of an increased initial dye concentration **[25]**. Used equations of the zero-order, first order, and second-order kinetics types for photocatalytic dye degradation by the nanoparticles at various initial dye concentrations, linear plots of C_o - C versus irradiation time (t) for zero-order model **Figure 11**, ln (C_o/C) versus irradiation time (t) for first-order order model **Figure 12**, and 1/C against irradiation time (t) for second order type of **Figure 13** are plotted. The values of ko, k_1, and k_2, R^2 (correlation coefficient values) are shown in **Tables 2**. The outcome showed that the kinetics of photocatalytic dye degeneration by BiOl/SrHA at various initial dye concentrations followed the first-order kinetic type.

The following experiments were performed at pH 7 and temperature 30±5 ^oC.

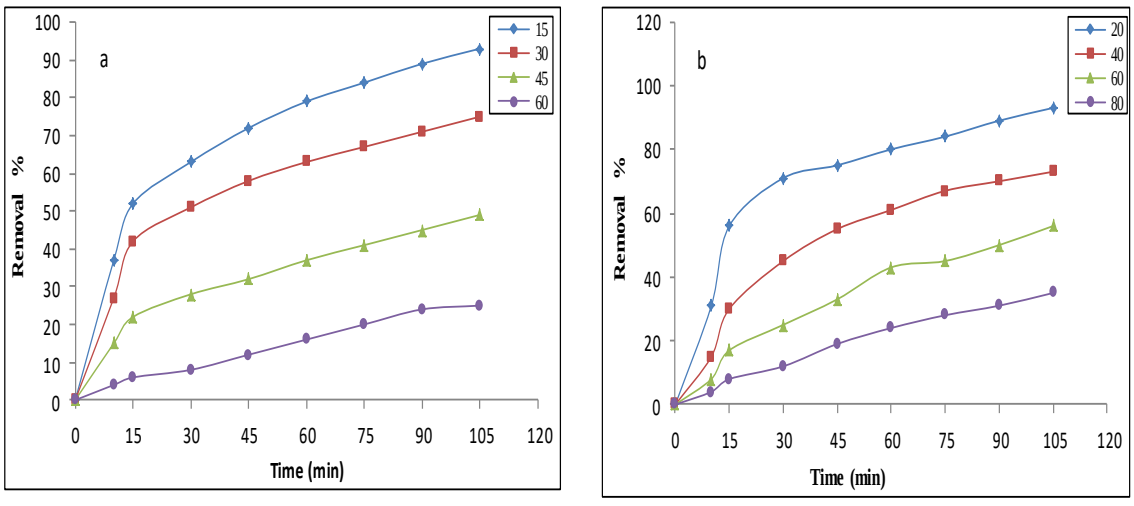

Figure 10: dye concentration effect on the degradation of dyes using UV/BiOI/ SrHA (a) BF, and (b) CV

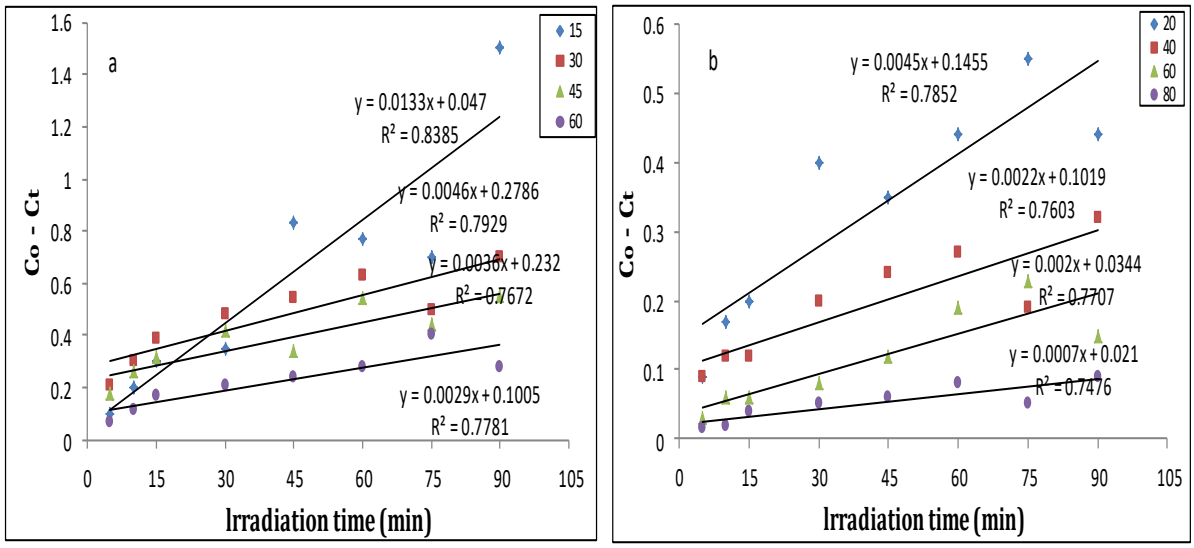

Figure 11: The zero-order kinetic of photocatalytic dye degradation by BiOI/ SrHA different dye concentrations (a) BF, and (b) CV

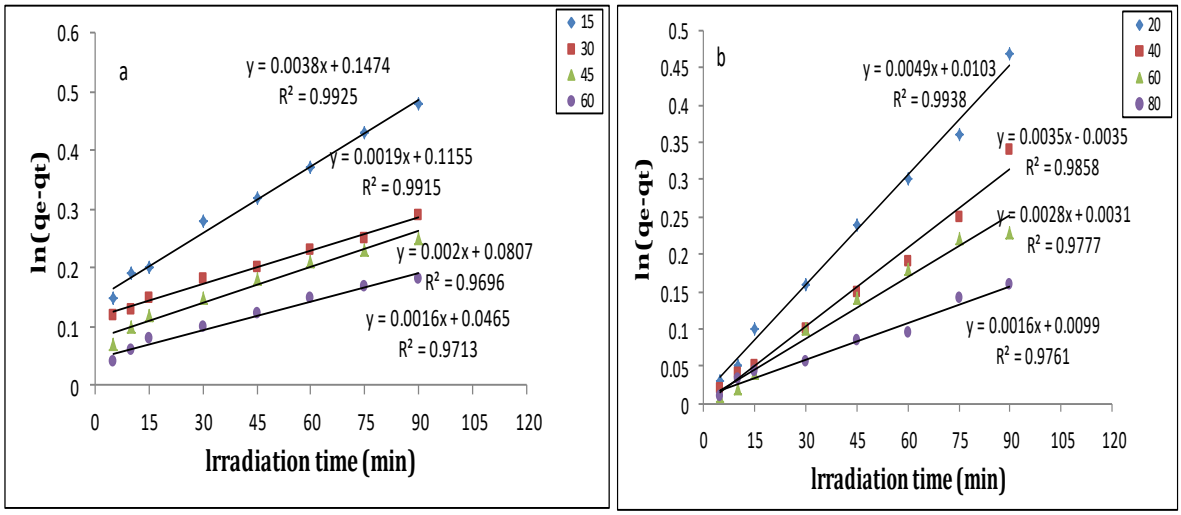

Figure 12: The first-order kinetic of photocatalytic dye degradation by BiOI/ SrHA different dye concentrations (a) BF, and (b) CV

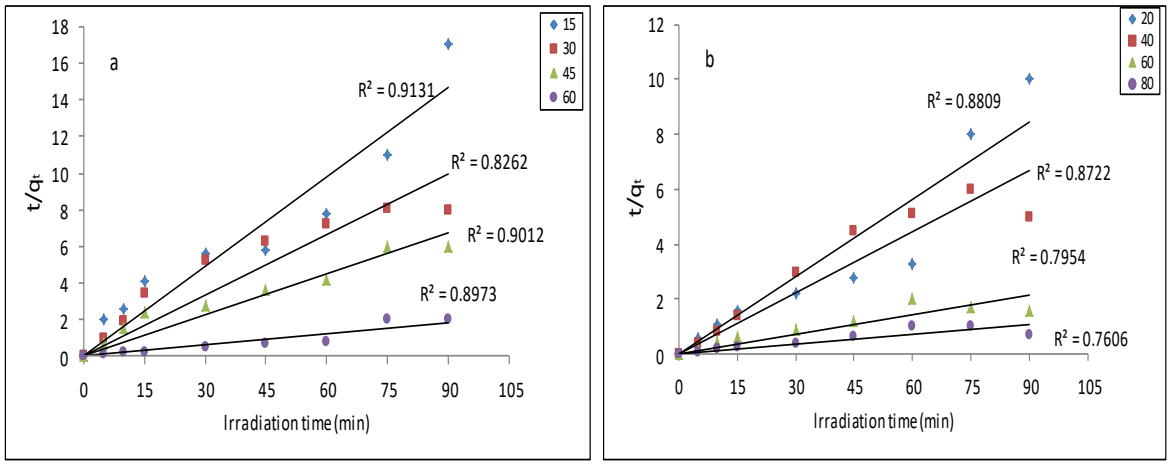

Figure 13: The second-order kinetic of photocatalytic dye degradation by BiOI/ SrHA different dye concentrations (a) BF, and (b) CV

Table 2: The kinetics constants of photocatalytic dye degradation by BiOl/SrHA at various Basic Fuchsin and Crystal Violet dye concentrations

dye (mg/l)	Pseudo-zero order		Pseudo-first order		Pseudo-second order	
BF	K_0	R^2	K_1	R^2	K_2	R^2
15	0.0133	0.8385	0.037	0.9925	0.0002	0.9189
30	0.0046	0.7929	0.0295	0.9865	9.2E-05	0.8456
45	0.0036	0.7672	0.0191	0.9468	0.00016	0.8178
60	0.0029	0.7781	0.0112	0.9852	0.00017	0.7685
CV						
20	0.0045	0.7852	0.0528	0.9809	0.0011	0.9200
40	0.0022	0.7603	0.0361	0.9715	0.0013	0.9028
60	0.002	0.7707	0.0197	0.9776	0.0014	0.8636
80	0.0007	0.7476	0.008	0.9614	0.0023	0.7801

6. Conclusion

The results show that BiOI-supported SrHA is an efficient adsorbent for the removal of Basic Fuchsin (BF) and Crystal Violet (CV) dyes from aqueous solutions, and because of its higher capacity, it can be used in wastewater treatment. The increased photocatalytic activities of BiOI/SrHA could be referred to as the formation of a heterojunction between BiOI and SrHA, which helpfully restrains the recombination of electron-hole pairs. Both the photocatalytic process and the photosensitizer process would work concurrently, $^{\bullet}OH$ and $O_2^{-\bullet}$ are the two main active types in the photocatalytic process. In the photocatalytic process, N-de-methylation and conjugated structure of CV and BF dyes occur during the decomposition process with BiOI/SrHA starting the catalyst. Therefore, it can be concluded that BiOI/SrHA provides a heterogeneous surface for the adsorption of dyes. The outcome displays that the modified adsorbent is a strong UV photocatalyst.

7. REFERENCES

[1] Rakness, Kerwin L., et al. "Wastewater disinfection with ozone-process control and operating results." Ozone: science & engineering 15.6 (1993): 497-513.

[2] Raizada, Pankaj, et al. "Fabrication of Ag3VO4 decorated phosphorus and sulphur co-doped graphitic carbon nitride as a high-dispersed photocatalyst for phenol mineralization and E. coli disinfection." Separation and purification technology 212 (2019): 887-900.

[3] Pare, Brijesh, Pardeep Singh, and S. B. Jonnalagadda. "Visible light-driven photocatalytic degradation and mineralization of neutral red dye in a slurry photoreacter." (2010).

[4] B. Pare, P. Singh, S.B Jonnalagadda, Artificial light assisted photocatalytic degradation oflissamine fast yellow dye in ZnO suspension in a slurry batch reactor, Indian J. Chem., Sect A 48 A (2009) 1364-1369

[5] Zhang, Lisha, et al. "Sonochemical synthesis of nanocrystallite Bi2O3 as a visible-light-driven photocatalyst." Applied Catalysis A: General 308 (2006): 105-110.

[6] Asahi, R. Y. O. J. I., et al. "Visible-light photocatalysis in nitrogen-doped titanium oxides." science 293.5528 (2001): 269-271.

[7] Khan, Shahed UM, Mofareh Al-Shahry, and William B. Ingler. "Efficient photochemical water splitting by a chemically modified n-TiO2." science 297.5590 (2002): 2243-2245.

[8] Al-Rubaie, Ali Z., Inas K. Mohammed, and Zaki N. Kadhim. "Synthesis and Characterization of New Organotellurium (IV) Compounds Containing Carbodithioate Ligands." IOP Conference Series: Materials Science and Engineering. Vol. 928. No. 5. IOP Publishing, 2020.

[9] Singh, Pardeep, et al. "Preparation of BSA-ZnWO4 nanocomposites with enhanced adsorptional photocatalytic activity for methylene blue degradation." International Journal of Photoenergy 2013 (2013).

[10] Li, Shijie, et al. "A novel heterostructure of BiOI nanosheets anchored onto MWCNTs with excellent visible-light photocatalytic activity." Nanomaterials 7.1 (2017): 22.

[11] Xiang, Yuhui, et al. "Chemical etching preparation of the Bi2WO6/BiOI p–n heterojunction with enhanced photocatalytic antifouling activity under visible light irradiation." Chemical Engineering Journal 288 (2016): 264-275.

[12] Chen, Lang, et al. "Room-Temperature Synthesis of Flower-Like BiOX (X⍰ Cl, Br, I) Hierarchical Structures and Their Visible-Light Photocatalytic Activity." Inorganic chemistry 52.19 (2013): 11118-11125.

[13] Radhi, Ibtighaa Kadhim, Mouayed Abdulaali Hussein, and Zaki Naser Kadhim. "Investigation of nigrosine, alizarin, indigo and acid fuchsin removal by modification of CaO derived from eggshell with AgI: Adsorption, kinetic and photocatalytic studies." *European Journal of Chemistry* 10.1 (2019): 64-71.

[14] Jiang, Zaiyong, et al. "Enhancing visible light photocatalytic degradation performance and bactericidal activity of BiOI via ultrathin-layer structure." Applied Catalysis B: Environmental 211 (2017): 252-257.

[15] Luan, Jingfei, et al. "Growth, structural and photophysical properties of i2GaTaO7."

Journal of crystal growth 273.1-2 (2004): 241-247.

[16] Di, Jun, et al. "Bidirectional acceleration of carrier separation spatially via N-CQDs/atomically-thin BiOI nanosheets nanojunctions for manipulating active species in a photocatalytic process." Journal of Materials Chemistry A 4.14 (2016): 5051-5061.

[17] Jiang, Zaiyong, et al. "Enhancing visible light photocatalytic degradation performance and bactericidal activity of BiOI via ultrathin-layer structure." Applied Catalysis B: Environmental 211 (2017): 252-257.

[18] Di, Jun, et al. "Reactable ionic liquid-assisted rapid synthesis of BiOI hollow microspheres at room temperature with enhanced photocatalytic activity." Journal of Materials Chemistry A 2.38 (2014): 15864-15874.

[19] Hasan, Jaafar, et al. "Efficient visible-light-driven photocatalysis of flower-like composites of AgI nanoparticle dotting BiOI nanosheet." Journal of Solid-State Chemistry 297 (2021): 122044.

[20] Ye, Liqun, et al. "Synthesis of highly symmetrical BiOI single-crystal nanosheets and their {001} facet-dependent photoactivity." Journal of Materials Chemistry 21.33 (2011): 12479-12484.

[21] Xiao, Xiufeng, et al. "Structural characterization of zinc-substituted hydroxyapatite prepared by hydrothermal method." Journal of materials science: Materials in medicine 19.2 (2008): 797-803.

[22] Radhi, Ibtighaa Kadhim, Mouayed Abdulaali Hussein, and Zaki Naser Kadhim. "Investigation of nigrosine, alizarin, indigo and acid fuchsin removal by modification of CaO derived from eggshell with AgI: Adsorption, kinetic and photocatalytic studies." European Journal of Chemistry 10.1 (2019): 64-71.

[23] AS Alassadi, Erfan, Zaki N Kadhim, and Mazin N Mousa. "The In Vitro Release Study Of Ceftazidime drug From Synthesized Strontium Flourapatite And Strontium Hydroxyapatite Coated Particles." *karbala journal of pharmaceutical sciences* 8.13 (2017): 137-151.

[24] Simon, V., et al. "Microscopic analysis of sintered titanium-hydroxyapatite implant materials." Journal of Optoelectronics and Advanced Materials 7.6 (2005): 2823.

[25] Kumar, Ankit, and G. Pandey. "A review on the factors affecting the photocatalytic degradation of hazardous materials." Mater. Sci. Eng. Int. J 1.3 (2017): 1-10.

https://doi.org/10.32441/kjps.06.01.p3

Al-Kitab Journal for Pure Sciences
ISSN: 2617-1260 (print), 2617-8141(online)
www.kjps.isnra.org

Comparative Study between Metformin and Insulin in Controlling uncomplicated Gestational Diabetes Mellitus

Enas Yahya Ibraheem*, Israa Hashim Abid Al-Karim

Tikrit University, Iraq

*Corresponding Author: enasaltemem@gmail.com

Citation: Ibraheem EY, Abid Al-Karim IH. Comparative Study between Metformin and Insulin in Controlling uncomplicated Gestational Diabetes Mellitus. *Al-Kitab Pure Sci KJPS*. 2022; 6(1): 30-41. https://doi.org/10.32441/kjps.06.01.p3.

Keywords
Metformin, Insulin, GDM.

Article History

Received	20 Feb.	2022
Accepted	12 July	2022
Available online	30 Aug	2022

Abstract:

Gestational diabetes always accompanies an increased maternal and neonatal risk. Insulin is the standard therapy but causes multiple complications. Metformin has less complications. This study aims to assess the efficacy of metformin in controlling maternal blood glucose level compared to insulin in women with gestational diabetes.

A randomized controlled trial conducted in the obstetric department in Salah Al-Deen general Hospital during the period from 1st February - 31st July 2022. Total sample of 100 pregnant women suffered from gestational diabetes at (24-28week) gestational age were recruited randomly. The patients were divided into two groups: 1-Metformin group (50 patients). 2-Insulin Group (50 patients). Fasting and post prandial blood glucose levels 2 h after breakfast were done at each visit and HbAlc each trimester. Follow up was continued till delivery to evaluate the pregnancy outcome .

The mean HbAlc was significantly higher among Insulin group (5.8± 0.5) than in Metformin group (5.4 ± 0.8). Preeclampsia was lower among Metformin group (14%) than Insulin group (19.6%). hypoglycemia episode was significantly lower among Metformin group (14%) than Insulin group (41.3%), Caesarean delivery was higher among Insulin group (58.7%) than Metformin group (37.2%). The mean birth weight was significantly higher among Insulin group (3761.4±470) than Metformin group (3540.9±338). Prematurity was found among (8.7%) of the Insulin group in comparison to (4.7%) of the Metformin group. Prematurity was non significantly higher among Insulin group (8.7%) than Metformin group (4.7%).

Metformin is effective and safe in the glycemic control of gestational diabetes, with better maternal and neonatal outcomes.

Keywords: Metformin, Insulin, GDM.

دراسة مقارنة بين الميتفورمين والأنسولين في السيطرة على الحمل السكري غير المعقدة

إيناس يحيى إبراهيم*، إسراء هاشم عبد الكريم

جامعة تكريت، العراق

* enasaltemem@gmail.com

الخلاصة:

يصاحب سكري الحمل دائمًا زيادة أخطار الأمهات والمواليد. الأنسولين هو العلاج القياسي ، ولكنه يسبب مضاعفات متعددة. الميتفورمين له مضاعفات أقل. تهدف هذه الدراسة إلى تقييم فعالية الميتفورمين في السيطرة على مستوى السكر في الدم لدى الأمهات مقارنة بالأنسولين لدى النساء المصابات بسكري الحمل.

أجريت دراسة سريريه منضبطة أجريت في قسم النسائية والتوليد بمستشفى صلاح الدين العام خلال الفترة من ١ فبراير - ٣١ يوليو ٢٠٢٢. تم تجنيد ما مجموعه ١٠٠ حامل مصابة بسكري الحمل بعمر الحمل (٢٤-٢٨ أسبوعًا). تم تقسيم المرضى عشوائياً إلى مجموعتين: ١ - مجموعة الميتفورمين (٥٠ مريضاً. ٢ - مجموعة الأنسولين (٥٠ مريضاً). تم إجراء فحص نسبه السكر في الدم بعد الصيام وبعد تناول الطعام بساعتين بعد الإفطار في كل زيارة وقياس HBA1C كل ثلاثة أشهر. استمرت المتابعة حتى الولادة لتقييم نتيجة الحمل.

كان متوسط HBA1C أعلى بشكل ملحوظ بين مجموعة الأنسولين (٥,٨ ± ٠,٥) منه في مجموعة METFORMIN (٥,٤ ± ٠,٨). كانت مقدمات الارتعاج أقل بين مجموعة الميتفورمين (١٤٪) من مجموعة الأنسولين (١٩,٦٪). كانت نوبة نقص السكر في الدم أقل بشكل ملحوظ بين مجموعة الميتفورمين (١٤٪) من مجموعة الأنسولين (٤١,٣٪) ، وكانت الولادة القيصرية أعلى بين مجموعة الأنسولين (٥٨,٧٪) من مجموعة الميتفورمين (٣٧,٢٪). كان متوسط وزن الولادة أعلى بشكل ملحوظ بين

مجموعة الأنسولين (٣٧٦١,٤ ± ٤٧٠) من مجموعة الميتفورمين (٣٥٤٠,٩ ± ٣٣٨). وُجدت الخداج عند (٨,٧٪) من مجموعة الأنسولين مقابل (٤,٧٪) في مجموعة الميتفورمين. كانت الخداج غير أعلى معنويا بين مجموعة الأنسولين (٨,٧٪) من مجموعة الميتفورمين (٤,٧٪).

الميتفورمين فعال وآمن في السيطرة على نسبة السكر في الدم لمرض سكري الحمل ، مع نتائج أفضل للأمهات والأطفال حديثي الولادة.

الكلمات المفتاحية: الميتفورمين والأنسولين في سكري الحمل ، مقارنة الميتفورمين والأنسولين في سكري الحمل.

1. INTRODUCTION:

Gestational Diabetes Mellitus (GDM) is said to occur late in pregnancy as a transient condition with less severe hyperglycemia [1], differing from diabetes in pregnancy (DIP) where diabetes overt in pregnancy and likely to continue after birth. However, recent literature suggests there may also be an entity related to early-onset GDM which may be distinct from DIP and a separate subset of hyperglycemia in Pregnancy (HIP) [2], as GDM typically appears in the second or third trimester. GDM exhibits a large proportion of HIP, with estimates that it represents 75–90% of all HIP cases [3].Insulin is the standard therapy for GDM management in cases refractory to nutrition therapy and exercise. Insulin therapy can be difficult for pregnant women due to multiple injection requirements, risk of hypoglycemia, and weight gain. In addition, hypoglycemia occurs in 70% of women who use insulin in their pregnancy. [4] Metformin is a type of oral hypoglycemic medications called Biguanides. Metformin decreases hepatic gluconeogenesis, improves peripheral and hepatic sensitivity to insulin and does not induce hypoglycemia or maternal weight gain. However, as Metformin crosses the placenta and the long-term effects in the offspring are unknown. There are more than 10 studies assessing Metformin safety and efficacy. Globally, the results have been favorable to Metformin. Compared to women taking insulin, those under Metformin have no difference in maternal glycemic control, congenital abnormalities, macrosomia, rates of neonatal hypoglycemia or other maternal or neonatal adverse outcomes. [5] This study aims to assess the efficacy of metformin in controlling maternal blood glucose level compared to insulin in women with GDM.

3. Patients and Methods

This study is a Randomized controlled trial was conducted in obstetric department in Salah Al-Deen general Hospital during the period from 1st February to the 31st of July 2022. Total

of 100 pregnant patients that diagnosed with GDM with gestational age (24-28week) were randomly selected from the outpatient clinic and divided for two groups randomly into: group metformin (50 patients), and insulin group (50 patients). Inclusion criteria were patients diagnosed to have GDM were treatment initiated before 34 weeks of gestation. Exclusion Criteria were essential hypertension, preeclampsia, Intra uterine growth retardation, Abnormal glucose tolerance before pregnancy, unbalanced chronic disease, twin pregnancy, and treatment initiated before 12 weeks or after 34 weeks of gestation. Data Collection done through a questionnaire: by direct interview with the pregnant women, taking information about demographic variable, & obstetrical history. Careful general clinical examination including body weight, height, blood pressure and lower limb edema. Maternal body mass index. & Abdominal examination for assessment of estimated fetal weight, fetal movement. Ultrasonography to confirm gestational age, to exclude Intra uterine growth retardation, congenital fetal malformation, and twin pregnancy. Preterm was diagnosed as gestational age at delivery < 37 completed weeks. Laboratory examination: blood samples were collected from the mothers for the diagnosis of GDM which made with at least two out of three elevated glucose levels & FBG. These testes were done for pregnant women with high risk for GDM on booking visit and pregnant women with low risk for GDM were screened at 24-28 weeks. Before intervention patients were advised to take standard nutritional instruction for three meals and four snakes daily.

Metformin Group: Metformin was started at dose of 500 mg and increased up to 1500 mg in 3 divided doses as tolerated until glycemic control was achieved **[6]**. Insulin group: Insulin was prescribed as a combination of short acting and intermediate acting human insulin, twice daily before meals in the morning and in the evening. A 24 h total insulin dose was calculated using 1 units/kg body weight. Two thirds of total dose was given in morning before breakfast and one third at night before dinner **[6]**.

Follow up: Follow up visits will arrange every 2 weeks till 36 weeks then weekly till delivery. All patients were taught self-blood sugar monitoring using home glucose monitors and will advised to maintain written record of blood sugar levels. Fasting and post prandial blood glucose levels 2 h after breakfast were done at each visit and Glycated hemoglobin (HbAlc) each trimester. Primary outcome measure is control of diabetes mellitus; monitored by fasting blood sugar level, two hours postprandial, and HbA1C. Secondary outcome measure is obstetric complications; macrosomia, shoulder dystocia, and rate of cesarean section.

3. Results

Enrollment of 100 pregnant women with gestational diabetes, 11 were lost to follow and 3 of the Metformin group were shifted to insulin management due to irresponsive to metformin and excluded from the study. The droop out rate was 11% lower than the accepted rate <20%, as shown in **Figure 1**.

Most of the patients in both groups insulin group and metformin group were aged (31-40 years), (47.83%), and (48.84%) respectively, this relation was statistically not significant. Most of the patients in both groups' insulin group and metformin group from urban areas, (63.04%), and (62.29%) respectively, this relation was statistically not significant. Most of the patients in insulin group and metformin group were with parity ≥3 (50%), (48.84%), respectively, this relation was statistically not significant .

Positive history of previous GDM found among (23.91%), and (20.93%) among insulin group, and metformin group respectively. Positive family history of diabetes mellitus found among (47.83%), and (53.49%) among insulin group, and metformin group respectively, this relation was statistically not significant. The mean gestational age at diagnosis was (28.3±5.2 week) among insulin group, and (29.5± 4.9 week) among metformin group as shown in **Table 1**.

Most of the patient were obese (BMI ≥30Kg/m 2) among insulin group (47.8%) and metformin group (46.5%), followed by overweight 13(28.3%), and 14(32.6%) respectively as shown in **Table 2**.

The mean systolic blood pressure among insulin group was (115.5±14.3), in comparison with metformin group (117.3±12.4), as shown in **Table 3**. The mean diastolic blood pressure among insulin group was (77.3±9.8), in comparison with metformin group (75.3±10.3), as shown in **Table 3**.

After the end of the treatment the results show that: The mean FBS was higher among insulin group (89.5± 7.2) than in metformin group (87.3± 5.01), this relation was statistically significant as shown in **Table 4**. The mean post prandial blood glucose2 h after breakfast was higher among insulin group (125.5± 5.7) than in metformin group (122.8± 4.1), this relation was statistically significant as shown in **Table 4**. The mean HbAlc was higher among insulin group (5.8± 0.5) than in metformin group (5.4 ± 0.8), this relation was statistically significant as shown in **Table 4**.

Preeclampsia non significantly was lower among metformin group 6(14%) than insulin group (19.6%). hypoglycemia episode was lower among metformin group (14%) than insulin group (41.3%), this relation was statistically significant (P value < 0.05), as shown in **Table 5**. Caesarean delivery was higher among insulin group (58.7%) than metformin group (37.2%), this relation was statistically significant as shown in **Table 5**.

The mean birth weight was higher among group I (3761.4±470) than group M (3540.9±338) this relation was statistically significant as shown in **Table 6**. Prematurity was found among 4(8.7%) of the insulin group in comparison to 2(4.7%) of the metformin group, this relation was statistically non-significant as shown in **Table 6**.

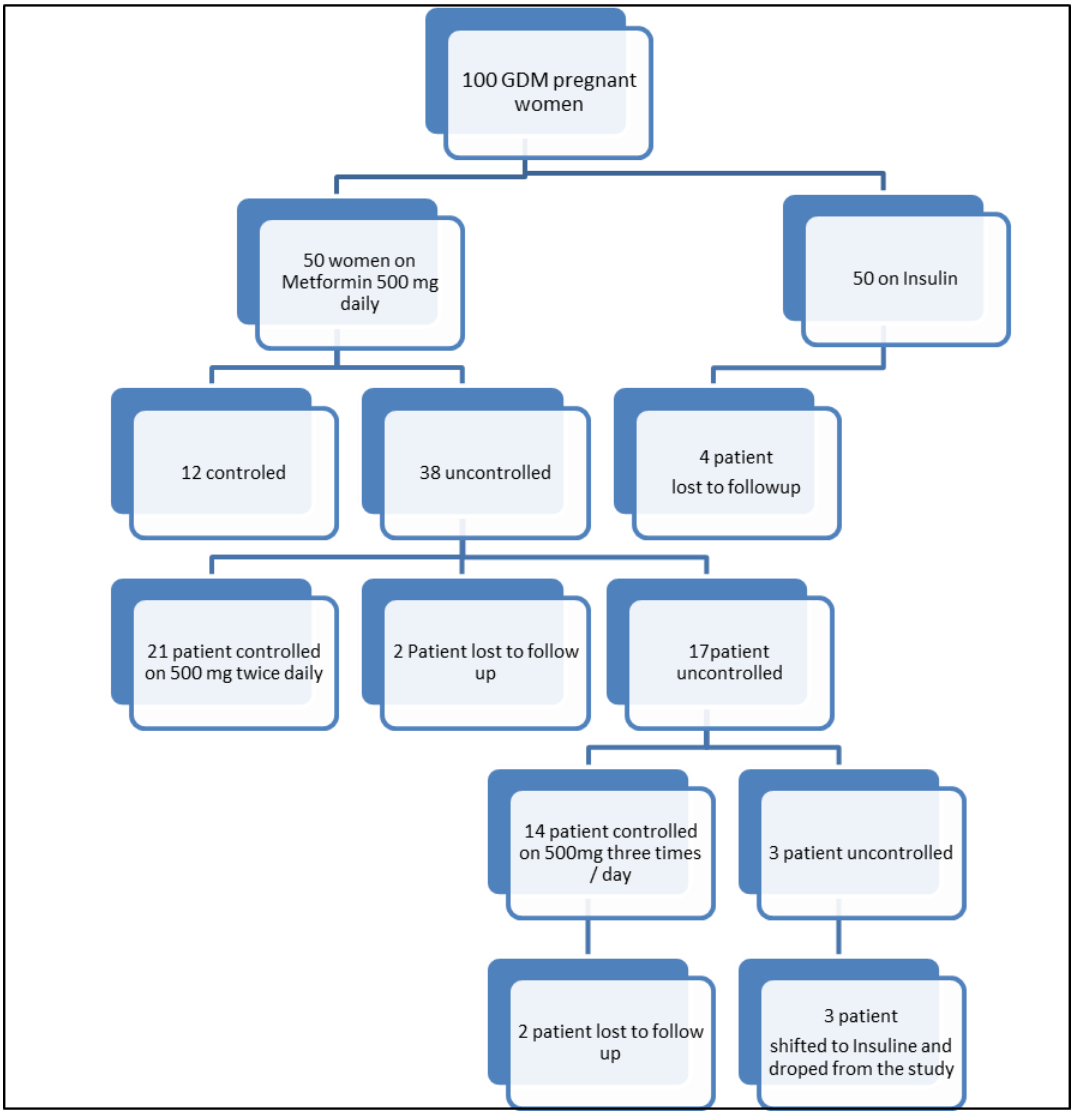

Figure 1. The study participant's flowchart.

Table 1. The general baseline characteristics of the sample.

	Insulin Group (n=46)		**Metformin Group (n=43)**		
Age	Frequency	%	Frequency	%	P value
<20 years	6	13.04	5	11.63	> 0.05 NS
21-30 years	18	39.13	17	39.53	
31- 40 years	22	47.83	21	48.84	
Total	46	100.00	43	100.00	
Urban	29	63.04	27	62.79	
Rural	17	36.96	16	37.21	> 0.05 NS
Parity					
Nulliparous	10	21.74	8	18.60	
1_2	13	28.26	14	32.56	> 0.05 NS
≥3	23	50.00	21	48.84	
Total	46	100.00	43	100.00	
previous GDM					
positive	11	23.91	9	20.93	> 0.05 NS
Negative	35	76.09	34	79.07	
Total	46		43		
DM Family history		0.00		0.00	
Positive	22	47.83	23	53.49	> 0.05 NS
Negative	24	52.17	20	46.51	
Total	46	100.00	43	100.00	
Gestational age at diagnosis of GDM (week)		28.3±5.2	29.5± 4.9		> 0.05 NS

Table 2. the sample distribution according to pre pregnancy BMI

BMI	**Insulin Group**		**Metformin Group**	
	Frequency	%	Frequency	%
Normal (18.5-24.9) Kg/m 2	11	23.9	9	20.9
Overweight (25-29.9) Kg/m 2	13	28.3	14	32.6
Obese (≥30) Kg/m 2	22	47.8	20	46.5
Total	46	100.0	43	100.0

Table 3. The sample distribution according to blood pressure

BP	**Insulin Group**		**Metformin Group M**		**P value**
	Mean	SD	Mean	SD	
Systolic	115.5	14.3	117.3	12.4	>0.05
Diastolic	77.3	9.8	75.3	10.3	>0.05

Table 4. The sample distribution according to blood glucose indices

Blood Glucose Indices	Insulin group		Metformin group		
	Mean	SD	Mean	SD	
FBS (mg/dl)	89.5	7.2	87.3	5.01	<0.05(2.8)
Post prandial blood glucose 2 h after breakfast (mg/dl)	125.5	5.7	122.8	4.1	<0.05(2.8)
HbAlc	5.8	0.5	5.4	0.8	<0.05(2.8)

Table 5. The sample distribution according to maternal outcomes

Maternal outcomes	**Insulin group**		**Metformin group**		**P value**
	Frequency	**%**	**Frequency**	**%**	
Preeclampsia	9	19.6	6	14.0	>0.05 NS
hypoglycemia episode	19	41.3	6	14.0	<0.05 S
mode of delivery					
vaginal delivery	19	41.3	27	62.8	
Caesarean	27	58.7	16	37.2	<0.05 S
Total	46	100	43	100	

Table 6. The sample distribution according to Neonatal outcomes

Neonatal outcomes	**Insulin group**		**Metformin Group**		**P value**
	Frequency	%	Frequency	%	
Birth weight (gr) mean± SD*	3761.4±470		3540.9±338		<0.05 S*
Prematurity	4	8.7	2	4.7	>0.05 NS***

*SD: standard deviation, **S: significant, ***NS: non-significant

4. Discussion

In both groups of the current study, Insulin group and Metformin group most of the patients were aged (31-40 years), (47.83%), and (48.84%) respectively, this goes with Baiee HA et al 2014 [7] who found that the women with gestational diabetes are older (49.3%) aged > 30 years , and with Mdoe MB et al 2021[7] found that maternal age above 35 years associated with GDM. Most of our patients from urban area in both groups; Insulin group (63.04%) and Metformin group (62.29%), this goes with Baiee HA et al 2014 [7] who found that most cases are living in urban regions. Mdoe MB et al 2021[8] found that most of GDM women were from urban areas (63%).

In current study the mean FBS was significantly higher among Insulin group (89.5± 7.2) than in Metformin group (87.3± 5.01). This goes with Aboud AL Hayani, and Nasir A 2020, [9] Found that patients on metformin treatment had significantly lower glucose levels

(78.7±3.2) than insulin treated group (86.92±3.31). Ghomian N et al 2019 **[10]** found that fasting plasma glucose (FPG) was controlled well by both groups' metformin treatment (91.22 ± 4.37) and insulin treatment (92.21 ± 4.41) without any significant difference. Simeonova-Krstevska S 2018 **[11]** found that the mean FPG was statistically significantly lower in metformin group (5.3±0.7 mmol/l) than in insulin group (5.8± 1.4 mmol/l). The mean post prandial blood glucose 2 h after breakfast was significantly higher among insulin group (125.5± 5.7) than in metformin group (122.8± 4.1), this goes with Ghomian N et al 2019 **[10]** found that postprandial glycemia control an metformin treated group (119.38 ± 4.03) was lower than among insulin treated group (118.99 ± 6.24), and with Simeonova-Krstevska S 2018 **[11]** found that the mean postprandial glycaemia was statistically significantly lower in metformin group (7.0 ± 1.2 mmol/l) than in insulin group (7.9 ± 1.9 mmol/l).

In current study the mean HbAlc was significantly higher among insulin group (5.8± 0.5) than in metformin group (5.4 ± 0.8). this supported by the findings of Sarwat A et al 2022 **[12]** found that maternal HbA1c levels before birth were 6.1±1.1 in metformin group and 6.0±1.2 in insulin group, and with Simeonova-Krstevska S 2018 **[11]** found that the mean glycosylated hemoglobin (HbA1c) at 37 gestation week was significantly lower in metformin groups (5.3±0.7) than in insulin group (6.2±1.8). Preeclampsia non significantly was lower among metformin group (14%) than insulin group (19.6%). This supported by what found by Kalafat ER et al 2018 **[13]** found that metformin use was associated with a reduced risk of pregnancy-induced hypertension when compared with insulin and a non-significantly reduced risk of pre-eclampsia. Hypoglycemia episode was significantly lower among metformin group (14%) than insulin group (41.3%). This goes with Picón-César, M.J et al 2021 **[14]** found that insulin treated group had more hypoglycemic episodes (55%) than the metformin treated group (17.7%). Ruholamin S et al 2014 **[15]** described only 2 women having hypoglycemia on insulin and none on metformin, and Ashoush et al 2016 **[16]** published a non-significant difference for maternal hypoglycemic episodes. Caesarean delivery was significantly higher among insulin group (58.7%) than metformin group (37.2%). This goes with Picón-César, M.J et al 2021 **[14]** found that cesarean deliveries (27.6% [metformin] vs 52.6% [insulin.]). Aboud AL Hayani, and Nasir A 2020 **[9]** found a significant difference between insulin and metformin groups as regards mode of delivery as insulin group (59.4%) has higher percentage than metformin groups (40-57.1%) according to metformin dose in cesarean delivery.

A meta-analysis done by Guo L et al 2019 **[17]** published a lower incidence of labor induction and a tendency to fewer elective cesarean deliveries for metformin treatment. The

mean birth weight was significantly higher among group insulin (3761.4±470) than metformin group M (3540.9±338). This goes with Aboud AL Hayani, and Nasir A 2020 **[9]** found that there were statistically significant differences between insulin group (4.1±0.12 kg) and metformin sub-groups patients as regards birth weight. Wang X et al 2021**[18]** and Jiang YF et al 2015 **[19]** found that metformin was with lower neonatal birth weight, in which the results were the same as a previous study. Ghomian N et al 2019 **[15]** found no different between metformin group (3,450 ± 548), insulin group (3,544 ± 57) regarding birth weight. Zhou et al 2021 **[20]** suggested that the level of triglyceride in maternal blood was positively correlated with neonatal birth weight. Metformin is also confirmed to reduce the level of triglyceride in non-obese type 2 DM patients, as a result, the potential mechanism for metformin to reduce neonatal birth weight is improved maternal lipid metabolism **[20].**

5. Conclusions

Metformin is effective and safe in the glycemic control of GDM, Metformin treated women had better maternal and neonatal outcomes, less hypoglycemic attacks and less preeclampsia, macrosomia and preterm labour. Larger multicenter studies are recommended to establish the long-term outcomes.

6. References

[1] American Diabetes Association (ADA). Classification and Diagnosis of Diabetes: Standards of Medical Care in Diabetes-2020. Diabetes Care (2020); 43(Supplement 1): S14–S31.

[2] Immanuel J, Simmons D. Screening and treatment for early-onset gestational diabetes mellitus: a systematic review and meta-analysis. Curr Diab Rep. 2017;17(11). https://doi.org/10.1007/s11892-017-0943-7.

[3] International Diabetes Federation. IDF Diabetes Atlas. Brussels, Belgium: International Diabetes Federation 2017.

[4] Catherine A, Elie S and Julie M (2014): Gestational Diabetes Mellitus Identification Based on SelfMonitoring of Blood Glucose. Canadian Diabetes Association, 5:1-9. 3.

[5] Kristi WK, Dana GC and Allison M: A review of current, treatment strategies for gestational diabetes mellitus. Drugs Context(2015), 4:212-222. 5.

[6] Jahanara A, Nasam K and Sanower AH. Metformin versus insulin treatment in gestational diabetes in pregnancy in a developing country. A randomized control trial. Diabetes Res Clin Pract (2014); 107(2):290-9.

[7] Baiee HA, Fliah M, Abd Alkareem D, Hamid S, Salim A. Factors Associated with Gestational Diabetes Mellitus in Babylon, Iraq During The Year 2014. Medical Journal of Babylon. 2016;13(1):24-31.

[8] Mdoe MB, Kibusi SM, Munyogwa MJ, Ernest AI. Prevalence and predictors of gestational diabetes mellitus among pregnant women attending antenatal clinic in Dodoma region, Tanzania: an analytical cross-sectional study. BMJ Nutrition, Prevention & Health. 2021;4(1):69.

[9] Aboud AL Hayani, NASIR A. Metformin versus Insulin in Treatment of Gestational Diabetes. The Medical Journal of Cairo University. 2020 Sep 1;88(September):1967-74.

[10] Ghomian N, Vahed SH, Firouz S, Yaghoubi MA, Mohebbi M, Sahebkar A. The efficacy of metformin compared with insulin in regulating blood glucose levels during gestational diabetes mellitus: a randomized clinical trial. Journal of cellular physiology. 2019 Apr;234(4):4695-701.

[11] Simeonova-Krstevska S, Bogoev M, Bogoeva K, Zisovska E, Samardziski I, Velkoska-Nakova V, Livrinova V, Todorovska I, Sima A, Blazevska-Siljanoska V. Maternal and neonatal outcomes in pregnant women with gestational diabetes mellitus treated with diet, metformin or insulin. Open access Macedonian journal of medical sciences. 2018 May 20;6(5):803

[12] Sarwat A, Perveen N, Saleem A, Rehman F, Zafar I, Iftikhar G. Comparison of Efficacy of Metformin and Insulin in management of Gestational Diabetes. An experience in Social Security Teaching Hospital, Ferozepur Road Lahore. Pakistan Journal of Medical & Health Sciences. 2022 Jun 1;16(05):242-6.

[13] Kalafat ER, Sukur YE, Abdi A, Thilaganathan B, Khalil A. Metformin for prevention of hypertensive disorders of pregnancy in women with gestational diabetes or obesity: systematic review and meta-analysis of randomized trials. Ultrasound in Obstetrics & Gynecology. 2018 Dec;52(6):706-14.

[14] Picón-César, M.J., Molina-Vega, M., Suárez-Arana, M., González-Mesa, E., Sola-Moyano, A.P., Roldan-López, R., Romero-Narbona, F., Olveira, G., Tinahones, F.J. and González-Romero, S.,. Metformin for gestational diabetes study: metformin vs insulin in gestational diabetes: glycemic control and obstetrical and perinatal outcomes: randomized prospective trial. American Journal of Obstetrics and Gynecology2021,; 225(5):517-e1.

[15] Ruholamin S, Eshaghian S, Allame Z. Neonatal outcomes in women with gestational diabetes mellitus treated with metformin in compare with insulin: a randomized clinical trial. J Res Med Sci 2014;19:970–5

[16] Ashoush S, El-Said M, Fathi H, Abdelnaby M. Identification of metformin poor responders, requiring supplemental insulin, during randomization of metformin versus insulin for the control of gestational diabetes mellitus. J Obstet Gynaecol Res 2016;42:640–7

[17] Guo L, Ma J, Tang J, Hu D, Zhang W, Zhao X. Comparative Efficacy and Safety of Metformin, Glyburide, and Insulin in Treating Gestational Diabetes Mellitus: A Meta-Analysis. J Diabetes Res 2019;2019: 9804708

[18] Wang X, Liu W, Chen H, Chen Q. Comparison of insulin, metformin, and glyburide on perinatal complications of gestational diabetes mellitus: a systematic review and meta-analysis. Gynecologic and Obstetric Investigation. 2021;86(3):218-30

[19] Jiang YF, Chen XY, Ding T, Wang XF, Zhu ZN, Su SW. Comparative efficacy and safety of OADs in management of GDM: network meta-analysis of randomized controlled trials. J Clin Endocrinol Metab. 2015;100(5):

2071

[20] Zhou J, Bai J, Guo Y, Fu L, Xing J. Higher levels of triglyceride, fatty acid translocase, and toll-like receptor 4 and lower level of HDL-C in pregnant women with GDM and their close correlation with neonatal weight. Gynecologic and Obstetric Investigation. 2021;86(1):48-54.

https://doi.org/10.32441/kjps.06.01.p4

Al-Kitab Journal for Pure Sciences
ISSN: 2617-1260 (print), 2617-8141(online)
www.kjps.isnra.org

Emotional Response using Power Spectrum Approach

Wafaa Khazaal Shams*, Qusay Kanaan Kadhim, Noor Ahmed Hameed, Wijdan Mahommd Khuthqair

Bilad Alrafidan University, Iraq.

*Corresponding Author: dr.wafaa@bauc14.edu.iq

Citation: Shams WK, Kadhim QK, Hameed NA, Khuthqair WM. Emotional Response using Power Spectrum Approach *Al-Kitab Pure Sci KJPS*. 2022; 6(1): 42-53. https://doi.org/10.32441/kjps.06.01.p4

Keyword
EEG, Alpha wave, Emotional states, classification,

Article History
Received May 3, 2022
Accepted August 12, 2022
Available online September 20,2022

Abstract:

The objective of this study is to detect affective response of children to facial expression based on alpha power density of brain activity. Electroencephalography data were collected from 10 typical children. The alpha power temporal information of active brain regions was extracted. Performance of the power spectrum feature was evaluated in emotion recognition process using K nearest neighbor, a regularized least square and multilayer perceptron classifier. A statistical analysis indicated right alpha activity during negative and calm emotional states. Statistical results showed significant difference between rest conditions and emotional state. The best accuracy we got to detect emotional states is by using regularized least square that is 70%.

Keywords: EEG, Alpha wave, Emotional states, classification.

الكشف عن استجابة العاطفية بتحليل الطيفي لإشارة الكهربائية للدماغ

وفاء خزعل شمس*، قصي كنعان كاظم، نورا حمد حامد، وجدان محمود خضير

كلية بلاد الرافدين الجامعة، العراق.

*dr.wafaa@bauc14.edu.iq

الخلاصة:

يقدم البحث دراسة تحليلية عن استجابة العاطفية للأطفال عند النظر الى صور وجوه أطفال تمثل حالات من الحزن والسعادة والخوف والحالة الطبيعة.. تم التحليل بسحب إشارة الدماغ من عشرة أطفال أعمارهم بيت الخامسة والرابعة . وتم استخدام مصنفات (MLP ,RLS , KNN) التحليل الإحصائي بين نشاط موجة ألفا من الجهة اليمنى للدماغ خلال حالة الحزن والطبيعية . وكذلك بين الاختلاف العالي في نشاط الفا بين حالة الهدوء خلال إغلاق العين أو فتح العين وحالة النظر للصور التي تمثل حالات عاطفية مختلفة . نسبة الدقة لتصنيف الحالة العاطفية باستخدام تقنيات الذكاء الصناعي وصلت الى 70 بالمئة.

الكلمات المفتاحية: الإشارة الكهربائية للدماغ، موجة ألفا، الحالة العاطفية، التصنيف.

1. INTRODUCTION:

Since the early studies of emotion, researches focused on the facial expression of emotion and reported that different facial expressions are related to different emotional state **[1-3]**. Aboard of studies by cognitive scientists and psychologists have been showing that facial expression is one of the important factors to develop the cognitive process and emotional state of the child. In early age, infants develop their ability to recognize emotion influenced by their parents or caregiver's facial expression **[4-6]**. However, some children have problem in processing facial information such as autism spectrum disorder and other children with learn disability **[7-9]**. Therefore, it is important to examine children response to emotional stimuli.

Emotion is psycho-physiological phenomena that can measure based on expressive movement **[10]** or skin conductance, heart rate and blood pressure**[11,12]**that present the physiological responses of autonomic nervous system. Further emotion is measured by neurophysiologic measurement such as functional magnetic resonance imaging (fMRI) and electroencephalogram (EEG) which are noninvasive techniques that detect the emotion from the central nervous system (CNS) with respect to spatiotemporal resolution **[13,14]**. Regarding emotional measurement tools, EEG has used extensively for emotional studies. Nevertheless, the low spatial resolution of EEG, EEG provides direct measurement of brain activity with high temporal resolution that enables of recording the instantaneous responses to emotional stimuli.

EEG is less cost-effective, safe for infants and less physical restriction. These markers make it the most appropriate tool to study neurons activity correlated to brain functions [15,16].Aboard of studies have done in this area which focusing on EEG asymmetry in the alpha band at the frontal and pre-frontal regions [14, 17-19] following the study of Davidson [20,21]. The left frontal alpha activity is associated with positive response whereas the right frontal alpha activity is related to negative emotion for adults and infants. However, studies on children were inconsistent. Feng et al [22] didn't report a difference in the activation between happy and sad stimuli. Pickens et al [23] reported left frontal activation for both happy and sad stimuli. This may be due to issue in the methodology or may interpret as a lack in stimuli intensity.

Other studies were concern on emotion recognition model to predicate human emotional states. A various feature extraction methods have been implied for emotion recognition including power spectrum [24] , higher order crossing [25], connectivity [26,27], wavelet coefficient [28], fractal dimension [29], statistical features of ERP [30], and EEG asymmetry at the frontal and pre-frontal regions [20]. Studies done on brain connectivity showed great potential for improving emotion recognition system [26, 27]. This can be related to that emotion process integrates among different brain regions. Neuroscience studies reported activation of different brain region during emotional stimuli and there are; amygdale, prefrontal cortex, anterior cingulated cortex, insula , hippocampus and hypothalamus [31]. Further brain imaging studies have shown that there is no specific location of EEG patterns [32,33]. This finding is quite consistent with the distribution theory whereby emotion is produced through interactions among brain regions rather than a specific brain location [34].

In this study we characterize the underlying process of emotion by computed alpha power density (PSD) for left and right brain regions during negative and positive emotional sessions. Further it will be used in a pattern recognition paradigm to recognize brain activity patterns under the emotional states. For this reason three classifiers are used; K-nearest neighbor (Knn) [35] a multilayer perceptron (MLP) with back propagation [36, 37]and regularized least squares (RLS) [38].

2.Method:

A. Emotion Stimuli

In this study we used the data from Othman et al [39].The experiment was designed to induce positive and negative emotion in two dimensional affective space model [40]. Combinations of pictures with different valence and arousal levels were selected from Radboud

database that presented four emotional stimuli, each composed of eight pictures of children faces [41]. The negative emotion is labeled as low valence = -1, and positive emotion are labeled as high valence = 1. Calm emotion is labeled when Arousal =-1, presenting in this study as low arousal (LA) and excited emotion is labeled when Arousal =1, presenting in this study as high arousal (HA).

B. Data collection

Ten healthy children between 4 to 6 years old participated in this study. The subjects were from several pre-schools in Malaysia. The data was collected by Brain Development Group at the International Islamic university of Malaysia. Prior to data collection, experimental procedure was explained to the subjects and a consent form was signed by the participants' parents. The experiment was started with baseline condition of 1.5-minute closed eyes and 1.5-minute open eyes and then followed by 4 minutes for emotional stimuli. Subjects were seated in a comfortable chair and asked to minimize their body movements. The emotional stimuli were displayed on 15 inches screen, 75 cm away from the subjects. The emotional stimuli consisted of four emotions with different level of valence and arousal. The EEG data was recorded with eight channels BIMEC equipment (Brainmarker BV product, Netherlands). Electrodes were placed according to the international 10-20 system (C3, C4, F3, F4, P5, P6, T7, and T8 with Cz as referenced channel). Data was sampled at 250 Hz and band-pass filtered (0.5-50 Hz). Impedance of each electrode was kept below than 5 ohms. According to age group of children, EEG data was band pass filtered in range (7 to 11.5 Hz) to retain only the interesting band. Data were segmented to 2 second epoch. Each epoch was examined manually for blink eyes movement and muscles artifacts with excluded the epoch of amplitude ±70 microvolt from all channels. The free-artifact epoch was used for further analysis.

C. Feature extraction

A mean alpha power were computed for each artifact free epoch using Fast Fourier Transform (FFT) with 1 second hanning window and with 1 Hz frequency bin [42]. The mean alpha power was computed from each channel producing feature vector set to examine alpha activity associated with subject's affective states.

D. Classification Process

We used classification process to evaluate the performance of the proposed feature for identifying emotional pattern from EEG. The feature set was divided into training set to learn the classifier and testing set (unseen data), which was not labeled. The high performance was

achieved when the classifier maps out the unseen data accurately. Further, the performance of the classification process is based on the classifier and the feature set itself. Three classifiers were used in this study. A K-nearest neighbor classifier is a feed forward learning method that based on computing the standard Euclidean distance of a new instance to the nearest given classes [35]. The second classifier was Regularized least squares classifier which reflects as the Tikhonov regularization problem [38]. The regularized parameter (lambda value) was determined by one-leave out cross validation of the training data set and a Gaussian kernel was considered. The RLS was applied using MIT toolbox [43]. The last classifier was MLP with back propagation. The MLP network consisted of one input layer with number of nodes representing the features set and one output layer to present the predicated value and two hidden layers. Functions of hidden layers were set to a tangent-sigmoid and a linear function was considered for the output layer [44]. In this model, the initial values of the weights were randomly set, and the learning rate was set to 0.01. In addition, 10 nodes were used for each hidden layer and number of iterations was set to 10000. Consequently, leave one out cross validation technique was used to evaluate the performance of each classifier with the training set. The classification process was done with subject independent classification. The extracted features were divided into training and a test set with ratio of 0.8 and 0.2, respectively.

2. Result

In this study we have two purposes of using PSD; (1) to investigate alpha frontal activity on our data set of children and (2) to compare between EEG recognition system based on PSD with different classifiers respectively.

A. Alpha

Regarding Davidson study[45], we computed the mean alpha power for each brain region during affective state. **Figure 1**. presents the mean alpha power with standard derivation for left and right brain regions for negative (LV) and positive emotions (HV). Results indicate alpha right frontal activity during negative emotion. This confirms with previous studies that during negative emotion alpha activity increased in right frontal rather than in left frontal of brain region. However, there is no difference between left and right frontal alpha activity during positive emotional state. This also confirms with studies by Feng et al [22] and Davdiosn et al [45]. For arousal level, results show alpha right activity in frontal brain regions during low arousal stimuli as demonstrate in **Figure 2**. However, there is alpha right activity in temporal region responding to high arousal stimuli.

An ANOVAs test was conducted to investigate the difference in PSD value among brain regions for valence and arousal levels. For each domain, we have two classes. For valence level, the electrodes F3, F4, C3, C4 and T7 indicate significant difference between positive and negative emotion ($p<0.05$). For arousal level, the electrodes F3 and C3 show significant difference between low and high arousal with ($p<0.05$). These results will be used later in classification process. Further, we examined the changes in mean alpha power during both eyes open and eyes-closed with emotional session. The statistical results indicate that there is a great difference between rest conditions and emotional states ($p <0.005$) as shown in **Table 1**. The increase of alpha activity in whole brain region during emotion stimuli indicates the response of participants to emotion stimuli. **Figure 3**. shows the mean alpha power for rest conditions and emotional state.

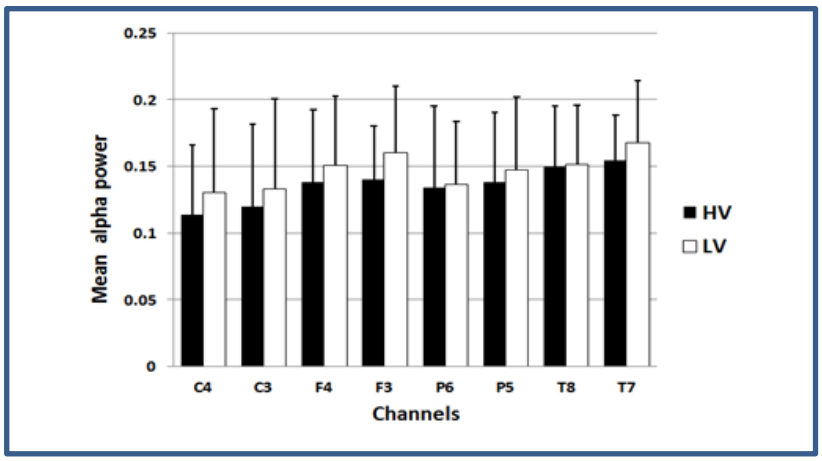

Fig 1. Mean alpha power with standard derivation for different brain regions for high and low valence level.

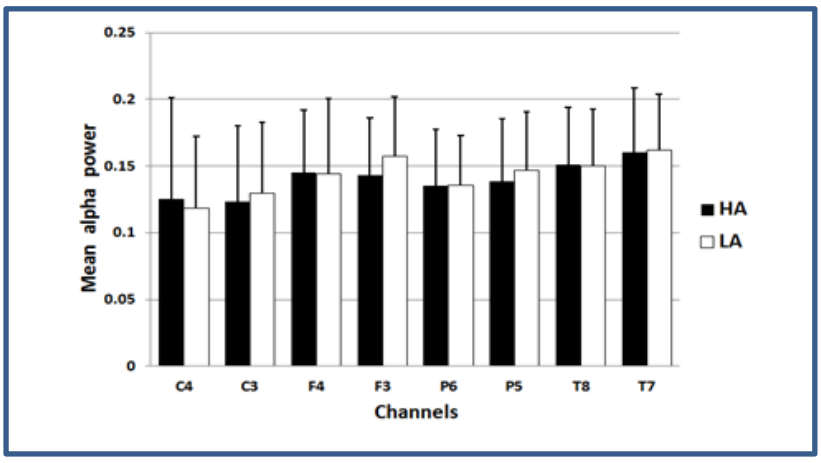

Fig 2.Mean alpha power with standard derivation for different brain regions for high and low arousal level.

Table 1. F test value for different comparison

Channel	HV-LV	HA-LA	EO-emotion	EC-emotion
C3	3.4*	2.6	6**	20**
C4	3.5*	3*	6.5**	19**
F3	4*	0.1	15**	22**
F4	12*	6*	15**	23**
P5	0.16	2	14**	26**
P6	2	0.2	15**	24.5**
T7	3.2*	0.08	14**	22**
T8	0.01	0.04	13**	19**

HV high valence; LV low valence; HA high arousal; LA low arousal; EO eyes- open; EC eyes-closed; *p < 0.05; **p << 0.005

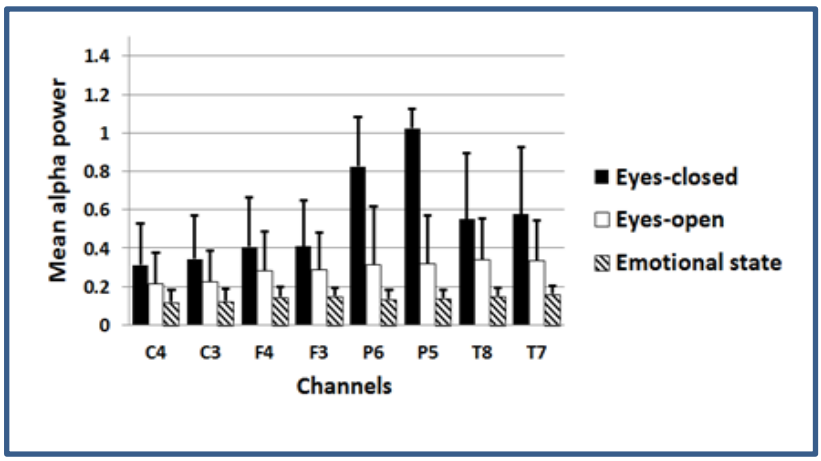

Fig 3. Mean alpha power with standard derivation for eyes closed , eyes open and emotional state.

B. Classification process of detection emotional states

We evaluated the performance of (PSD) to detect emotional states in affective space domains (valence and arousal). The data was divided into training and testing group with ratios 0.8 and 0.2 respectively as mentioned before. The accuracy was computed using repeated random sub-sampling validation. The highest accuracy was 61 % using Knn for valence and 58 % using RLS for arousal level. **Table 2** summarizes the average accuracy and standard derivation for each class and method.

To find best discriminate between classes, we evaluated the performance of PSD after feature selection. Feature selection was performed based on repeated ANOVAs as mentioned previously with alpha value less than 0.05. The feature selection was done using all population

of our dataset. Then the selected features were applied for both training and testing sets. A pair test was applied to compare the accuracy of each method. Table III summarizes the mean classification accuracy without features selection and with features selection. Obviously, there was improvement in classification accuracy using PSD with knn and RLS classifiers ($p<<0.01$).

Classification accuracy for PSD feature was improved with feature selection. The frontal, central and temporal regions are involved in discriminate among affective states. Comparison with other studies has many difficulties though each study has used different emotion stimuli, aged group and modality. However, we compared our results with methods based on using PSD and connectivity among brain regions. Regarding recent studies, Gupta et al **[46]** got 60% accuracy for detection arousal and valence using PSD and support vector machine (SVM). Soleymain et al **[47]** reported 50% classification accuracy for valance and 62% for arousal. Khosrowabadi et al [26] got 71.43% and 70.8 % for valence and arousal level respectively using coherence and Lee et al **[27]** reported 62% using Phase synchronization index (PSI) of alpha band. Our classification results are compatible with the previous studies and indicate the capability of RST feature to identify brain activity. Overall EEG feature based on interaction among brain region such as connectivity and our proposed approach showed high ability to detect emotional state compared to method based on specific brain region.

Table 2. Mean classification accuracy with standard derivation of detection emotional states

Method	HV	LV	HA	LA
PSD-Knn	0.60(0.03)	0.63(0.07)	0.525(0.02)	0.51(0.01)
PSD-RLS	0.58(0.06)	0.60(0.06)	0.595(0.08)	0.585(0.02)
PSD-MLP	0.49(0.37)	0.50(0.34)	0.50(0.1)	0.54(0.3)

HV;High valence ,LV;low valence,HA;high arousal,LA;low arousal

Table 3. classification accuracy with standard derivation of detection emotional states.

Methods	Without feature selection	With feature selection	P
PSD-Knn	0.55(0.018)	0.65(0.019)	2.50E-04**
PSD-RLS	0.58(0.057)	0.70(0.037)	2.00E-04**
PSD-MLP	0.50(0.28)	0.63(0.03)	0.012

HV;High valence ,LV;low valence,HA;high arousal,LA;low arousal

4. Conclusions

This study showed the benefit of characterizes brain activity by spatial temporal information to discriminate different emotional states. This study used 8 channels present different brain

region with temporal domain. The power alpha wave has been computed. Different classifiers have been used to detect between high valence and low valence as well as high arousal and low arousal. Our results indicate that EEG of frontal, partial and cortex region can characterize emotional states. Further RLS classifier show good performance to detect brain activity compared to Knn and MLP classifiers.

5- References

[1] Ekman, P.: 'Darwin and facial expression: A century of research in review' (Ishk, 2006. 2006)

[2] Ekman, P. Are there basic emotions?. 1992

[3] Darwin, C., and Prodger, P. The expression of the emotions in man and animals.Oxford University Press, USA, 1998.

[4] Izard, C.E. Measuring emotions in infants and children. Cambridge University Press, 1982.

[5] Feldman, R.Parent–infant synchrony and the construction of shared timing; physiological precursors, developmental outcomes, and risk conditions. Journal of Child psychology and Psychiatry, 2007, 48, (3-4), pp. 329-354

[6] Pollak, S.D., and Sinha, P.Effects of early experience on children's recognition of facial displays of emotion.Developmental psychology, 2002, 38, (5), pp. 784

[7] Dapretto, M., Davies, M.S., Pfeifer, J.H., Scott, A.A., Sigman, M., Bookheimer, S.Y., and Iacoboni, M.: 'Understanding emotions in others: mirror neuron dysfunction in children with autism spectrum disorders', Nature neuroscience, 2006, 9, (1), pp. 28

[8] El-Haddad, C., and Laouris, Y.: 'The ability of children with mild learning disabilities to encode emotions through facial expressions': 'Toward Autonomous, Adaptive, and Context-Aware Multimodal Interfaces. Theoretical and Practical Issues' (Springer, 2011), pp. 387-402

[9] Holder, H.B., and Kirkpatrick, S.W.Interpretation of emotion from facial expressions in children with and without learning disabilities.Journal of Learning Disabilities, 1991, 24, (3), pp. 170-177

[10] Marrero-Fernández, P., Montoya-Padrón, A., Jaume-i-Capó, A., and Buades Rubio, J.M. Evaluating the research in automatic emotion recognition, IETE Technical Review, 2014, 31, (3), pp. 220-232

[11] Meena, S.M., Vimala, K., and Kalaivani, V.Emotional stress recognition using multi-modal bio-signals.Biometrics and Bioinformatics, 2015, 7, (1), pp. 17-22

[12] Dan-Glauser, E.S., and Gross, J.J.The temporal dynamics of emotional acceptance: Experience, expression, and physiology.Biological Psychology, 2015, 108, pp. 1-12

[13] Costafreda, S.G., Brammer, M.J., David, A.S., and Fu, C.H.Predictors of amygdala activation during the processing of emotional stimuli: a meta-analysis of 385 PET and fMRI studies. Brain research reviews, 2008, 58, (1), pp. 57-70

[14] Schmidt, L.A., and Trainor, L.J.Frontal brain electrical activity (EEG) distinguishes valence and intensity of musical emotions', Cognition & Emotion, 2001, 15, (4), pp. 487-500.

[15] Mauss, I.B., and Robinson, M.D.Measures of emotion: A review. Cognition and emotion, 2009, 23, (2), pp. 209-237

[16] Smith, C.L., Diaz, A., Day, K.L., and Bell, M.A.Infant frontal electroencephalogram asymmetry and negative emotional reactivity as predictors of toddlerhood effortful control.Journal of experimental child psychology, 2016, 142, pp. 262-273

[17] Angus, D.J., and Harmon-Jones, E.On the neuroscience of approach and withdrawal motivation, with a focus on the role of asymmetrical frontal cortical activity.Recent Developments in Neuroscience Research on Human Motivation' (Emerald Group Publishing Limited, 2016), pp. 37-63

[18] Zhang, J., Hua, Y., Xiu, L., Oei, T.P. and Hu, P., 2020. Resting state frontal alpha asymmetry predicts emotion regulation difficulties in impulse control. Personality and Individual Differences, 159, p.109870.

[19] Li, W., Li, Y. and Cao, D., 2021. The effectiveness of emotion cognitive reappraisal as measured by self-reported response and its link to EEG alpha asymmetry. Behavioural Brain Research, 400, p.113042.

[20] Davidson, R.J.Anterior cerebral asymmetry and the nature of emotion. Brain and cognition, 1992, 20, (1), pp. 125-151

[21] Davidson, R.J., and Fox, N.A.Frontal brain asymmetry predicts infants' response to maternal separation. Journal of abnormal psychology, 1989, 98, (2), pp. 127

[22] Feng, X., Forbes, E.E., Kovacs, M., George, C.J., Lopez-Duran, N.L., Fox, N.A., and Cohn, J.F.Children's depressive symptoms in relation to EEG frontal asymmetry and maternal depression', Journal of abnormal child psychology, 2012, 40, (2), pp. 265-276

[23] Pickens, J., Field, T., and Nawrocki, T.: 'Frontal EEG asymmetry in response to emotional vignettes in preschool age children. International Journal of Behavioral Development, 2001, 25, (2), pp. 105-112

[24] Bekkedal, M.Y., Rossi III, J., and Panksepp, J.Human brain EEG indices of emotions: delineating responses to affective vocalizations by measuring frontal theta event-related synchronization. Neuroscience & Biobehavioral Reviews, 2011, 35, (9), pp. 1959-1970

[25] Petrantonakis, P.C., and Hadjileontiadis, L.J.Adaptive emotional information retrieval from EEG signals in the time-frequency domain. IEEE Transactions on Signal Processing, 2012, 60, (5), pp. 2604-2616

[26] Khosrowabadi, R., Quek, C., Ang, K.K., and Wahab, A.ERNN: A biologically inspired feedforward neural network to discriminate emotion from EEG signal. IEEE transactions on neural networks and learning systems, 2014, 25, (3), pp. 609-620

[27] Lee, Y.-Y., and Hsieh, S.: 'Classifying different emotional states by means of EEG-based functional connectivity patterns', PloS one, 2014, 9, (4), pp. e95415

[28] Murugappan, M., Ramachandran, N., and Sazali, Y.: 'Classification of human emotion from EEG using discrete wavelet transform', Journal of Biomedical Science and Engineering, 2010, 3, (04), pp. 390

[29] Sourina, O., and Liu, Y.A Fractal-based Algorithm of Emotion Recognition from EEG using Arousal-Valence Model', in Editor.Ed..Book A Fractal-based Algorithm of Emotion Recognition from EEG using Arousal-Valence Model' (2011, edn.), pp. 209-214

[30] Frantzidis, C.A., Bratsas, C., Klados, M.A., Konstantinidis, E., Lithari, C.D., Vivas, A.B., Papadelis, C.L., Kaldoudi, E., Pappas, C., and Bamidis, P.D. On the classification of emotional biosignals evoked while viewing affective pictures: an integrated data-mining-based approach for healthcare applications. IEEE Transactions on Information Technology in Biomedicine, 2010, 14, (2), pp. 309-318

[31] Pelachaud, C.: 'Emotion-oriented systems.John Wiley & Sons, 2013.

[32] Uttal, W.R.Reliability in cognitive neuroscience: A meta-meta-analysis.MIT Press, 2013.

[33] Guillory, S.A., and Bujarski, K.A.Exploring emotions using invasive methods: review of 60 years of human intracranial electrophysiology. Social cognitive and affective neuroscience, 2014, 9, (12), pp. 1880-1889

[34] Uttal, W.R.Reliability in cognitive neuroscience: A meta-meta-analysis.MIT Press, 2013

[35] Aha, D.W., Kibler, D., and Albert, M.K.Instance-based learning algorithms.Machine learning, 1991, 6, (1), pp. 37-66

[36] Rumelhart, D., Hinton, G.E., and Williams, R.Learning internal representations by error propagation.Parallel distributed processing: explorations in the microstructure of cognition, 1986, 1

[37] Jemberie, A.A.Information theory and artificial intelligence to manage uncertainty in hydrodynamic and hydrological models. CRC Press,2014

[38] Evgeniou, T., Pontil, M., and Poggio, T.Regularization networks and support vector machines. Advances in computational mathematics, 2000, 13, (1), pp. 1

[39] Othman, M., Qayoom, A., and Wahab, A.Affective mapping of eeg during executive function tasks', in Editor (Ed.)^(Eds.).Book Affective mapping of eeg during executive function tasks' (IEEE, 2012, edn.), pp. 144-149

[40] Russell, J.A.A circumplex model of affect. Journal of personality and social psychology, 1980, 39, (6), pp. 1161

[41] Langner, O., Dotsch, R., Bijlstra, G., Wigboldus, D.H., Hawk, S.T., and Van Knippenberg, A.Presentation and validation of the Radboud Faces Database.Cognition and emotion, 2010, 24, (8), pp. 1377-1388

[42] Durak L., Arikan O.Short-time Fourier transform: Two fundamental properties and an optimal implementation.IEEE Trans. Signal Process. 2003.51, 1231–1242,

[43] Tacchetti, A., Mallapragada, P.S., Santoro, M., and Rosasco, L.GURLS: a Toolbox for Regularized Least Squares Learning.2012

[44] Simard, P.Y., LeCun, Y.A., Denker, J.S., and Victorri, B.: 'Transformation invariance in pattern recognition—tangent distance and tangent propagation': 'Neural networks: tricks of the trade' (Springer, 1998), pp. 239-274

[45] Davidson, R.J., Ekman, P., Saron, C.D., Senulis, J.A., and Friesen, W.V.Approach-withdrawal and cerebral asymmetry: Emotional expression and brain physiology. Journal of personality and social psychology, 1990, 58, (2), pp. 330

[46] Gupta, R., and Falk, T.H.Relevance vector classifier decision fusion and EEG graph-theoretic features for automatic affective state characterization.Neurocomputing, 2016, 174, pp. 875-884

[47] Soleymani, M., Pantic, M., and Pun, T.Multimodal emotion recognition in response to videos', in Editor (Ed.)^(Eds.).Book Multimodal emotion recognition in response to videos' (IEEE, 2015, edn.), pp. 491-497

Al-Kitab Journal for Pure Sciences
ISSN: 2617-1260 (print), 2617-8141(online)
www.kjps.isnra.org

Association between ICSI cycle outcome and response in women with infertility

Sara Samir Sadoon[1*], Amal Abdulwahid Mohammed[2], Ali Ibrahim Rahim[3]

[1*]Kirkuk Health Directorate, Iraq
[2]Lecturer at higher institute for diagnosis of infertility and assisted reproduction techniques, Iraq
[3]Al-Ameed University, College of Medicine; Al-Kafeel Specialized Hospital, IVF Center; Karbala, Iraq

*Corresponding Author: sara.samir@ierit.nahrainuniv.edu.iq

Citation: Sadoon SS, Mohammed AA, Rahim AI. Association between ICSI cycle outcome and response in women with infertility. *Al-Kitab Pure Sci KJPS*. 2022; 6(1): 54-64. https://doi.org/10.32441/kjps.06.01.p5

Keyword
ISCI, Infertility, AMH, Pregnancy Rate, Ovarian Response.

Article History
Received May 3, 2022
Accepted August 12, 2022
Available online September 20, 2022

Abstract:

Background: Infertility is the inability to achieve a clinical pregnancy after 12 months of regular and unprotected sexual activity. Increases in child-bearing delay and maternal age at first pregnancy significantly impact the rise of age-related infertility and the demand for treatment using assisted reproduction techniques (ART). As a result, many women with a low ovarian reserve and a poor ovarian response (POR) to conventional stimulation seek medical assistance at infertility clinics. Aim: The study aimed to evaluate the quality of oocytes and embryos, as well as the rates of conception, in infertile women who were candidates for fresh intracytoplasmic sperm injection between good and poor-responder women (ICSI). Patients and methods: The study was conducted on 45 infertile women undergoing ICSI at the High Institute for Infertility Diagnosis and Assisted Reproductive Technologies/ Al-Nahrain University/ Baghdad/ Iraq from October 2021 to April 2022, regardless of whether they had previously undergone ICSI. The morphology of the oocytes and the quality of the resulting embryos were assessed. The patients' ages ranged from 20 to 42 years old. There was primary and secondary infertility ranging from one to 20 years. Every couple had a basic reproductive assessment. The

antagonist protocol was used for all infertile females. All females had their serum levels of AMH, luteinizing hormone (LH), follicle-stimulating hormone (FSH), and oestradiol (E2) measured on the second or third day of their cycle. The serum oestradiol (E2) level was re-measured on the day of the hCG injection. Results: The participants in the study were 32.6 ± 5.3 years old. The findings showed that 57.8% of the patients had a well response, and 24.4% of the women were pregnant. In those who became pregnant, anti-müllerian hormone (AMH) levels were significantly higher, and follicle-stimulating hormone (FSH) levels were noticeably lower (p> 0.05). The E2, LH, prolactin, and progesterone levels were not statistically different (P> 0.05). Conclusion: In conclusion, the findings revealed a positive relationship between response and ICSI outcomes in infertile women.

Keywords: ISCI, Infertility, AMH, Pregnancy Rate, Ovarian Response.

العلاقة بين نتائج دورة الحقن المجهري والاستجابة عند النساء المصابات بالعقم

ساره سمير سعدون[١]، آمال عبد الواحد محمد[٢]، علي إبراهيم رحيم[٣]

[١]مديرية صحة كركوك، العراق

[٢]المعهد العالي لتشخيص العقم وتقنيات الإنجاب، العراق

[٣]جامعة العميد ، كلية الطب، مستشفى الكفيل التخصصي، مركز أطفال الأنابيب، كربلاء، العراق

*sara.samir@ierit.nahrainuniv.edu.iq

الخلاصة:

يُعرَّف العقم بأنه عدم القدرة على تحقيق الحمل السريري بعد ١٢ شهرًا من النشاط الجنسي المنتظم وغير المحمي. تؤثر الزيادة في تأخر الإنجاب وعمر الأم عند الحمل الأول بشكل كبير على زيادة العقم المرتبط بالعمر والطلب على العلاج باستخدام تقنيات الإنجاب المساعدة (ART). يتسبب هذا في وجود عدد كبير من النساء ذوات احتياطي المبيض المنخفض واستجابة المبيض الضعيفة (POR) للتحفيز التقليدي يطلبن المساعدة الطبية في عيادات العقم. كان الهدف من الدراسة هو تقييم جودة البويضات والأجنة وكذلك معدلات الحمل لدى النساء المصابات بالعقم والمرشحات لحقن الحيوانات المنوية الجديدة داخل الهيولى في كل من النساء المستجيبات الطبيعيات والضعيفات (الحقن المجهري). المرضى والأساليب: أجريت الدراسة على ٤٥ امرأة مصابة بالعقم يخضعن للحقن المجهري في المعهد العالي لتشخيص العقم والتقنيات الإنجابية المساعدة / جامعة النهرين / بغداد / العراق من أكتوبر ٢٠٢١ إلى أبريل ٢٠٢٢، بغض النظر عما إذا كانوا قد خضعوا سابقًا للحقن المجهري. تم تقييم مورفولوجيا البويضات ونوعية الأجنة الناتجة. تراوحت أعمار المرضى من ٢٠ إلى ٤٢ عامًا. كان هناك عقم أولي وثانوي يتراوح من عام إلى ٢٠ عامًا، خضع جميع الأزواج لتقييم الإنجاب الأساسي. كان بروتوكول جميع الإناث المصابات بالعقم هو البروتوكول المضاد. تم قياس مستويات مصل الدم من AMH ، وهرمون (LH) LUTEINIZING ، وهرمون تحفيز الجريب

(FSH) ، والإستراديول (E2) في اليوم الثاني أو الثالث من الدورة. تم إعادة قياس مستوى مصل الاوستراديول (E2) في يوم حقن (HCG). النتائج: تراوحت أعمار المشاركين في الدراسة بمتوسط عمر ٣٢,٦ ± ٥,٣ سنة. وأظهرت النتائج أن ٥٧,٨٪ من المرضى لديهم استجابة طبيعية، وأن ٢٤,٤٪ من النساء كن حوامل. كان الهرمون المضاد للمولر (AMH) أعلى بشكل ملحوظ وكان الهرمون المنبه للجريب (FSH) أقل بشكل ملحوظ (P> 0.05) في النساء الحوامل. لم تكن مستويات E2 وLH والبرولاكتين والبروجسترون مختلفة إحصائياً (P> 0.05) بينهما. الخلاصة: في الختام أوضحت النتائج وجود علاقة إيجابية بين الاستجابة ونتائج الحقن المجهري في النساء المصابات بالعقم.

الكلمات المفتاحية: ISCIK، العقم، AMH، معدل الحمل استجابة المبيض.

1. INTRODUCTION:

Infertility is a worldwide medical and financial issue that can cause stress and psychological distress. Infertility is the inability to obtain a clinical pregnancy following at least one year of regular unprotected sexual intercourse. Lifestyle has had a significant impact on the decline of fertility and the rise of assisted reproductive technologies in recent years [1]. Infertile patients undergoing in vitro fertilization (IVF) programs have a poor ovarian response in 9 to 24 % of cases [2]. Follicles that respond to FSH are fewer in women with a poor ovarian response, resulting in poor IVF outcomes and presenting a significant challenge to clinicians worldwide [3]. Several standards for determining POR have been proposed. However, none had been accepted as the international standard for defining POR until the development of Bologna standards in 2011[4]. Treatment of poor-responder patients during Assisted Reproductive Technologies (ART) is still a controversial topic [3].The main goal is to determine the optimum treatment strategy for them depending on their ovarian capacity to enhance pregnancy potential while remaining clinically safe. It is most likely to reduce the risk of treatment failure, improve IVF outcomes, raise the chances of conception, provide proper counseling to patients, and set realistic expectations for ovarian stimulation outcomes. Increasing the gonadotropins or decreasing the GnRH agonist (GnRH-a) doses, as well as the use of adjunctive growth hormone, clomiphene citrate, aromatase inhibitors, or the use of a micro dose flare regimen with or without oral contraceptive pretreatment, or the use of a GnRH antagonist regimen, have all been suggested for the management of the poor-responder patient to improve the ovarian responses as well as the IVF outcomes [5]. The study's goal was to assess oocyte and embryo quality as well as conception rates in women with infertility who were candidates for fresh intracytoplasmic sperm injection in both well and poor responder women (ICSI).

2. Patients and Methods:

The study included 45 infertile women who underwent ICSI who underwent ICSI at the High Institute for Infertility Diagnosis and Assisted Reproductive Technologies/Al-Nahrain University/Baghdad, Iraq, from October 2021 to April 2021, regardless of whether they had previously undergone ICSI. The morphology of the oocytes and the quality of the generated embryos were assessed in the same institute's laboratory. The age of patients was between 20 and 42. Primary and secondary infertility were also present, with a period of 1 to 20 years. All couples underwent a basic reproductive assessment, which included a history, physical examination, hormone measurement, and the exclusion of uncontrolled endocrine problems, as well as sperm analysis for their partner. The protocol for all infertile females was the antagonist protocol. All patients had their serum levels of AMH, luteinizing hormone (LH), follicle-stimulating hormone (FSH), as well as oestradiol (E2) tested on the second or third day of their periods. The serum oestradiol (E2) level was re-measured the day after the hCG injection. The average age of the females included in this study was 20 to 42, had normal BMI, or weighed less than 30 kg, and had a partner with adequate normal sperm. Females with uncontrolled endocrine and systemic diseases, as well as those who had a partner with severe oligospermia or azoospermia, were excluded from the study.

Methods: To discover the reason for infertility, each infertile couple who participated in this study had a thorough medical history and physical examination. Questions about medical history include medical history (thyroid illness symptoms, diabetes, hirsutism, weight gain or loss, nipple discharge, lower abdomen or pelvic pain, mumps history, medication allergies, oral contraceptive pill use, steroids, chemotherapy, radiation, and non-steroidal anti-inflammatory medications, etc.). Past surgical history includes (cesarean section, appendectomy, diagnostic or therapeutic curettage, thyroid surgery, abdominal surgery, etc). Menstrual history includes (age of menarche, length of cycle, character of menstrual cycle, and presence of dysmenorrhea). Past gynecological history includes a history of vaginal discharge, pelvic pain, previous exposure to pelvic inflammatory disease, and history of PAP smears, a history of marriage, date of marriage, coital timing and frequency, methods of contraception if present, etc. Fertility history includes the type, duration, causes, previous investigations, and treatments, including IVF-ICSI trials and their outcomes. Past obstetrical conditions include the following: a history of gravidity and parity; a history of pregnancy-induced hypertension, gestational diabetes, a miscarriage; vaginal bleeding; a previous history of cervical cerclage; the birth of an abnormal

child; and post-partum hemorrhage). Family history; includes a history of infertility, premature ovarian failure, diabetes mellitus, thyroid diseases, or congenital abnormalities, etc.). Social history includes occupation, smoking, alcohol, address, and animal contacts. Both partners underwent physical examinations, including body mass index (BMI), general, cardiovascular, abdominal, central nervous system, thyroid, and breast examinations. Gynecological examination, including vaginal and cervical abnormalities, discharge, and uterine size. The Hormonal Assay was used to assess ovarian reserve, whereas serum prolactin, progesterone, and 17 estradiol (E2) were all used to evaluate hypothalamic-pituitary-ovarian (HPO) axis function. Based on their ovarian response, women were divided into two groups. Women with a poor ovarian response to stimulation had a reduced follicular response and low levels of oestradiol (E2) to stimulation according to the "Bologna criteria" developed by the European Society of Human Reproduction and Embryology (ESHRE).

3-Result

Figure 1 depicts the distribution of study patients based on general characteristics. Patients in the study ranged in age from 23 to 42 years old, with a mean of 32.6±5.3 years old. However, the majority of participants (57.8%) were under the age of 35.

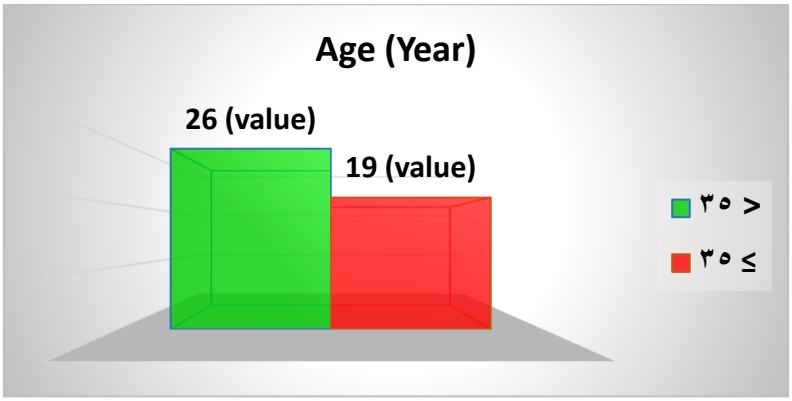

Fig 1. Distribution of participants by age

According to the findings, (57.8%) of patients had well responses, as shown in **Table 2**.

Table 1. Distribution of study patients by response

Response	No. (n= 45)	Percentage (%)
Poor responder	19	42.2
Well responder	26	57.8

Figure 2 shows the distribution of study patients by ICSI cycle outcome. The prevalence of pregnancy was (24.4 %).

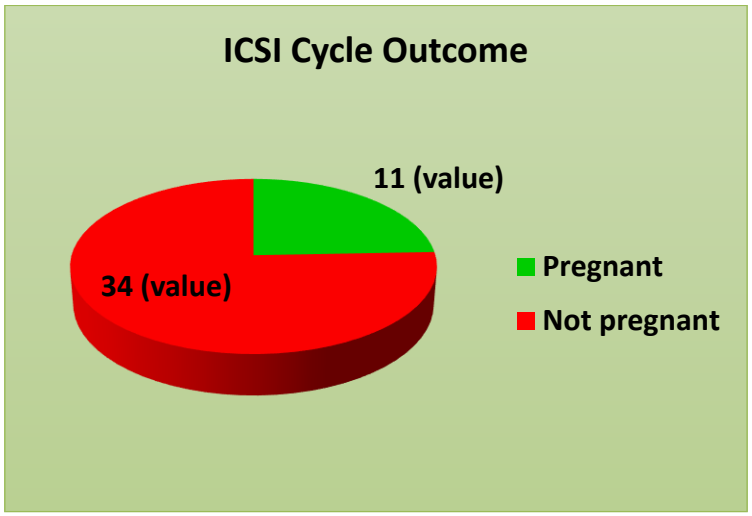

Figure 2: Distribution of study patients by ICSI outcome

Furthermore, pregnant women have considerably increased AMH and significantly lower FSH, as seen in **Table 2** ($p<0.05$). There were no statistically significant differences ($p>0.05$) between E2, LH, prolactin, and progesterone.

Table 2: Comparison of hormonal parameters based on ICSI cycle outcome

Hormonal Parameter	ICSI cycle outcome		P - Value
	Pregnant Mean ± SD	Not pregnant Mean ± SD	
Estradiol (pg/ml)	1590.01 ± 631.1	1261.13 ± 929.7	**0.209**
AMH (ng/ml)	2.85 ± 1.6	1.51 ± 1.1	**0.032**
FSH (IU/L)	6.97 ± 1.8	9.02 ± 2.6	**0.01**
LH (IU/L)	7.62 ± 2.4	7.22 ± 2.4	**0.651**
Prolactin (ng/ml)	13.21 ± 4.2	14.11 ± 5.1	**0.321**
Progesterone (ng/ml)	1.69 ± 1.1	1.71 ± 1.2	**0.833**

As shown in **Table3**, there was no statistically significant difference in response between pregnant and non-pregnant women (P= 0.063).

Table 3: Association between ICSI cycle outcome and response

Response	ICSI cycle outcome		Total (%) n= 45	P - Value
	Pregnant (%) n= 11	Not pregnant (%) n= 34		
Poor responder	1 (9.09%)	18 (52.9%)	19 (42.2%)	**0.027**
Well responder	10 (90.91%)	16 (47.1%)	26 (57.8%)	

Table 4 compares clinical indicators based on the outcome of an ICSI cycle. Those who got pregnant had a considerably larger mean number of grades I embryos (p = 0.03) than those who did not. All other clinical measures' means did not show statistically significant changes (P> 0.05).

Table 4: Comparison in clinical parameters by ICSI cycle outcome

Clinical Parameter	ICSI cycle outcome		P - Value
	Pregnant Mean ± SD	Not pregnant Mean ± SD	
Endometrial Thickness (mm)	9.36 ± 1.2	8.89 ± 1.3	**0.306**
No. of oocyte retrieved	12.9 ± 5.5	8.91 ± 6.5	**0.07**
No. of ruptured follicle	0.8 ± 1.31	0.54 ± 0.85	**0.571**
No. of GV stage oocyte	2.0 ± 1.9	0.82 ± 1.8	**0.101**
No. of M1 stage oocyte	2.4 ± 1.7	1.65 ± 1.8	**0.25**
No. of M2 stage oocyte	7.0 ± 4.1	5.34 ± 4.8	**0.292**
No. of embryos	5.9 ± 3.4	4.31 ± 3.5	**0.217**
No. of grade I embryo	4.1 ± 2.9	2.25 ± 2.1	**0.03**
No. of grade II embryo	1.3 ± 1.1	0.97 ± 0.92	**0.39**
No. of grade III embryo	0 ± 0	0.25 ± 0.78	**0.059**

4. Discussion

Despite advances in reproductive technology, significant proportions of patients remain poor responders (PORs) to aspects of oocyte retrieval and pregnancy rates **[6]**. According to the current findings, 57.8% of patients responded well to ART treatment programs, whereas 42.2% responded poorly. Furthermore, the prevalence of pregnancy was 24.4%. A previous study estimated that the pregnancy rate was about 26%, which is highly approximate to the result of the present study **[7].**

In contrast to the results of Hassan et al.'s 2020 study, better results were published, with an overall prevalence of pregnancy after ICSI of 32.3% **[8]**. In other studies, 33 patients out of 90 in Kamkar et al.'s study in 2018 got pregnant (36%), only 27 of which were clinical pregnancies, giving a 30% clinical pregnancy rate **[9]**. In the Ashrafi et al. study from 2013, 1492 infertile women were enrolled and underwent ICSI, and the overall clinical pregnancy rate was 33.9% **[10]**.

As shown in **Table 3**, there was no statistically significant difference in response between women who became pregnant and those who did not, as shown in **Table 3** (P = 0.063). Similarly, there was a non-significant response difference between those who became pregnant and those who did not **[8]**. Another study found a significant difference in ovarian response between the two groups, with clinical pregnancy rates of 14.8 percent in poor-responder women and 36.7 percent in normal-responder women **[11]**.

In addition, in the current study, AMH, FSH, LH, prolactin, and E2 were measured for females' ovarian reserve assessment, which is critical before any ICSI trial **[12]**. Furthermore, this information can be used to analyze and advise couples before ICSI stimulation, as well as optimize stimulation techniques. The current study found that AMH levels differed significantly between pregnant and non-pregnant women ($P< 0.05$), with pregnant women having higher levels. Other studies have supported the current study's findings. **[13, 14, and 15]** .

According to Gomez et al. (2016), women with low serum AMH levels can become pregnant. However, the findings revealed significant differences in FSH levels between pregnant and non-pregnant women, with the mean FSH being significantly lower in pregnant women than in non-pregnant women ($P<0.05$). Tulic also confirmed that lower basal FSH levels are associated with a positive assisted reproduction outcome **[16]**. According to Salama et al. **[17]**, lower basal FSH levels are associated with chemical and clinical pregnancies.

Moreover, the current study showed no significant differences with E2, LH, prolactin, and progesterone ($P \geq 0.05$). In contrast, Al-Ghazali et al. found that E2 levels were higher in pregnant women than in non-pregnant women in 2013, indicating significant ovarian response **[18]**. Jiang et al. found that, despite having normal FSH, women with elevated basal E2 had poor pregnancy outcomes **[19].**

In a 2020 study, Pizarro et al. discovered that FSH, LH, and serum estradiol were higher, while serum progesterone was lower on the day of hCG in those who got pregnant versus those who couldn't after ICSI, with no significant relationship observed among these

parameters (P>0.05). [11]. According to a different conclusion from a 2013 study by Ashrafi and other co-authors, the mean LH serum concentration in the pregnant group was significantly higher than that in the non-pregnant group (p = 0.04). Despite this, the serum concentrations of FSH and prolactin measured on day three did not differ significantly between the two groups (P>0.05) [10]. However, basal LH and E2 levels are not assumed to be appropriate markers for differentiating infertile patients who respond differentially to ovarian stimulation [19]. The ability to assess embryos quality is critical for decreasing the chance of multiple pregnancies and rising pregnancy rates by transferring the best embryos [21].

In the current study, there was no significant difference in oocyte quality, MII, or MI germinal vesicles between pregnant and non-pregnant women. However, pregnant women had a higher GI embryo count than non-pregnant women, which was statistically significant (P = 0.03). The overall number of embryos, the number of GII embryos, and the number of GIII embryos were not significantly different (P ≥ 0.05). On the other hand, Sivrikoz discovered that high-quality embryos improve pregnancy rates [20]. According to a study published in 2020 by Hassan et al., there is no difference in total oocytes, aberrant oocytes, germinal vesicle oocytes, MII, or MI oocytes between pregnant and non-pregnant women (p>0.05). Furthermore, there was no discernible difference in the percentage of grade I, II, III, IV, as well as selected embryos between pregnant and non-pregnant women after ICSI (p>0.05)[8].

5- Conclusions

In conclusion, the study showed that oocyte quality affects the pregnancy rate. Furthermore, the results of ICSI have strong associations with AMH and FSH levels.

6- References

[1] Wischmann, T 2020,'Psychological Impact of Infertility and Assisted Reproduction 1', in, Handbook of Perinatal Clinical Psychology, Routledge, pp.61–81.

[2] Bentov, Y., Hannam, T., Jurisicova, A., Esfandiari, N. and Casper, R.F., 2014. Coenzyme Q10 supplementation and oocyte aneuploidy in women undergoing IVF-ICSI treatment. Clinical Medicine Insights: Reproductive Health, 8, pp.CMRH-S14681.

[3] Esteves, S.C., Roque, M., Bedoschi, G.M., Conforti, A., Humaidan, P. and Alviggi, C., 2018. Defining low prognosis patients undergoing assisted reproductive technology: POSEIDON criteria—the why. Frontiers in endocrinology, 9, p.461.

[4] Younis, J.S., Ben-Ami, M. and Ben-Shlomo, I., 2015. The Bologna criteria for poor ovarian response: a contemporary critical appraisal. Journal of ovarian research, 8(1), pp.1-10.

[5] Gat, I., Blanco Mejia, S., Balakier, H., Librach, C.L., Claessens, A. and Ryan, E.A., 2016. The use of coenzyme Q10 and DHEA during IUI and IVF cycles in patients with decreased ovarian reserve. Gynecological Endocrinology, 32(7), pp.534-537.

[6] Safdarian, L., Aghahosseini, M., Alyasin, A., Samaei-Nouroozi, A., Rashidi, S., Shabani-Nashtaei, M., Najafian, A. and Lak, P., 2019. Growth hormone (GH) improvement of ovarian responses and pregnancy outcome in poor ovarian responders: a randomized study. Asian Pacific Journal of Cancer Prevention: APJCP, 20(7), p.2033.

[7] Zargar, M., Najafian, M. and Zamanpour, Z., 2018. Relationship between follicular fluid and serum anti-Mullerian hormone levels and pregnancy rate in ART cycles. Perinatología y Reproducción Humana, 32(1), pp.3-8.

[8] Hasan NA, Abdulhameed WA, Rahim AI. Correlation Among Obesity, Oocyte Characteristics, Embryo Characteristics and Maternal Plasma Folate Level in a Sample of Iraqi Women Undergoing Intracytoplasmic Sperm Injection (ICSI). Iraqi Journal of Embryos and Infertility Researches. 2020;10(1):1-19

[9] Kamkar, N., Ramezanali, F. and Sabbaghian, M., 2018. The relationship between sperm DNA fragmentation, free radicals and antioxidant capacity with idiopathic repeated pregnancy loss. Reproductive biology, 18(4), pp.330-335.

[10] Ashrafi M, Jahanian Sadatmahalleh S, Akhoond MR, Ghaffari F, Zolfaghari Z. ICSI Outcome in Infertile Couples with Different Causes of Infertility: A Cross-Sectional Study. Int J Fertil Steril. 2013;7(2):88-95.

[11] Pizarro BM, Cordeiro A, Reginatto MW, Campos SPC, Mancebo ACA, Areas PCF, et al. Estradiol and Progesterone Levels are Related to Redox Status in the Follicular Fluid During In vitro Fertilization. J Endocr Soc. 2020;4(7):bvaa064-bvaa.

[12] Scheffer, JAB, Scheffer, B, Scheffer, R, Florencio, F, Grynberg, M, & Lozano, DM 2018, 'Are age and anti-Müllerian hormone good predictors of ovarian reserve and response in women undergoing IVF?', JBRA assisted reproduction, vol. 22, no. 3, p. 215.

[13] Gomez, R, Schorsch, M, Hahn, T, Henke, A, Hoffmann, I, Seufert, R, & Skala, C 2016, 'The influence of AMH on IVF success', Archives of gynecology and obstetrics, vol. 293, no. 3, pp. 667–673.

[14] Sacha, C.R., Chavarro, J.E., Williams, P.L., Ford, J., Zhang, L., Donahoe, P.K., Souter, I.C., Hauser, R., Pépin, D. and Mínguez-Alarcón, L., 2020. Follicular fluid anti-Müllerian hormone (AMH) concentrations and outcomes of in vitro fertilization cycles with fresh embryo transfer among women at a fertility center. Journal of Assisted Reproduction and Genetics, 37(11), pp.2757-2766.

[15] Mohammed, ZI & Qasim, MT 2021, 'Correlation of AMH and LH Levels in PCOS Patients with Pregnancy Rate', Annals of the romanian society for cell biology, pp. 945–951.

[16] Tulic, L., Tulic, I., Bila, J., Nikolic, L., Dotlic, J., Lazarevic-Suntov, M. and Kalezic, I., 2020. Correlation of progesterone levels on the day of oocyte retrieval with basal hormonal status and the outcome of ART. Scientific Reports, 10(1), pp.1-9.

[17] Salama, S., Sharaf, M., Salem, S.M., Rasheed, M.A., Salama, E., Elnahas, T. and Lotfy, R., 2021. FSH versus AMH: age-related relevance to ICSI results. Middle East Fertility Society Journal, 26(1), pp.1-8.

[18]Al-Ghazali BS, Al-Jarrah DM. Factors Affecting Intra-Cytoplasm Sperm Injection (ICSI) and Pregnancy Outcome in the Fertility Center of Al–Najaf City. The Iraqi Postgraduate Medical Journal. 2013;12.

[19] Kassab, A., Sabatini, L., Lieberman, G., Tozer, A., Zosmer, A., Davis, C. and Al-Shawaf, T., 2007. Does measuring early basal serum follicular lutinising hormone assist in predicting In vitro fertilization (IVF)/Intracytoplasmic sperm injection (ICSI) outcome?. Reproductive Biology and Endocrinology, 5(1), pp.1-6.

[20] Sivrikoz, Ts, Özgör, By, Bilgiç, Be, & Kutlu, Ht 2021, 'Investigation of factors affecting the success rates of in vitro fertilization followed by a failed cycle', Journal of istanbul faculty of medicine, vol. 84, no. 1, pp. 20–26.

[21] Li, H., Xu, X., Jing, Y., Liu, L. and Wang, Y., 2020. Associations between a new day 4 embryo grading system and implantation rates in frozen embryo transfer (FET) cycles. Medicine, 99(42).

Al-Kitab Journal for Pure Sciences (2022); 6(1):65-77.

https://doi.org/10.32441/kjps.06.01.p6

Al-Kitab Journal for Pure Sciences
ISSN: 2617-1260 (print), 2617-8141(online)
www.kjps.isnra.org

Studying the IVF Laboratory Performance Indicators the Vienna Consensus 2017 for the High Institute According to Diagnosis and Assisted Reproductive for Infertility Technologies, Al-Nahrain University, Iraq

Zahraa Abdulsalam Hussein[1*], Ali Ibrahim Rahim[2], Wasan Adnan Abdul-Hameed[1]

[1]High Institute of Infertility Diagnosis and Assisted Reproductive Technologies, Iraq.
[2]Al- Ameed University, College of Medicine; Al-Kafeel Specialized Hospital, IVF Center; Karbala, Iraq

*Corresponding Author: zahraaabdulsalm95@gmail.com

Citation: Hussein ZA, Rahim AI, Abdul-Hameed WA. Studying the IVF Laboratory Performance Indicators According to the Vienna Consensus 2017 for the High Institute for Infertility Diagnosis and Assisted Reproductive Technologies, Al-Nahrain University, Iraq. *Al-Kitab Pure Sci KJPS*. 2022; 6(1): 65-77. https://doi.org/10.32441/kjps.06.01.p6.

Keyword
KPI, ICSI, Pregnancy rate.

Article History

Received	June 7, 2022
Accepted	August 25, 2022
Available online	September 30, 2022

Abstract:

Background: Performance indicators are used to assess patient safety, efficacy, equity, patient-centeredness, punctuality, and efficiency. The benchmark values for each Key Performance Indicator are aspirational values, and the minimum performance level values are the number of fertilized oocytes on Day 1 and the Normal Fertilization Rate, respectively (presence of 2Pro Nucleus and 2Polar Body measured at 17 h post-injection) as a Failed fertilization rate is calculated as the proportion of IVF cycles (excluding cycles with intracytoplasmic injection) on Day 1 (17 hours after insemination) with no signs of pregnancy [1].

During fertilization (i.e., 0 oocytes with 2Pro Nucleus). The percentage of zygotes on Day 2 (44 hours after insemination) is known as the cleavage rate, and it can suggest an issue with sperm quality (sperm function, oocyte activation, and gamete receptors), sperm processing, or the quantity of spermatozoa used for insemination. which cleaves to create embryos [1]. The

percentage of cleaved embryos per successfully fertilized egg that are at the 4-cell stage on Day 2 (44 hours post-insemination) or at the 8-cell stage on Day 3 (68 hours post-insemination) is known as the embryo development rate. This evaluates the viability and quality of the embryos as well as the capacity of the culture system to promote cleavage at the necessary stages. The critical factor is the proportion of blastocysts observed at 116 hours after insemination as a function of the number of correctly fertilized oocytes. Measures of performance blastocyst development rate. The viability of the embryo as well as the culture system's capacity to support blastocyst formation from fertilized oocytes (i.e., the formation of an intracellular mass and a blastocoele cavity) are both determined by this factor. It should be noted that this phrase only considers blastocyst formation and not blastocyst stage or quality. The damage rate is the proportion of oocytes that are injured or have deteriorated by the time of fertilization assessment on Day 1 as a result of the intracytoplasmic injection. The percentage of biopsied and tubed/fixed samples where DNA is found represents the success rate of the biopsy. It serves as a gauge of the embryologists' ability to transfer biopsied samples to test tubes, as shown by successful DNA amplification. The number of gestational sacs divided by the total number of transplanted embryos is how one calculates the implantation rate, which is dependent on the cleavage stage **[1]**. By dividing the number of gestational sacs by the total number of transplanted blastocysts, the implantation KPI (blastocyst stage) is calculated **[1].**

Aim

Compare the annual results of our institute with the ESHRE-defined international KPI, the Performance Indicators (Fertilization rate, cleavage rate, development day 2, development day 3, blastocyst rate, blastocyst cryosurvival rate, damage rate, successful biopsy rate, implantation rate depends on cleavage stage, implantation rate depends on blastocyst stage).

Patients and Methods: From November 2015 to December 2021, 699 infertile couples who were having intracytoplasmic sperm injection were included in a retrospective study done at the high institution for infertility diagnosis and assisted reproductive technologies at Al Nahrain University in Baghdad, Iraq. The information gathered from the lab and the archive room was classified and divided. Comparing each year to the previous years as well as comparing with the performance indicators (fertilization rate, cleavage rate, development day 2, development day 3, blastocyst rate, blastocyst cryosurvival rate, damage rate, success rate of biopsy, implantation rate dependent on cleavage stage, implantation rate dependent on blastocyst

stage), as well as with ESHRE. Except for the successful biopsy rate and implantation rate, all markers were identified in this investigation.

Results

The fertilization and cleavage rates closely to ESHRE's Key Performance Indicators. The outcomes from days two and three were also close to the ESHRE competency and benchmark standards. Comparison of the mean blastocyst rate revealed a substantial amount of fluctuation, with the highest year being 2016 and the lowest being 2019. 2015 and 2016 are the highest and lowest years for a blastocyst of cryosurvival, respectively. 2020 and 2021 both saw the highest ICSI damage rate. 2015 and 2020 are the highest and lowest pregnancy result years respectively.

Keywords: KPI, ICSI, Pregnancy rate.

دراسة مؤشرات أداء مختبر التلقيح الاصطناعي حسب إجماع فيينا ٢٠١٧ للمعهد العالي للعقم التشخيص والمساعدة على الإنجاب، جامعة النهرين، العراق

زهراء عبد السلام حسين[١]، علي إبراهيم رحيم[٣]، وسن عدنان عبد الحميد[١]

[١]المعهد العالي لتشخيص العقم والتكنولوجيات المساعدة على الإنجاب، العراق
[٢]جامعة العميد ، كلية الطب، مستشفى الكفيل التخصصي، مركز أطفال الأنابيب، كربلاء، العراق

*zahraaabdulsalm95@gmail.com

الخلاصة:

تُستخدم مؤشرات الأداء لتقييم سلامة المريض والفعالية والإنصاف والتركيز على المريض والالتزام بالمواعيد والكفاءة. القيم المعيارية لكل مؤشر أداء رئيسي هي قيم طموحة ، والحد الأدنى لقيم مستوى الأداء هو عدد البويضات المخصبة في اليوم الأول ومعدل الإخصاب الطبيعي ، على التوالي (نواه عدد ٢ والجسم القطبي تم قياسهما في ١٧ ساعة بعد الحقن) كمعدل الإخصاب الفاشل يتم حسابه كنسبة من دورات التلقيح الاصطناعي (باستثناء دورات الحقن داخل المجهري) في اليوم الأول (١٧ ساعة بعد التلقيح) مع عدم وجود علامات الحمل (علماء ألفا في الطب التناسلي المنظمة العالمية للأجنة والخصوبة) أثناء الإخصاب تُعرف النسبة المئوية للحيوانات الملقحة في اليوم الثاني (٤٤ ساعة بعد التلقيح) بمعدل الانقسام ، ويمكن أن تشير إلى مشكلة تتعلق بجودة الحيوانات المنوية (وظيفة الحيوانات المنوية ، وتفعيل البويضات ، ومستقبلات الأمشاج) ، أو معالجة الحيوانات المنوية ، أو كمية الحيوانات المنوية المستخدمة للتلقيح. التي تلتصق لتكوين الأجنة [1]. تُعرف النسبة المئوية للأجنة المشقوقة لكل بويضة مخصبة بنجاح في المرحلة المكونة من ٤ خلايا في اليوم الثاني (٤٤ ساعة بعد التلقيح) أو في المرحلة المكونة من ٨ خلايا في اليوم الثالث (٦٨ ساعة بعد التلقيح) باسم تطور الجنين معدل. يقوم هذا بتقييم صلاحية وجودة الأجنة

وكذلك قدرة نظام الاستزراع على تعزيز الانقسام في المراحل اللازمة. العامل الحاسم هو نسبة الأكياس الأريمية التي لوحظت بعد ١١٦ ساعة من التلقيح كدالة لعدد البويضات المخصبة بشكل صحيح.

مقاييس أداء معدل تطور الكيسة الأريمية. يتم تحديد قابلية بقاء الجنين وكذلك قدرة نظام الاستزراع على دعم تكوين الكيسة الأريمية من البويضات المخصبة (أي تكوين كتلة داخل الخلايا وتجويف القيلة الأريمية) بواسطة هذا العامل. وتجدر الإشارة إلى أن هذه العبارة تتناول فقط تكوين الكيسة الأريمية وليس مرحلة الكيسة الأريمية أو جودتها. معدل الضرر هو نسبة البويضات المصابة أو التي تدهورت في وقت تقييم الإخصاب في اليوم الأول نتيجة الحقن داخل الهيولى. تمثل النسبة المئوية للعينات المأخوذة من الخزعة والأنابيب / الثابتة حيث تم العثور على الحمض النووي معدل نجاح الخزعة. إنه بمثابة مقياس لقدرة علماء الأجنة على نقل العينات المأخوذة من الخزعة إلى أنابيب الاختبار ، كما يتضح من تضخيم الحمض النووي الناجح. عدد أكياس الحمل مقسومًا على العدد الإجمالي للأجنة المزروعة هو كيفية حساب معدل الانغراس ، والذي يعتمد على مرحلة الانقسام بقسمة عدد أكياس الحمل على العدد الإجمالي للكيسات الأريمية المزروعة ، يتم حساب مؤشر الأداء الرئيسي (مرحلة الكيسة الأريمية).

الغرض

مقارنة النتائج السنوية لمعهدنا مع مؤشرات الأداء الرئيسية الدولية المحددة من قبل ايشري ومؤشرات الأداء (معدل الإخصاب ، معدل الانقسام ، يوم التطوير ٢ ، يوم التطوير ٣ ، معدل الكيسة الأريمية ، معدل البقاء على قيد الحياة في الكيسة الأريمية ، معدل الضرر ، معدل الخزعة الناجح ، معدل الزرع يعتمد في مرحلة الانقسام ، يعتمد معدل الانغراس على مرحلة الكيسة الأريمية)، المرضى وطرق العلاج: من تشرين الثاني (نوفمبر) ٢٠١٥ إلى كانون الأول (ديسمبر) ٢٠٢١ ، تم تضمين ٦٩٩ من الأزواج المصابين بالعقم والذين كانوا يخضعون لحقن الحيوانات المنوية داخل الهيولى في دراسة بأثر رجعي أجريت في المؤسسة العليا لتشخيص العقم وتقنيات الإنجاب المساعدة في جامعة النهرين في بغداد ، العراق. تم تصنيف وتقسيم المعلومات التي تم جمعها من المختبر وغرفة الأرشيف. مقارنة كل عام بالسنوات السابقة وكذلك المقارنة مع مؤشرات الأداء (معدل الإخصاب ، معدل الانقسام ، يوم التطوير ٢ ، يوم التطوير ٣ ، معدل الكيسة الأريمية ، معدل بقاء الكيسة الأريمية بالتبريد ، معدل الضرر ، معدل نجاح الخزعة ، معدل الانغراس يعتمد على الانقسام المرحلة ، ويعتمد معدل الانغراس على مرحلة الكيسة الأريمية) ، وكذلك مع . باستثناء معدل الخزعة الناجح ومعدل الزرع ، تم تحديد جميع العلامات في هذا التحقيق .

النتائج

معدلات الإخصاب والانقسام قريبة من مؤشرات الأداء الرئيسية لـ ESHRE. كانت نتائج اليومين الثاني والثالث قريبة أيضًا من معايير الكفاءة والمعايير ESHRE. كشفت مقارنة متوسط معدل الكيسة الأريمية عن قدر كبير من التقلبات ، حيث كان أعلى عام هو عام ٢٠١٦ وأدنى عام هو عام ٢٠١٩، يُعد عامي ٢٠١٥ و٢٠١٦ هما الأعلى والأدنى بالنسبة إلى الكيسة الأريمية للبقاء بالتبريد ، على التوالي. شهد كل من عامي ٢٠٢٠ و٢٠٢١ أعلى معدل ضرر للحقن المجهري. ٢٠١٥ و٢٠٢٠ هما أعلى وأدنى نتيجة حمل على التوالي.

الكلمات المفتاحية: مؤشرات الأداء الرئيسية، حقن الحيوانات المنوية داخل السايتو بلازم، الحمل.

1. INTRODUCTION:

Infertility is the medically recognized inability to get pregnant after at least a year of unbroken, unprotected sexual activity. [2] estimates that 8–12% of couples who are of reproductive age will be impacted. Demographers describe infertility as a woman's inability to conceive a live child despite engaging in sexual activity and without using contraception [3]. Infertility for women over 35 was previously defined as the inability to conceive after at least six months or a year of unrestricted sexual engagement.

With the aid of assisted reproductive technology (ART), infertility may be treated (ART). In reproductive procedures, it describes both the male sperm and the female ovum. It works by removing the eggs from the lady. Embryos are produced when sperm and eggs are joined. After that, the embryos are returned to the woman's body. In vitro fertilization is the most widely used and successful kind of ART (IVF) Occasionally, ART procedures may involve the use of frozen embryos, donor eggs, or sperm. Surrogacy or the use of a gestational carrier may also be used. A woman who uses her male partner's sperm to carry the couple's kid is known as a surrogate. Pregnancy occurs in the gestational carrier as a result of the union of the male and female partners' sperm and eggs.[4-6].

Types of ART :

Different ART procedures employ various methodologies and reproductive cells. A doctor can advise on the most suitable ART method based on the situation. The most common technique of conception is by in vitro fertilization [7]. One of the top methods for treating infertility is ICSI, ICSI, or intracytoplasmic sperm injection are all names for the procedure. One live sperm is injected into the center of an egg by means of this procedure.

The process is completed by stimulating the release of a significant number of mature eggs from the female partner's ovaries using fertility medications. The eggs are then carefully removed from the uterus using vaginal ultrasonography and stored in an embryology facility. To prepare the sperm sample, centrifugation is utilized, which involves spinning sperm cells in a certain medium. The majority of the living and dead sperm can then be distinguished from debris in this way. The embryologist will then use a glass needle to place the last sperm into the egg [8]. The international organization ESHRE created Performance Indicators to be used in the laboratory to carry out the ICSI process.

Because they enable evaluation of the efficacy, efficiency, equity, and patient-centeredness of treatment, performance indicators (PIs) are a crucial part of the quality management system (QMS) (ESHRE Guideline Group on Good Practice in IVF**[9,10]**. Currently, laboratories using assisted reproductive technology (ART) lack performance indicators (PIs) and have limited published data **[11]**. The objectives of this international workshop were to reach consensus on the key performance indicators (KPIs) for oocyte and embryo cryopreservation using slow freezing or vitrification, as well as on the minimum performance level values for each KPI, which represent fundamental competency, and aspirational benchmark values for each KPI, which represent best practice goals. This study provides overviews of current practice and important standards for creating KPIs. All 14 KPIs have benchmarks available **[12]**.

KPIs IN THE ART LABORATORY

Because of the work that is done with gametes and embryos in the lab, the ART technique is most crucial there. Above all, it is crucial to take into account these strategies and the surrounding surroundings **[13]**.

2. Patients and Methods

Material

The embryologist is responsible for keeping the books' notes neat and organized. Paper and hard copies were used for the data collection process from the IVF laboratory. These notebooks are kept safe from any potential hazards, such as fire, water, and electrical sources. The information gathered from the archive room is also kept on paper, albeit it is not organized enough to guarantee finding anything. Data was gathered to be compared to the international organization ESHRE's KPI.

Methods

At the start of the study, a form with information was given; complete it as directed. Along with his address, education, occupation, whether or not he smokes, what sort of smoking he does, and any illnesses he may have, the husband's name, height, weight, blood type, absence day, volume of semen, concentration, motility, agglutination, and round cell are all mentioned on this form. What previous health issues, like diabetes or high blood pressure, did he have? How many procedures has he had in the past, Name, weight, blood type, age, and hormone

analyses for FSH, LH, prolactin, and AMH (Anti Mullerian hormone), among other details, were found.

It's also important to know details about embryos, such as how many are implanted every day, how many pro nuclei or embryos are injected, how many follicles, oocytes, or ruptured oocytes, germinal vesicles, MI, or MIII, how many are retrieved, when those are transferred, and how many are of different grades. This study The IVF operation room and the archives should work together to gather all the data. 2015, 2016, 2017, 2018, 2019, 2020, and 2021 were the years for which data was gathered. About 699 instances made up the data. was unable to find certain names or files, possibly because they had been relocated from the operating room to the archive room to display the medical reports.

3-Result

Key performance indicators compared according to year

CSI normal fertilization rate: Table 1 compares the normal fertilization rate for ICSI according to year. Because the categorical feature (cleavage rate) is a constant and not a variable, statistical analysis cannot be done with respect to competency values of 65% because the rate in all years is more than 65%. Because the categorical characteristic (cleavage rate) is a constant and not a variable, the rate in all years exceeds the benchmark value of 80%, making statistical analysis impossible.

Table 1: Comparison of ICSI normal fertilization rate according to year

Characteristic	2015		2016		2017		2018		2019		2020		2021		Total	
INFRC (Competency value)	n= 21		n=73		n=144		n= 216		n=231		n=27		n=127		n=839	
≥ 65 %	21	100	73	100	144	100	216	100	231	100	27	100	127	100	839	100
<65 %	0	0	0	0	0	0	0	0	0	0	0	0	0	0	0	0
INFRB (Benchmark value)	n= 21		n=73		n=144		n= 216		n=231		n=27		n=127		n=839	
≥ 80 %	21	100	73	100	144	100	216	100	231	100	27	100	127	100	839	100
<80 %	0	0	0	0	0	0	0	0	0	0	0	0	0	0	0	0

Cleavage rate :

Table 2 compares the cleavage rate with time according to year. Because the categorical feature (cleavage rate) is a constant and not a variable, the rate in all years is greater than 95% with respect to the competency value of less than 95%, making statistical analysis impossible.

Because the categorical characteristic (cleavage rate) is a constant and not a variable, the rate in all years exceeds the benchmark value of 99%, making statistical analysis impossible.

Table 2 Comparison cleavage rate according to year

Characteristic	2015		2016		2017		2018		2019		2020		2021		Total	
CRC (Competency value)	**n= 24**		**n=78**		**n=148**		**n= 216**		**n=229**		**n=27**		**n=111**		**n=833**	
≥ 95 %	24	100	78	100	148	100	216	100	229	100	27	100	111	100	833	100
<95 %	0	0	0	0	0	0	0	0	0	0	0	0	0	0	0	0
CRB (Benchmark value)	**n= 24**		**n=78**		**n=148**		**n= 216**		**n=229**		**n=27**		**n=111**		**n=833**	
≥ 99 %	24	100	78	100	148	100	216	100	229	100	27	100	111	100	833	100
<99 %	0	0	0	0	0	0	0	0	0	0	0	0	0	0	0	0

Day 2 embryo development rate: In **Table 3**, the rate of embryo development on day 2 is compared by year. With regard to Competency Value, the rate of 50% was between 67.2% and 86.7%, and the difference was not statistically significant ($p > 0.05$). In terms of benchmark value, the rate of 80% varied from 25.9% to 63.3%, and the difference between 2015 and 2020 was not significant ($p > 0.05$); nevertheless, a substantial decline was found in the year 2021 ($p = 0.0$).

Table 3: Comparison of day 2 embryo development rate according to year

Characteristic	2015		2016		2017		2018		2019		2020		2021		Total	
D2EDRC (Competency value)	**n= 4**		**n= 30**		**n= 33**		**n = 70**		**n= 137**		**n= 22**		**n= 58**		**n= 353**	
≥ 50 %	3	75.0	26	86.7	27	81.8	51	72.9	113	82.5	18	81.8	39	67.2	277	78.2
<50 %	1	25.0	4	13.3	6	18.2	19	27.1	24	17.5	4	18.2	19	32.8	77	21.8
			0.536 NS		0.599 NS		0.322 NS		0.106 NS		0.940 NS		0.198 NS			
D2EDRB (Benchmark value)	**n= 4**		**n= 30**		**n= 33**		**n = 70**		**n= 137**		**n= 22**		**n= 58**		**n= 353**	
≥ 80 %	2	50.0	19	63.3	13	39.4	31	44.3	71	51.8	11	50.0	15	25.9	162	45.8
<80 %	2	50.0	11	36.7	20	60.6	39	55.7	66	48.2	11	50.0	43	74.1	192	54.2
			0.606 NS		0.058 NS		0.640 NS		0.305 NS		0.874 NS		0.040 *			

Day 3 embryo development rate: **Table 4** compares the pace of embryo development on day 3 according to year. The rate of 45% for Competency Value ranged from 52.6% to 81.0%, and the difference was not statistically significant ($p > 0.05$). Regarding Benchmark value, the rate of ≥ 70 % was ranging from 20.0 % to 69.4 % and the difference was among years 2015 through 2017 was not significant ($p > 0.05$); but significant reduction was reported in year 2019 ($p = 0.007$), but later on the fluctuation in rate became not significant ($p > 0.05$).

Table 4: Comparison of day 3 embryo development rate according to year

Characteristic	2015		2016		2017		2018		2019		2020		2021		Total	
D3EDRC (Competency value)	**n= 25**		**n= 71**		**n= 131**		**n= 188**		**n= 211**		**n= 27**		**n= 96**		**n= 749**	
≥ 45 %	20	80	57	80.3	106	80.9	141	75.0	169	80.1	21	77.8	59	61.5	573	76.5
<45 %	5	20	14	19.7	25	19.1	47	25.0	42	19.9	6	22.2	37	38.5	176	23.5
			0.976 NS		0.913 NS		0.214 NS		0.222 NS		0.778 NS		0.116 NS			
D3EDRB (Benchmark value)	**n= 25**		**n= 71**		**n= 131**		**n= 188**		**n= 211**		**n= 27**		**n= 96**		**n= 749**	
≥ 70 %	15	60	43	60.6	81	61.8	116	61.7	102	48.3	12	44.4	30	31.3	399	53.3
<70 %	10	40	28	39.4	50	38.2	72	38.3	109	51.7	15	55.6	66	68.8	350	46.7
			0.960 NS		0.860 NS		0.981 NS		0.007 **		0.703 NS		0.201 NS			

Blastocyst development rate: Table 5 displays a comparison of the Blastocyst formation rate by year. When it came to competency value, the rate of 40% ranged from 0% to 90.0%; there was a significant difference between 2015 and 2016 ($p = 0.016$), but no significant change was observed in subsequent years ($p > 0.05$). With regards to the benchmark value, the rate of 60% ranged from 0% to 75.0%; however, the difference was not statistically significant ($p > 0.05$).

Table 5: Comparison of Blastocyst development according to year

Characteristic	2015		2016		2017		2018		2019		2020		2021		Total	
BDRC (Competency value)	**n = 2**		**n = 8**		**n = 12**		**n = 11**		**n = 21**		**n = 0**		**n = 6**		**n = 60**	
≥ 40 %	0	0.0	7	87.5	8	66.7	10	90.9	15	71.4	0	0.0	4	66.7	44	73.3
<40 %	2	100.0	1	12.5	4	33.3	1	9.1	6	28.6	0	0.0	2	33.3	16	26.7
			0.016 *		0.292 NS		0.159 NS		0.205 NS				0.822 NS			
BDRB (Benchmark value)	**n = 2**		**n = 8**		**n = 12**		**n = 11**		**n = 21**		**n = 0**		**n = 6**		**n = 60**	
≥ 60 %	0	0.0	6	75.0	7	58.3	9	81.8	11	52.4	0	0.0	4	66.7	37	61.7
<60 %	2	100.0	2	25.0	5	41.7	2	18.2	10	47.6	0	0.0	2	33.3	23	38.3
			0.053 NS		0.444 NS		0.221 NS		0.102 NS				0.535 NS			

Blastocyst cryosurvival rate: Table 6 presents a comparison of the Blastocyst cryosurvival rate by year. When it came to competency value, the rate of 90% ranged from 50% to 100%; there was no significant difference between 2015 and 2016 ($p = 0.747$), but a significant decline was observed in the next year ($p = 0.021$), and the rate fluctuation in subsequent years was not

significant (p > 0.05). The benchmark value ranged from 50% to 91.7%, but the difference was not statistically significant (p > 0.05).

Table 6: Comparison of Blastocyst cryosurvival rate according to year

Characteristic	2015		2016		2017		2018		2019		2020		2021		Total	
BCSRC (Competency value)	**n = 2**		**n = 8**		**n = 12**		**n = 11**		**n = 21**		**n = 0**		**n = 6**		**n = 49**	
≥ 90 %	1	50.0	5	62.5	12	100.0	11	100	18	85.7	0	0.0	4	66.7	40	81.6
<90 %	1	50.0	3	37.5	0	0.0	0	0	3	14.3	0	0.0	2	33.3	9	18.4
			0.747 C NS		0.021 C *		---		0.188 C NS		---		0.289 C NS			
BCSRB (Benchmark value)	**n = 2**		**n = 8**		**n = 12**		**n = 11**		**n = 21**		**n = 0**		**n = 6**		**n = 49**	
≥ 99 %	1	50.0	5	62.5	11	91.7	10	90.9	18	85.7	0	0.0	4	66.7	39	79.6
<99 %	1	50.0	3	37.5	1	8.3	1	9.1	3	14.3	0	0.0	2	33.3	10	20.4
			0.747 C NS		0.110 C NS		0.949 C NS		0.673 C NS		---		0.289 C NS			

ICSI damage rate: In Table 7, the damage rate for ICSI is compared by year. ICSI damage rates greater than 10% ranged from 7.4% to 25.9%, with an upward trend over time. Year 2018 shown a significant increase in this rate in contrast to the year before (p = 0.012). When comparing benchmark values of > 5%, the rate varied from 2.7% to 26.6% with an upward trend over time; the level of p-value was greater than 0.05 when comparing succeeding years to prior years; however, some p-values, like 0.080 and 0.052, were extremely close to the threshold of significance of 0.05.

Table 7: Comparison of ICSI damage rate according to year

Characteristic	2015		2016		2017		2018		2019		2020		2021		Total	
IDR (Competency value)	**n= 27**		**n= 79**		**n= 172**		**n= 216**		**n= 247**		**n= 30**		**n= 139**		**n= 910**	
≤ 10 %	25	92.6	69	87.3	159	92.4	184	85.2	208	84.2	27	90.0	103	74.1	775	85.2
>10 %	2	7.4	10	12.7	13	7.6	32	14.8	39	15.8	3	10.0	36	25.9	135	14.8
p-value			0.457 NS		0.193 NS		0.027 *		0.772 NS		0.404 NS		0.061 NS			
IDR (Benchmark value)	**n= 27**		**n= 79**		**n= 172**		**n= 216**		**n= 247**		**n= 30**		**n= 139**		**n= 910**	
≤ 5 %	25	92.6	69	87.3	154	89.5	180	83.3	205	83.0	27	90.0	102	73.4	762	83.7
>5 %	2	7.4	10	12.7	18	10.5	36	16.7	42	17.0	3	10.0	37	26.6	148	16.3
p-value			0.457 NS		0.608 NS		0.080 NS		0.923 NS		0.326 NS		0.052 NS			

4. Discussion

Comparison of ICSI's average fertilization rate over time:

Compares the typical ICSI fertilization rate by year. All years' rates above the competency value of 65 percent since the category feature (cleavage rate) is a constant and not a variable, making statistical analysis impossible. Because the categorical characteristic (cleavage rate) is a constant and not a variable, the rate in all years exceeds the benchmark value of 80%, making statistical analysis impossible. The outcomes were quite close to the ESHRE KPI.

Comparison of the cleavage rate across years:

Compares the cleavage rate between years. Statistical analysis cannot be performed on these data because the categorical feature (cleavage rate), which has a competency value of 95%, is a constant and not a variable because the rate is always larger than 95%. Since the cleavage rate is a categorical trait and not a variable, it exceeds the benchmark figure of 99 percent every year, making statistical analysis impossible. The results closely matched the KPI for ESHRE.

Development on day two is contrasted by year:

In terms of competency value, the range for the 50% rate was 67.2 to 86.7 percent, with no statistically significant difference ($p > 0.05$). The benchmark value's 80% rate ranged from 25.9 to 63.3 percent, and the difference between 2015 and 2020 was not statistically significant ($p > 0.05$); however, the year 2021 showed a significant reduction ($p = 0.04$). It is most likely due to the lack of instances in 2020. A comparison of annual rates of day 2 embryo development.

Day 3 embryo development rates:

The rate of embryo development on day 3 is contrasted by year. In terms of competency value, the difference between the rates of 45 percent and 52.6 percent to 81.0 percent was not statistically significant ($p > 0.05$). Regarding the benchmark value, the rate of 70% ranged from 20.0 to 69.4%, and the variation between 2015 and 2017 was not significant ($p > 0.05$); however, a substantial reduction was seen in 2019 ($p = 0.007$), after which the rate fluctuation became not significant ($p > 0.05$). There are no specific causes, however one of the following possibilities could exist: Sperm abnormality and an intrinsic factor (nearly normal oocyte) (DNA fragmentation ,defect in centriole, origin of sperm). Incubator and media type (poor media quality) are both negative.

Blastocyst development rate comparison between years compares the Blastocyst formation rate by year. Regarding Competency value, the rate of 40% ranged from 0% to 90.0 %; there was a significant difference between 2015 and 2016 ($p = 0.016$), but no significant change was observed in subsequent years ($p > 0.05$). Regarding Benchmark value, the rate of 60% ranged from 0 to 75.0 percent; nevertheless, the difference was not statistically significant ($p > 0.05$). The following are most likely the causes: low number of blastocyst cases because patients do not understand that the embryo develops to this stage and because the institute (doctors) does not encourage it.

comparison of the Blastocyst cryosurvival rate between years.

A comparison of the Blastocyst cryosurvival rate by year. Between 2015 and 2016 there was no significant change ($p = 0.747$), but in 2017 there was a significant fall ($p = 0.021$), and the rate variation in the years after that was not significant ($p > 0.05$). The rate of 90% for Competency Value ranged from 50% to 100%. The rate of less than 99 percent varied from 50 to 91.7% in terms of benchmark value, however the variation was not statistically significant ($p > 0.05$). Age, weight, the wife's hormonal balance, oocyte and sperm quality, as well as her age and weight, are potential contributing factors.

Comparison of ICSI damage rates between years

The damage rate for ICSI is contrasted by year. With an upward trend over time, the rate of ICSI damage rates greater than 10% ranged from 7.4 percent to 25.9 percent, and the year 2018 showed a noticeable increase in this rate compared to the year before ($p = 0.012$). The level of p-value was higher than 0.05 when comparing data from subsequent years to those from earlier years; yet, several p-values, such 0.080 and 0.052, were quite close to the level of significance of 0.05. The rate ranged from 2.7 percent to 26.6 percent with an increasing rate trend over time with respect to the benchmark value of > 5 percent.

5- Conclusions

The efficiency standard values, which are the minimum expected, the efficiency values that every laboratory should be able to achieve, and the efficiency values that can be used as best practice, were contrasted in this study. The outcomes are satisfactory and favorable.

6- References

[1] Zegers-Hochschild F, Adamson GD, De Mouzon J, Ishihara O, Mansour R, Nygren K, Sullivan E, and Van der Poel S. The international committee for monitoring assisted reproductive technology (ICMART) and the world health organization (WHO) revised glossary on ART terminology. *Human reproduction*. 2009; 24(11): 2683-2687.

[2] Altamimi SI, Snobar RO, Al-Fraihat A, Albuarki M, Rizk, D. Causes of infertility. *Bahrain Medical Bulletin*, 2019; 41(2): 93-96.

[3] Carrell DT, Krausz C. Guest Editors: Douglas T Carrell and Csilla. *Reproductive BioMedicine Online*, 2008; 16(4): 471-473.

[4] Pirtea P, de Ziegle, D, Ayoubi JM. Effects of endometriosis on assisted reproductive technology gone with the wind. *Fertility and Sterility*. 2021; 115(2): 321-322.

[5] Mneimneh AS, Boulet SL, Sunderam S, Zhang Y, Jamieson DJ, Crawford S, McKane P, Copeland G, Mersol-Barg M, Grigorescu V, Cohen B. States Monitoring Assisted

Reproductive Technology (SMART) Collaborative: data collection, linkage, dissemination, and use. *Journal of Women's Health*. 2013; 22(7): 571-577.

[6] Snoek J, Rippel O, Swersky K, Kiros R, Satish N, Sundaram N, Patwary M, Prabhat M, Adams R. Scalable bayesian optimization using deep neural networks. *In International conference on machine learning.* 2015; June. (2171-2180). PMLR

[7] Polkinghorne KR, Chin GK, MacGinley RJ, Owen AR, Russell C, Talaulikar GS, Vale E, Lopez-Vargas PA. KHA-CARI Guideline: vascular access-central venous catheters, arteriovenous fistulae and arteriovenous grafts. *Nephrology* (Carlton). 2013; 18(11): 701-705.

[8] Damani MN, Masters V, Meng MV, Burgess C, Turek P, Oates RD. Postchemotherapy ejaculatory azoospermia: fatherhood with sperm from testis tissue with intracytoplasmic sperm injection. *Journal of clinical oncology*. 2002; 20(4): 930-936.

[9] Suorsa M, Rossi F, Tadini L, Labs M, Colombo M, Jahns P, Kater MM, Leister D, Finazzi G, Aro EM, Barbato R. PGR5-PGRL1-dependent cyclic electron transport modulates linear electron transport rate in Arabidopsis thaliana. *Molecular Plant*. 2016; 9(2):271-288.

[10] Laranjo L, Arguel A, Neves AL, Gallagher AM, Kaplan R, Mortimer N, Mendes GA, Lau AY. The influence of social networking sites on health behavior change: a systematic review and meta-analysis. *Journal of the American Medical Informatics Association*. 2015; 22(1): 243-256.

[11] Donaldson MS, Corrigan JM, Kohn LT. To err is human: building a safer health system. 2000.

[12] Wang HT, Hong PP, Li HY, Zhou W., Li T. Use of a new set of key performance indicators for evaluating the performance of an in vitro fertilization laboratory in which blastocyst culture and the freeze-all strategy are the primary treatment in patients with in vitro fertilization. *Journal of International Medical Research*. 2021; 49(9).

[13] Hammond ER, Morbeck DE. Tracking quality: can embryology key performance indicators be used to identify clinically relevant shifts in pregnancy rate?. *Human Reproduction*. 2019; 34(1): 37-43.